DESIGN METHODS FOR ACTIVE-PASSIVE HYBRID SPACE HEATING SYSTEMS

BY

BRIAN L. EVANS

A thesis submitted in partial fulfillment of the requirements for the degree of

MASTER OF SCIENCE
(Mechanical Engineering)

at the

UNIVERISITY OF WISCONSIN-MADISON

1983

ACKNOWLEDGMENTS

I would like to thank Professer Sanford Klein for his help and encouragement throughout this project. Without his insight and understanding this work would have been much more painful and time consuming. The assistance of Professors John Duffie and William Beckman has also had an important impact upon the content and presentation of this work.

I am likewise grateful for the support of Professor John Mitchell and the rest of the Solar Lab staff. Jim and Daryl in particular have lent assistance which greatly eased the development of the generalized Un-utilizability design method. And to Beth, who has shared the ups and downs, thank you.

ABSTRACT

In this thesis, design methods for three different types of active-passive hybrid space heating systems are presented. The three types of systems are: active system-passive system hybrids; active collection-passive storage hybrids; and active collection-passive plus direct-gain hybrids.

The active system-passive system design method is for systems composed of either a direct-gain or collector-storage wall passive system combined with an active space heating system. This method is based upon the application of existing analysis methods (i.e The SLR (3), Un-utilizablity (4,5), and f-Chart (2) Methods) successively on the passive and active subsystems. Two correction factors are presented to modify the existing analysis methods for interactions between the active and passive subsystems.

The design methods for the active collection-passive storage and the active collection-passive storage plus direct-gain systems are based on Monsen's Un-utilizability method for direct-gain systems (4). The Un-utilizability method is modified into a generalized Un-utilizability method which can be used on either direct-gain or active-passive hybrid systems.

Also presented is a review of the concept of "effective" building capacitance. A short term (72 Hr.) simulation technique is presented for determining the effective capacitance of particular building constructions, using the TRNSYS 12.1 transfer function building model.

TABLE OF CONTENTS

LIST OF FIGURES

LIST OF TABLES

NOMENCLATURE

$A_{c,a}$	Active collector area
$A_{c,p}$	Passive collector area
β_a	Active collector slope
β_p	Passive collector slope
$\overline{\beta}$	Average collector slope
γ_a	Active collector azimuth
γ_p	Passive collector azimuth
$\overline{\gamma}$	Average collector azimuth
C	Building effective capacitance
C_{min}	Active system load heat exchanger minimum capacitance rate
DD	Monthly heating degree-days
ε	Active system load heat exchanger effectiveness
f_a	Active solar fraction (monthly basis)
$f_{a,i}$	Monthly active solar fraction for building with infinite energy storage capacity
$f_{a,z}$	Monthly active solar fraction for building with zero energy storage capacity
f_p	Passive solar fraction (monthly basis)
f_{a+p}	Solar fraction for active plus direct-gain passive storage systems
F_a	Active solar fraction (annual basis)
F'_a	Annual active solar fraction corrected

	for the load time distribution
F_p	Passive solar fraction (annual basis)
ΔF_a	The overprediction of the f-Chart Method relative to TRNSYS simulations (annual basis)
$\Delta F_{a,p}$	Difference between solar fractions of active systems with active and passive storage
F_{max}	Maximum attainable solar fraction for active collection-passive storage solar systems
$F_R U_L$	Negative of the slope of the ASHRAE 93-77 collector test
$F_R(\tau\alpha)_n$	Intercept of the ASHRAE 93-77 collector test
$\overline{H}_T$	Monthly average radiation incident upon a tilted surface
$I_{c,c}$	Collector critical radiation level
$I_{c,b}$	Building critical energy level
$I_{c,cb}$	Building critical radiation level
L	Heating load
L'	Heating load per square meter of floor area
L_o	Passive design method prediction of active system load
ΔL	Increase in active system load due to controller effects
N	Number of days in a month
$(mC_p)_s$	Active energy storage capacity per square meter of collector area per degree Celsius
$\overline{\phi}_c$	Collector utilizability factor
$\overline{\phi}_{cb}$, $\overline{\phi}_b$	Building un-utilizability factor

$\overline{\phi}_u$	System un-utilizability factor
$Q_{c,a}$	Monthly energy collected by the active collector array
$Q_{c,p}$	Monthly energy collected by the passive collector array
Q_{aux}	Auxiliary energy required by the building
$Q_{aux,i}$	Auxiliary energy required by a building with infinite energy storage capacity
$Q_{aux,z}$	Auxiliary energy required by a building with zero energy storage capacity
Q_{dump}	Energy dumped from a building with zero energy storage capacity
$Q_{s,a}$	Energy storage capacity of active solar storage device
$Q_{s,p}$	Passive energy storage capacity of building
$Q'_{s,p}$	Passive solar storage capacity per square meter of floor area
$T_{set,act}$	Active solar system set temperature
$T_{set,aux}$	Auxiliary system set temperature
$\overline{T}_{act}$	Average building temperature when the active solar system is operating
$\overline{T}_{aux}$	Average building temperature when the auxiliary system is operating
$\overline{T}_a$	Monthly average ambient temperature
$\overline{T}_b$	Monthly average building temperature
$\overline{T}_i$	Monthly average collector inlet temperature
UA_b	Building shell energy loss coefficient
$UA_{c,d}$	Daytime value of the passive collector energy loss coefficient

$UA_{c,n}$	Nighttime value of the passive collector energy loss coefficient
$\overline{UA}_c$	Average passive collector energy loss coefficient
X	Total solar to load ratio
X_a	Active solar to load ratio
X_p	Passive solar to load ratio
Y	Passive energy storage capacity to energy dump ratio

CHAPTER 1 INTRODUCTION

1.1 BACKGROUND

Solar energy for use in building space heating applications has been extensively studied. With the decrease in fuel availability, and the associated increase in energy costs, solar heating systems have become a viable means to conserve heating energy.

There are a number of different generic types of solar space heating systems currently in use. Active systems employ collectors through which a fluid, either air or a liquid, is circulated by a fan or pump. The energy collected is then delivered to either the building directly, or to a storage device such as a pebble bed or water tank.

Passive solar systems are integrated directly into the building construction, such as a south-facing window or collector storage wall. The energy storage for a passive system, rather than being a thermally separate storage device, is the building structure itself. The energy is transferred to the building mass by direct radiation or by convection of the indoor air. This necessitates that the indoor temperature rise when solar energy is available,

allowing excess energy to be conducted into the building mass. This energy is then used at some later time to offset building energy losses. The passive energy storage capacity is therefore limited by the effective capacitance of the building and the range of temperatures which are allowable on an occupant comfort basis. An additional limitation is that the building mass must be thermally coupled to the room air, allowing the necessary heat transfer to take place.

A number of combinations of active and passive systems are possible and are shown schematically in Figure 1.1.1. Active and passive systems can be installed on the same building. This active system-passive system hybrid has both active and passive collectors, and uses the building mass as well as a storage tank or pebble bed for energy storage. Each of the two subsystems is however, relatively independent of the other.

A second type of hybrid space heating system is the combination of active collectors and passive storage. Active collection-passive storage systems make use of the controllable nature of the active collectors but eliminate the added expense of an active storage device. Unlike passive systems, active collection-passive storage systems require no night insulation, as the fluid circulator can simply be turned off at night. Similarly, there is no difficulty with the building overheating during the summer

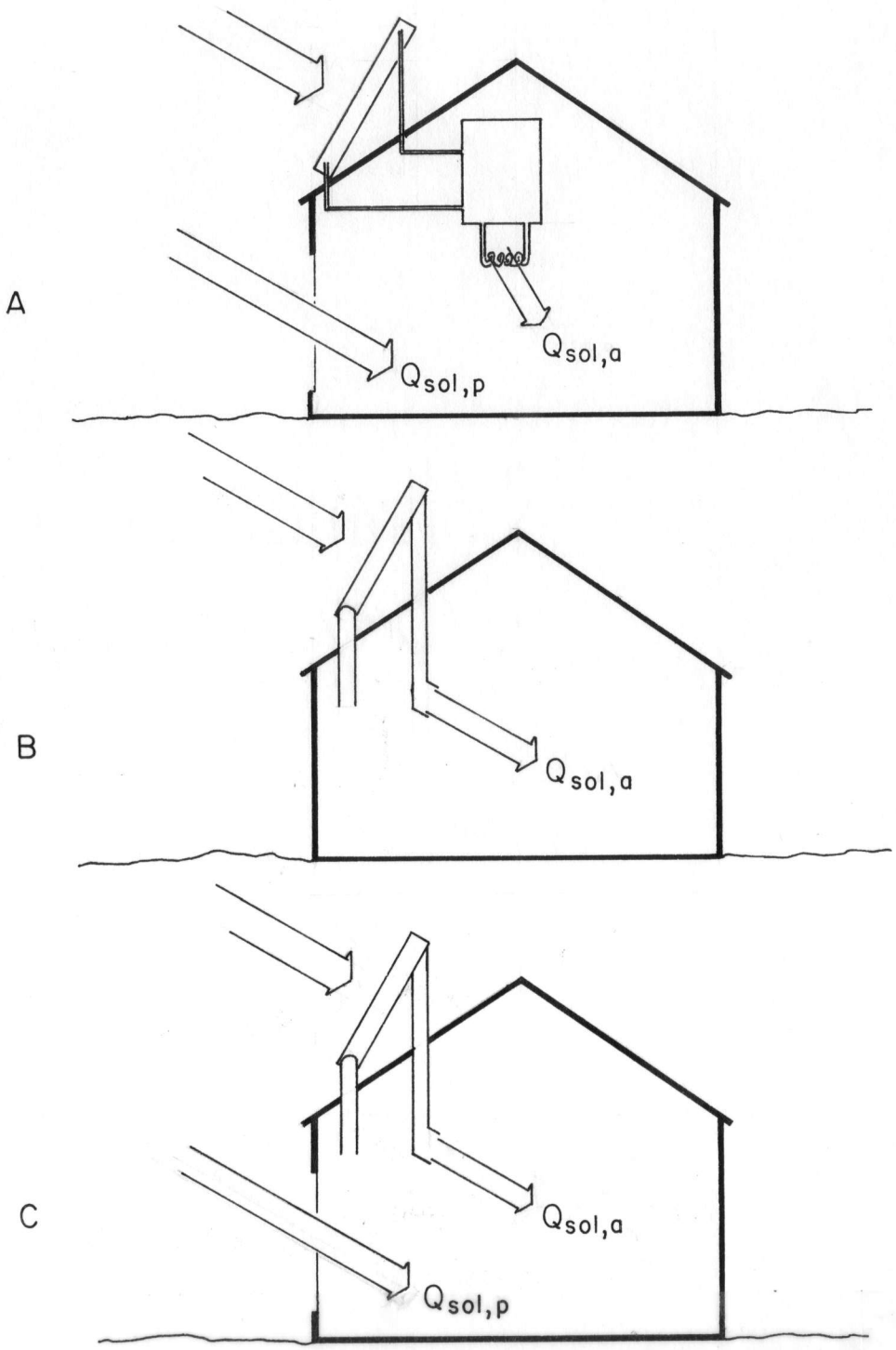

Figure 1.1.1 Schematic Representation of Three Active-Passive Hybrid Space Heating Systems. a) Active System-Passive system Hybrid. b) Active Collection-Passive Storage Hybrid. c) Active Plus Passive Collection-Passive Storage Hybrid.

months due to unwanted solar gains.

A third type of hybrid is a variation on the active collection-passive storage system, using both active collectors and direct-gain, with passive energy storage.

There are two basic means to perform a thermal analysis on a solar heating system. The first is to use a detailed computer simulation, such as the transient simulation program TRNSYS (1), to model the proposed system on an hourly (or shorter time interval) basis. This is the most versatile and most expensive way to do a system analysis. The flexability of programs such as TRNSYS is useful for unusual or large systems where a very detailed study is warranted. The design of simple solar systems by the use of detailed simulations could, however, end up costing more in computing and consulting costs than is saved by the final system design.

An alternative to detailed simulations is to use a simplified "design method" based on monthly or yearly calculations. Design methods are generally presented in the form of empirical correlations of solar system permformance as a function of several system parameters and weather data. The range of parameters which can be incorporated into a simplified design method is limited, leading to a number of design methods, each for a different "family" of solar systems. Several design methods exist for the analysis of active and passive solar space heating

systems. The f-Chart method (2) for active solar systems and the SLR method (3) for passive solar systems are perhaps the most widely used. Alternative passive design methods are the direct-gain and collector-storage wall Un-utilizability methods of Monsen, et al. (4,5). There have been, however, design methods for only a few specific configurations of hybrid space heating systems (6).

1.2 OBJECTIVES

The objective of this research was to develop general design methods for the three types of hybrid solar systems described above. The approach to this was to modify existing design methods wherever possible, either by altering the input parameters to correctly model hybrid systems, and/or developing correction factors which extend the limits of existing correlations.

Chapter 2 presents an analysis of active system-passive system hybrids. It uses any existing passive design method (i.e., the SLR method or Un-utilizability method) to predict the performance of the passive subsystem. The passive solar gains are then used to modify the inputs to the active system design method (i.e., the f-Chart method). Two correction factors have been developed to correct the active system design method for interactions between the passive and active subsystems.

Chapter 3 describes a modification of Monsen's direct-gain Un-utilizability method which allows it to be used for the analysis of active collection-passive storage systems. An additional modification is presented in Chapter 4 for active collection plus direct-gain, passive storage hybrid systems.

Chapter 5 reexamines the concept of an "effective" (lumped) building capacitance. The Un-utilizability method, whether for direct-gain or a hybrid system requires the calculation of the passive energy storage capacity. This is generally done using an effective capacitance and an allowable building temperature swing. Real buildings, however, have distributed capacitance. Chapter 5 presents a method for using short term (72 hour) simulations of detailed building models to determine an effective capacitance.

The remainder of this chapter reviews some of the pertinent design methods for solar space heating systems which will be referred to in the following chapters.

1.3 REVIEW OF PERTINENT DESIGN METHODS

This section summarizes the f-Chart design method (2) for active solar systems, which was used in the development of the design method for active system-passive system hybrids presented in Chapter 2. The Un-utilizability method for direct-gain systems (4), which is the basis of

the design methods presented in Chapters 3 and 4 is also briefly reviewed. The final design method outlined is the commonly used SLR Method, which is used for some of the design method-simulation comparisons in Chapter 2.

1.3.1 The f-Chart Method

The f-Chart method (2) was developed to predict the solar fraction, f_a, for a wide range of residential active solar system designs using either pebble bed or liquid storage. The solar fraction is calculated using equations which have been empirically correlated from hundreds of detailed simulations covering a wide range of system parameters and weather data. Three different equations have been developed. Two apply to space heating systems (or combined space heating and domestic hot water systems) with pebble bed or liquid storage. The third correlation is for systems which heat domestic hot water only.

The solar fraction is correlated against two independent, dimensionless parameters, X and Y. Y, the solar to load ratio, is approximately the ratio of the absorbed solar radiation to the total heating load. X is the ratio of the collector losses at some arbitrary reference temperature to the heating load. X and Y are defined below.

$$X = A_{c,a} F_R U_L (T_{ref} - \bar{T}_a) \Delta t / L \qquad (1.3.1)$$

$$Y = A_{c,a} F_R (\tau\alpha)_n \bar{H}_T N/L \qquad (1.3.2)$$

Pipe or duct losses, solar incidence angle effects, and the effects of a heat exchanger between the collector loop and the storage can be accounted for by modifying F_R, U_L, and $(\tau\alpha)_n$. The algorithms for these corrections are given in Appendix A.

A number of correction factors can be applied to X and/or Y to increase the range of parameters for which the f-Chart correlations are valid. Variations in storage capacity can be accounted for by correcting the dimensionless parameter X. For liquid systems:

$$X_c = X \left[\frac{\text{actual storage capacity (l)}}{75\ \text{l/m}^2 A_{c,a} F_R'} \right]^{-0.25} \qquad (1.3.3)$$

For pebble bed systems

$$X_c = X \left[\frac{\text{actual storage capacity (m}^3\text{)}}{0.25\ \text{m}^3/\text{m}^2 A_{c,a} F_R'} \right]^{-0.30} \qquad (1.3.4)$$

Liquid based solar systems also require modifications to the f-Chart parameter,Y , to account for the heat exchanger between the storage tank and the building air. The dimensionless parameter $\varepsilon C_{min}/UA_b$ is a measure of the size of the heat exchanger relative to the load it must meet. ε

is the heat exchanger effectiveness, C_{min} is the minimum fluid capacitance rate, and UA_b is the energy loss coefficient of the building.

$$Y_c = Y(0.39+0.65(\exp(-0.139UA_b/\varepsilon C_{min}))) \qquad (1.3.5)$$

The f-Chart correlation for pebble bed systems is based upon an air flow rate of 10 l/s per square meter of collector area. For flow rates other than this, the dimensionless parameter, X, can be corrected in addition to the correction for storage size.

$$X_c = X\left[\frac{\text{actual flow rate } (l/s\text{-}m^2)}{10\ (l/s\text{-}m^2)}\right]^{0.28} \qquad (1.3.6)$$

The limits for which all of these correction factors are applicable can be found in reference (7). The solar fraction correlations for air and liquid space heating systems are given below. For both correlations, the curve fits break down for values of X greater than 15, and for values of Y greater than 4. Caution should therefore be used if X or Y fall into these ranges. For liquid systems:

$$f_a = 1.029Y-0.065X-0.245Y^2+0.0018X^2+0.0215\ Y^3 \qquad (1.3.7)$$

For pebble bed systems:

$$f_a = 1.040Y-0.065X-0.159Y^2+0.00187X^2-0.0095Y^3 \quad (1.3.8)$$

1.3.2 The Un-utilizability Method

Monsen's direct-gain Un-utilizability (4,5) design method is based on the concept of solar radiation utilizability. The utilizability factor is the fraction of radiation incident upon a collector which is greater than some specified critical radiation level. In the case of a direct-gain passive system having no thermal storage, the un-utilizability factor is the fraction of the incident radiation which must be dumped from the building because it is in excess of the immediate heating needs of the building. Dumping can be accomplished either by venting the building, or by blocking the collector aperture.

Monsen developed upper and lower limits to the performance of a direct-gain system assuming that the building had zero and infinite energy storage capacity. He then correlated the results from a large number of simulations of buildings with realistic energy storage capacities to develop an equation which essentially interpolates between the two limits.

The passive solar fraction, f_p, is correlated against the independent dimensionless parameters X, Y and $\overline{\phi}_b$. X is the ratio of the absorbed solar radiation to the building heating load.

$$X = A_{c,p}\bar{H}_T(\overline{\tau\alpha})N/L \qquad (1.3.9)$$

Y, the storage to dump ratio, is the ratio of the energy storage capacity of the building to the amount of solar energy that would be dumped from the building if there were zero energy storage capacity.

$$Y = \frac{C\Delta T_s N}{A_{c,p}\bar{H}_T(\overline{\tau\alpha})N\bar{\phi}_b} \qquad (1.3.10)$$

The building storage capacity is presented here as the product of the effective building capacitance and the allowable temperature swing.

$\bar{\phi}_b$, is the building un-utilizability factor, which is the fraction of incident radiation which is greater than the radiation level necessary to just meet the heating requirements of the house, $I_{c,b}$.

$$I_{c,b} = (UA_b+UA_c)(T_b-\bar{T}_a)/(A_{c,p}(\overline{\tau\alpha})) \qquad (1.3.11)$$

$\bar{\phi}_b$ can be found as a function of $I_{c,b}$ using one of the methods outlined in Appendix B.

Equation 1.3.12 is the passive solar fraction correlation for direct-gain systems.

$$f_p=PX+(1-P)(3.082-3.142\bar{\phi}_B)(1-\exp(-0.329X)) \qquad (1.3.12)$$

where $P=(1-\exp(-0.294Y))^{0.652}$ (1.3.13)

The limitations of this correlation can be found in reference 4 or 8.

1.3.3 The SLR Method

The Solar Load Ratio (SLR) Method (3) for analyzing passive solar systems uses a somewhat different approach than the Un-utilizability Method. Only one dimensionless parameter is used to correlate system performance, the solar to load ratio. This is comprised of the load to collector ratio (LCR), which is the only building design variable, and a number of weather parameters. The coefficents used in the solar fraction correlation are presented for 94 different reference designs (3), and are valid only for buildings which closely match the characteristics of those designs. The effect of varying a single parameter other than the LCR can be accommodated by using the sensitivity analyses presented in reference (3) . Varying more than one additional parameter can lead to errors due to interaction effects between the different parameters. A more complete overview of the SLR Method is given by Balcomb in reference (9).

CHAPTER 2 ACTIVE-PASSIVE COMBINED HYBRID SYSTEMS

2.1 INTRODUCTION

The combination of active and passive solar space heating systems is attractive due to the complimentary nature of the two system types. Passive systems are typically less expensive and simpler than active systems. Yet in many climates, it is difficult to meet a high fraction of the heating requirement with passive heating alone because of the need for large glazing areas and the difficulty in storing energy in the building structure for extended periods of time with typical building construction. Active solar systems provide additional energy input and can efficiently store energy for later use. Combining these systems provides the efficient storage capacity of the active system and allows a reduction in active system size, hence cost, compared to an active only system because the passive system meets a portion of the heating load.

Almost all active systems can be considered active-passive hybrid systems since any windows which contribute a net solar gain can be considered to be a passive solar system. Although hybrid systems have great potential, there has been no generalized simple design method

available to analyze their performance. The objective of this chapter is to present a design method for hybrid systems through the combination of existing design methods for active and passive systems.

2.2 ANALYSIS METHODOLOGY

A possible procedure for analyzing a hybrid system is to first apply a passive design method (e.g., the Solar-Load Ratio (3,9), or Un-utilizabilty (4,5) methods), assuming that there is no active system. The additional energy needed to maintain the building above its set point is predicted by the passive design method and then is used as the heating load for the active system. The result of the active system design method (e.g., the f-Chart method (2)) is then the estimate of the auxiliary which must be supplied for the combined active-passive system. This infers that the passive system has the first opportunity to supply energy to the heating load, and the active system is essentially a backup, as it is more controllable than the passive system.

There are two problems with this approach to hybrid system analysis. First, the load on the active system will always be greater than the auxiliary energy predicted by the passive system design method (disregarding systematic or location dependent errors in the design method) because the active system controller causes the average building

temperature to be greater than it would be if the active solar system were not present.

The second problem is concerned with the time distribution of the load on the active system. Active system design methods such as f-Chart (2) assume that the space heating load is proportional to the difference between the indoor and outdoor temperatures. In a hybrid system, the passive component will supply much of the load during the day, shifting the load distribution for the active system to nighttime periods. These two problems can be accounted for by the use of two corrections that are part of the design method given in this chapter.

2.3 IDENTIFICATION OF IMPORTANT PARAMETERS

In order to investigate which system components and parameters are important in causing the interaction between active and passive components in hybrid systems , a series of TRNSYS (1) simulations were run in which timed, artificial "passive gains" were input into the building model. The distribution and intensity of the artifical passive gains were controlled in a manner which allowed the effect of changes in parameters and components on active system performance to be readily apparent.

In addition to the artificial "passive" energy gain parameters, a number of building and active solar system parameters were also investigated. Of these, four were

found to be possible causes of interactions between the active and passive system performance. These are: active system collector size relative to the building energy losses not met by passive; active system storage capacity per unit collector area; active system load heat exchanger size; and effective building energy storage capacity.

Using controlled "passive gains" allowed inexpensive screening to select parameters for further study using detailed passive models on an annual basis. In the subsequent detailed studies, standard components of the TRNSYS 11.1 simulation program are used for both the active and passive systems.

2.4 MAGNITUDE CORRECTION FOR ACTIVE SYSTEM LOAD

The error in the passive design method prediction of the magnitude of the active system load is primarily a function of the active system controller. The increase in load on the active system above that predicted by the passive system design method results from the active solar thermostat set temperature being higher than the auxiliary system thermostat set temperature. A higher set temperature is necessary to ensure that available solar energy is used before auxiliary energy is supplied. Higher active solar fractions mean that the building is at the higher set temperature more often, causing the average building temperature to be higher. Higher building

temperatures will result in additional energy losses from the building, hence more load on the active system.

A monthly energy balance on a hybrid system leads to a generalized correction factor for L/L_o, the ratio of the active system load, L, to the active system load as predicted by the passive design method, L_o. The correction factor is in terms of the monthly passive solar fraction, f_p, defined in Equation 2.4.1; the monthly active solar fraction, f_a, defined in Equation 2.4.2 ; the monthly heating degree days, DD (based on the building base temperature); the building shell energy loss coefficient (not including the passive collector) UA_b; and the passive collector energy loss coefficient UA_c.

$$f_p = 1 - L_o/(UA_b(DD)) \qquad (2.4.1)$$

$$f_a = 1 - Q_{aux}/L \qquad (2.4.2)$$

where Q_{aux} is the actual auxiliary energy required by the hybrid building.

To account for deadband settings in the active and auxiliary systems controllers, the assumption is made that when either system is operating, the average indoor temperature is equal to the respective lower set point plus one half of the controller deadband (defined in Equations 2.4.3 and 2.4.4). Figure 2.4.1 shows a plot of TRNSYS

simulation results of the building indoor temperature as a function of time. The period shown in the plot covers both active system and auxiliary system operation. These and other simulation results using a UA-degree day, lumped capacitance building model have shown that the average temperatures defined in Equations 2.4.3 and 2.4.4 are valid on a monthly basis.

$$\bar{T}_{aux} = T_{set,aux} + 0.5(deadband)_{aux} \qquad (2.4.3)$$

$$\bar{T}_{act} = T_{set,act} + 0.5(deadband)_{act} \qquad (2.4.4)$$

L, the actual load on the active system, can be derived by calculating the load on the active system as predicted by the passive design method and adding the increase in active system load due to the effects caused by the difference between the active and auxiliary setpoints. L_o can be expressed:

$$L_o = UA_b(DD)(1 - f_p) \qquad (2.4.5)$$

The increase in the active system load, ΔL, must be expressed in terms of the total building energy loss coefficient (the building shell energy loss coefficient plus the passive collector energy loss coefficient) as there will be increased losses from both the building shell

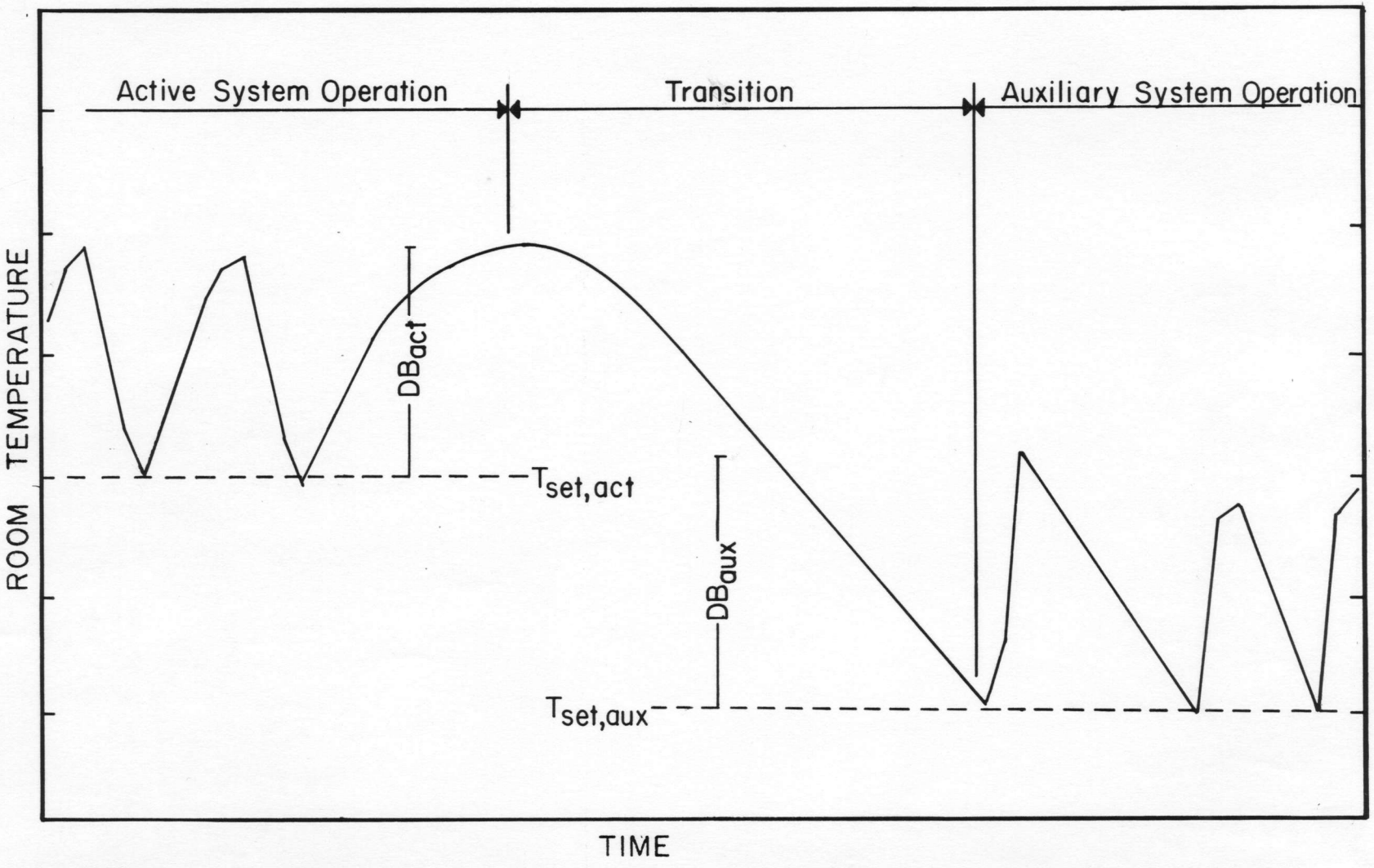

Figure 2.4.1 Instantaneous Indoor Building Temperature During Active Solar System Operation and During Auxiliary System Operation.

and the passive collector.

$$\Delta L = (UA_b + UA_c)(\bar{T}_{act} - \bar{T}_{aux})(N)f_a \qquad (2.4.6)$$

In equation 2.4.6, N is the number of days in the month. The product of the difference between the average temperatures and N is the additional heating degree-days due to the increase in average indoor temperature. Additional energy losses will occur only when the indoor temperature is greater than the degree-day base temperature, which is when the temperature is greater than T_{aux}. This occurs when the active solar system is operating, thus, the active solar fraction (which is related to the percentage of time that the active solar system is operating) becomes a factor. It is convenient to express the load magnitude correction factor in terms of L/L_o, which is simply $(L_o + \Delta L)/L_o$:

$$L = UA_b(DD)(1 - f_p) + (UA_b + UA_c)(\bar{T}_{act} - \bar{T}_{aux})(N)f_a \qquad (2.4.7)$$

$$\frac{L}{L_o} = 1 + \frac{(UA_b + UA_c)(\bar{T}_{act} - \bar{T}_{aux})(N)f_a}{UA_b(DD)(1 - f_p)} \qquad (2.4.8)$$

Equation 2.4.8 indicates that if $f_a = 0$ (i.e., no active system), then L, the energy required in addition to the passive contribution to maintain the building at the

set point temperature, is equal to L_o, the estimate provided by the passive system design method. As f_a is increased, the fraction of L provided by the active solar energy system is increased, and L/L_o becomes greater than 1 as shown in Figure 2.4.2. This is for a typical situation in which N = 31, DD = 403 C-Days, $(UA_b + UA_c)/UA_b = 1.5$, $\bar{T}_{aux}$=18.5 C, and $\bar{T}_{act}$ = 20.0 C. For example, a passive solar fraction of 0.4, and high active solar fractions can result in loads which are 25% greater than those calculated based on the auxiliary set point temperature. This correction factor can (and should) be applied to active only space heating systems (i.e., f_p = 0) as well, as the load estimates used in the design method calculations do not usually include the effect of elevated temperatures resulting from controller settings.

The use of Equation 2.4.8 requires an iterative calculation procedure. The monthly passive solar fractions (f_p) are calculated from a passive design method. The net loads obtained from the passive method (L_o) are used in the f-Chart method to obtain monthly active solar fraction estimates. The monthly active solar fractions and the monthly degree-days are then used to find correction factors from Equation 2.4.8 which can be multiplied by monthly values of L_o to obtain better estimates of the monthly loads. The f-Chart calculations are then repeated. One iteration is generally all that is needed.

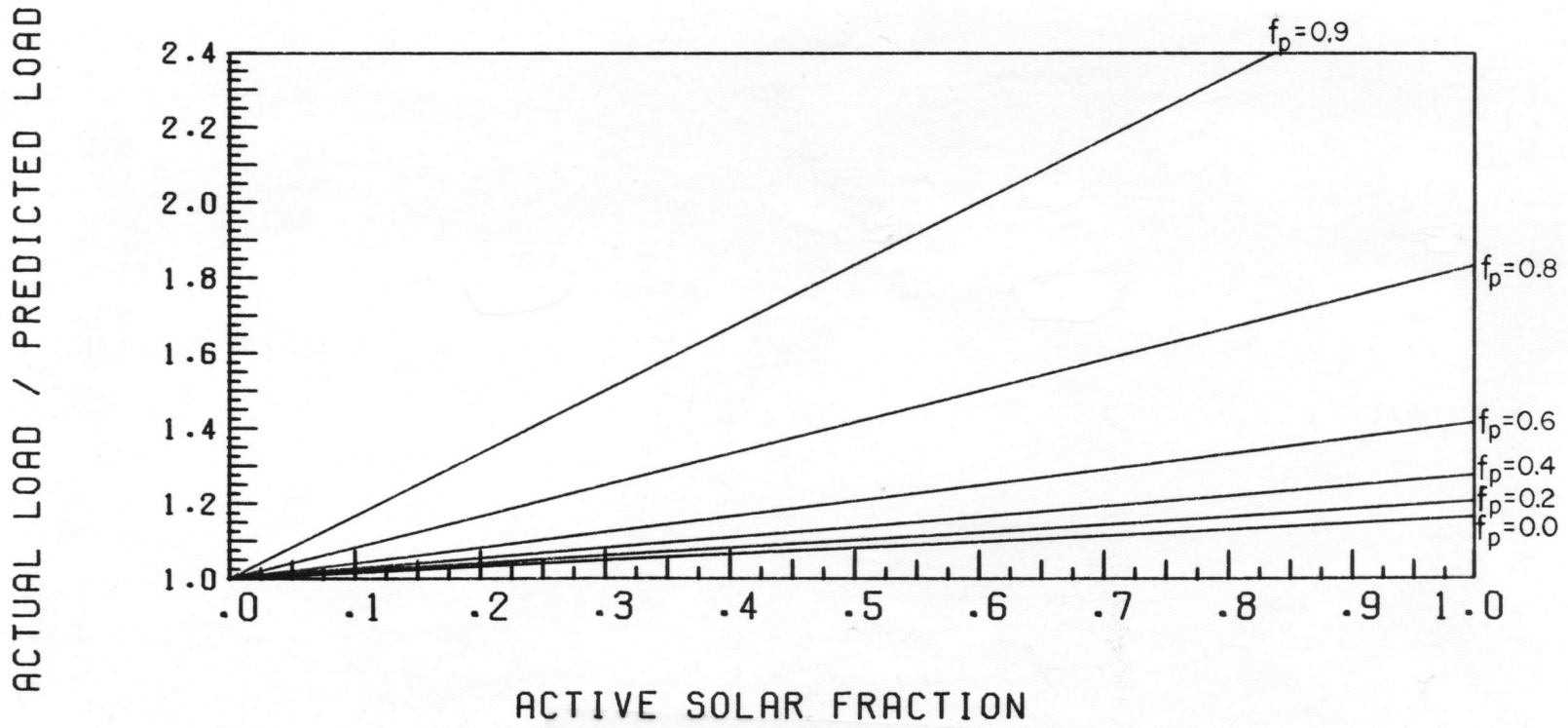

Figure 2.4.2 Load Magnitude Correction Factor for Active System Loads. This Plot is for N=31 days, DD= 403 C-days T_{aux}=18.5C, and T_{act}=20.0 C, and $(UA_B+UA_C)/UA_B$=1.5

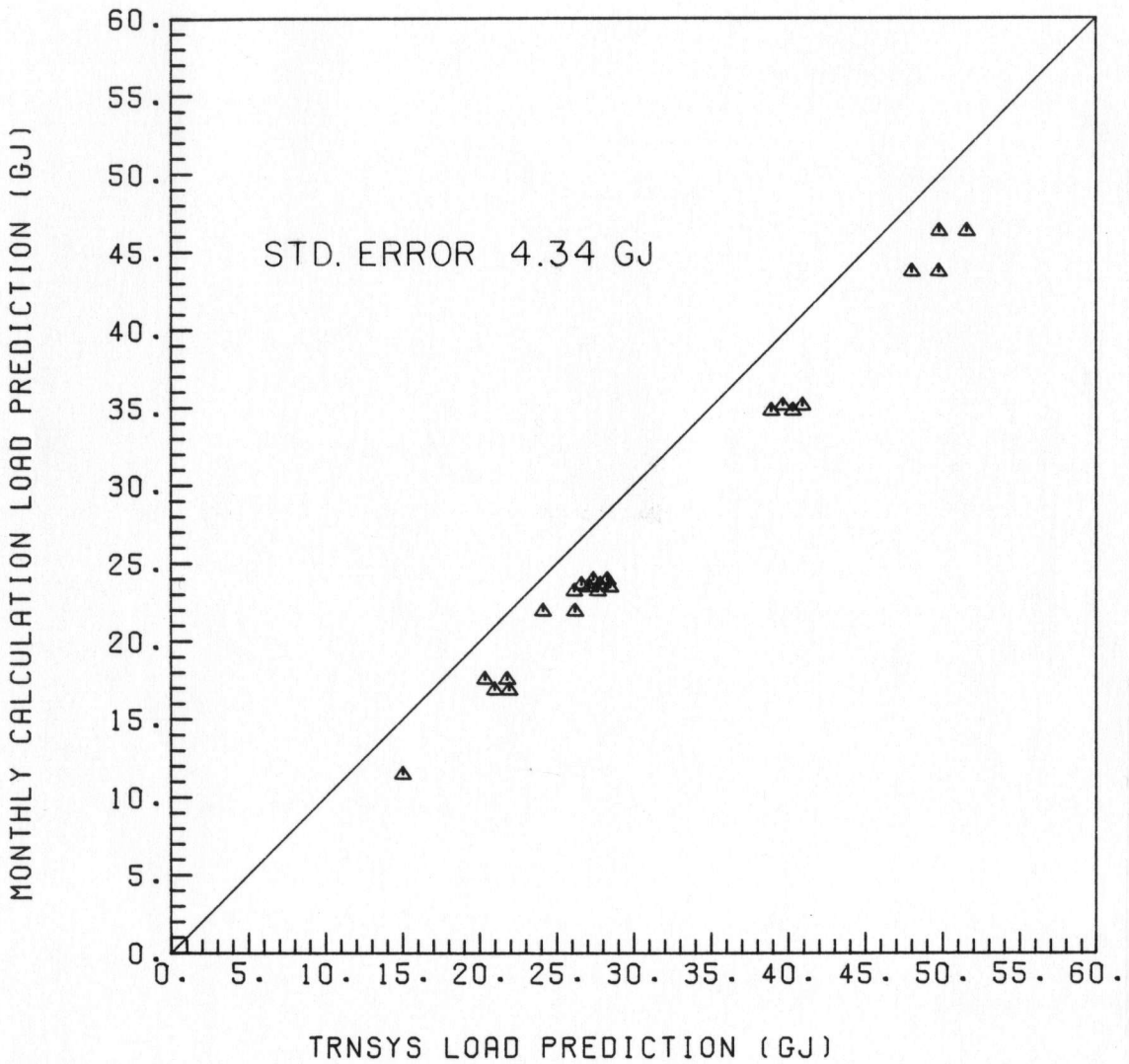

Figure 2.4.3 Uncorrected Annual Active System Loads Compared to TRNSYS Simulation Results. The Points are for Caribou, ME, Bismarck, ND, Columbia, MO, and New York, NY.

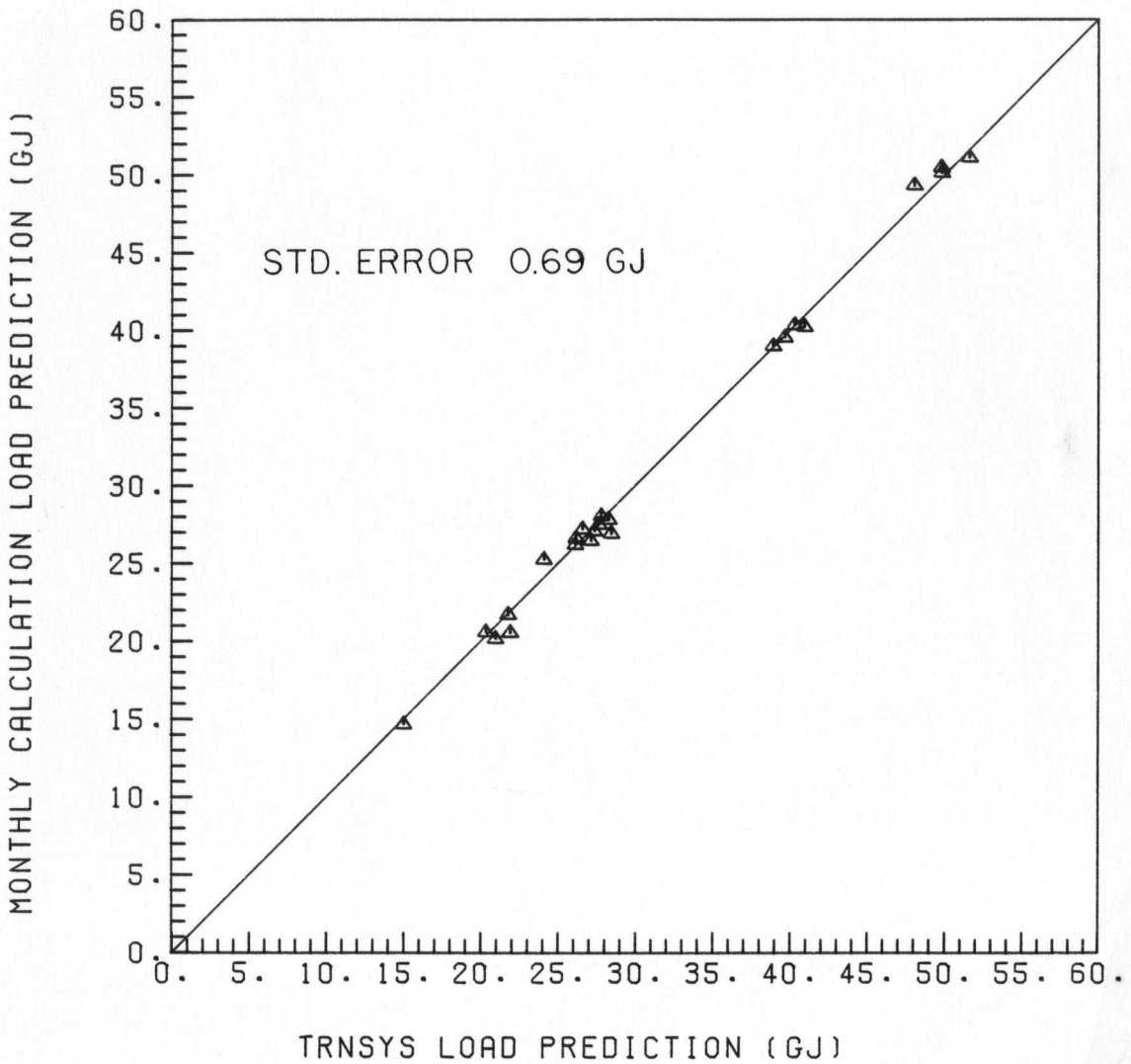

Figure 2.4.4 Corrected annual Active System Loads Compared to TRNSYS Simulation Results. The Locations are the same as in Figure 2.4.3.

Figure 2.4.3 shows predicted annual active system loads that have not been corrected for controller effects compared to detailed simulation results for four locations. Figure 2.4.4 shows a similar comparison, except that the predicted active system loads have been corrected by use of the correction factor given in Equation 2.4.8. (In both of these plots, simulation results rather than a passive design method were used to obtain the predicted active system loads thereby eliminating any error associated with the simplified passive design methods.) Comparison of the two plots shows that Equation 2.4.8 corrects the active system load for controller effects to within a standard deviation of $\pm 2\%$ on an annual basis for all locations. Somewhat more error is associated with the monthly calculations which were summed to get the annual values.

2.5 CORRECTION FACTOR FOR ACTIVE SYSTEM LOAD TIME DISTRIBUTION

The time distribution of the load on an active system is affected by the passive solar contribution. In a combined active, direct-gain system, for example , the load on the active system will be shifted more towards nighttime, causing the active system to store energy for longer periods. Storing energy raises the average collector inlet temperature and thereby reduces the efficiency of the active system. Design methods such as

f-Chart do not account for this effect. Comparisons of detailed TRNSYS simulations of hybrid systems and design method predictions were used to develop an empirical correction factor for the time distribution effect. The parameters used in the simulations and f-Chart calculations are listed in Table 2.5.1. The f-Chart calculations were done using the computer program F-CHART 3.0 (10), not to be confused with the $\overline{\phi}$,f-Chart method (11) used in F-CHART 4.1 (12).

Before evaluating active-passive interactions, it was first necessary to verify the accuracy of the f-Chart method for active systems alone, and to determine if there was any systematic bias which could mask the hybrid system interactions. As seen in Figure 2.5.1, each of the four cities has a certain bias curve, with the difference in annual solar fractions between f-Chart predictions and TRNSYS calculations (defined as ΔF_a) being plotted as a function of annual active solar fraction. Taken as a whole, the accuracy of f-Chart relative to TRNSYS appears to be $\pm$3%, as originally cited for the method (2). The one exception to this is Seattle, WA, a location for which f-Chart has been previously shown (7) to underpredict due to the fact that the relatively small amount of sunshine during the winter months has a high utilizability. The more detailed calculations required by the $\overline{\phi}$,f-Chart method (i.e., F-CHART 4.1) should agree more closely with

simulation results for Seattle.

A further study was conducted to determine the effect of building capacitance on active solar fraction predictions. Figure 2.5.2 shows a comparison of ΔF_a as a function of annual solar fraction and effective building capacitance. The heating system control strategy used in these simulations is as follows. If the building temperature drops below 19 C, energy from the solar storage (if available) is added to the house; if the temperature continues to drop, the auxiliary furnace is turned on at 18 C. Both solar and auxiliary thermostats have 2 C deadbands. This control strategy is called temperature level control. Also shown in Figure 2.5.2 are simulation results using energy rate control, the control strategy used in the development of the f-Charts. With energy rate control, the exact amount of energy needed during a given timestep is added to the building. This corresponds to a 0 degree deadband controller, keeping the indoor air temperature constant.

The product of the deadband and the building capacitance is a measure of the amount of energy which can be stored in the building mass. Temperature level control therefore allows additional energy storage. Figure 2.5.2 shows that the building capacitance does have a systematic effect on f-Chart calculations. However, between the extremes of 2000 KJ/C to 35000 KJ/C, which should encompass

TABLE 2.5.1

SIMULATION AND f-Chart PARAMETERS FOR ACTIVE SYSTEM-PASSIVE SYSTEM HYBRIDS

LOCATIONS:		
Seattle, WA Madison, WI Albuquerque, NM Boston MA		
PASSIVE COMPONENTS:		
Direct Gain Storage Wall		0.12m ; 0.25m Collector Storage Wall
$U_{Collector}$	Day	2.5 $W/m^2°C$
	Night	1.5 $W/m^2°C$
Collector Area		5-100m^2
ACTIVE COMPONENTS:		
$F_R(\tau\alpha)$		.7
F_RU_L		4.72 $W/m^2°C$
Collector Area		0-200m^2
Storage Capacity		37-75ℓ/m^2
$\frac{\varepsilon C_m}{UA}$		1.1-5.0
BUILDING:		
UA (without passive collector)		60-200 W/°C
Capacitance		2000-35000 KJ/°C
Auxiliary Set Temperature		18°C
Active Set Temperature		19°C
Deadbands		2°C
Allowable Passive Swing		4-8°C

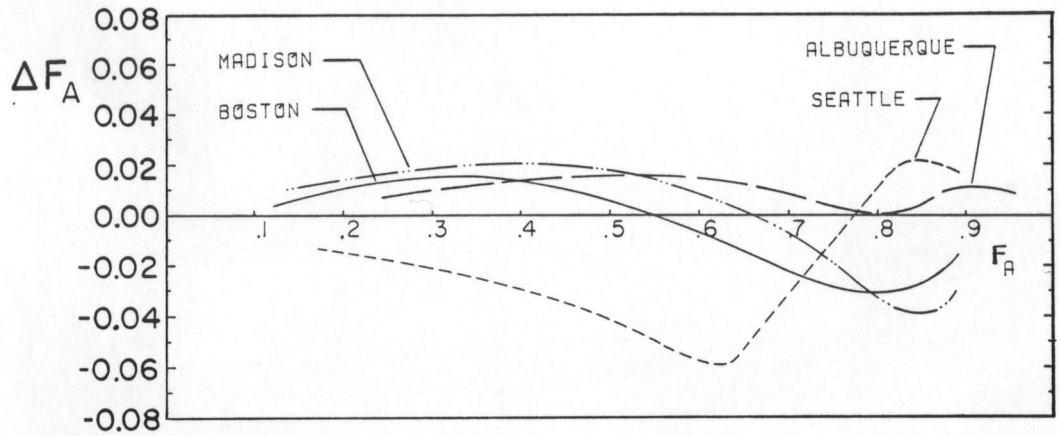

Figure 2.5.1 Overprediction Error in the f-Chart Method for Active Only Systems for Different Locations. All Other Parameters were Constant.

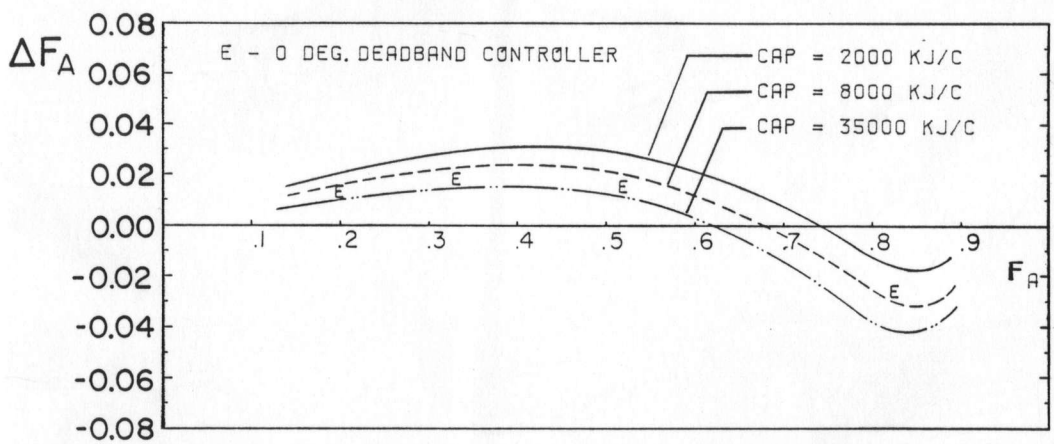

Figure 2.5.2 Overprediction Error in the f-Chart Method for Different Building Capacitances for an Active Only System in Madison, WI.

buildings of very light to heavy construction, there is a maximum variation in ΔF_a of only 2.5%.

A final comparison between TRNSYS and F-CHART for active systems shows the effect of the active system load heat exchanger size. In the f-Chart method, load heat exchanger size is represented by the dimensionless parameter $\varepsilon C_{min}/UA_b$, where ε is the heat exchanger effectiveness, C_{min} is the minimum capacitance rate of the heat exchanger, and UA_b is the total building energy loss coefficient. A standard value of 2.0 for this parameter was used to develop the f-Charts for liquid-based systems, and nonstandard values require a correction factor to the f-Chart dimensionless parameter, Y. Changes in $\varepsilon C_{min}/UA_b$ produce a small distortion of the basic f-Chart accuracy for a reasonable range of values (1.1 to 5.0), with the only notable variation (about 3%) being in the 70-90% solar fraction range.

The previous F-CHART--TRNSYS comparisons and the comparisons of hybrid systems to follow are all based on monthly loads in F-CHART as calculated by the corresponding TRNSYS simulations rather than load estimates obtained from a passive design method and Equation 2.4.8. This is done so that possible errors from these sources are not introduced into the time distribution correction factor derived from these comparisons.

A study of the use of the f-Chart method for estimating the active solar fraction in hybrid systems was based on TRNSYS simulations using the parameter values in Table 2.5.1. Comparisons of results from the simulations and f-Chart predictions were done in a manner similar to the previous studies, i.e., by plotting active ΔF_a (the over-prediction in f-Chart solar fraction) as a function of active solar fraction. The major difference was that the f-Chart bias for active systems alone was subtracted out so that the effect of hybrid interactions could be plotted independently. Following this procedure, it was found that building capacitance had little effect on hybrid interaction on a yearly basis, or in other words, the effect of building capacitiance on f-Chart predictions of hybrid system performance was no more pronounced than it was for active systems alone. Similarly, the effect of $\varepsilon C_{min}/UA_b$ was found to be minimal.

Based on these results, the important parameters in hybrid systems are: active solar fraction, passive solar fraction, and active system storage capacity relative to collector size. A range of active and passive annual solar fractions (0-90% for active, 0-60% for passive) were studied by varying their respective collector areas. Active system storage was investigated for the f-Chart standard storage (314 KJ/C-m^2) and for one-half of the standard storage (157 KJ/C-m^2). Different passive gain

time distributions were studied by using direct-gain, 0.25m concrete collector-storage wall, and 0.125m concrete collector-storage wall systems.

The change in the time distribution of the load on the active system will always be greater for direct-gain systems than for collector-storage walls. The direct-gain meets the load during the day, causing the active system to store energy during the day thereby raising the storage tank or pebble bed temperature more than it normally would be raised if a direct-gain system were not involved. This in turn raises the collector inlet temperature and reduces the collector efficiency. Collector-storage walls moderate this effect somewhat by delaying passive gains towards the evening, allowing some of the energy collected by the active system during the day to be used immediately, thereby lowering the average storage temperature and more closely resembling the load distribution assumed by the f-Chart method. Because direct-gain is the limiting case of hybrid interaction, and because the overall error in f-Chart predictions of active solar fractions in hybrid systems is relatively small, results of the direct-gain hybrid systems will be presented as the upper bound of f-Chart overprediction for hybrid systems. These results can be used directly to obtain a time distribution correction factor for active system performance in direct-gain hybrid systems calculated by the f-Chart method and will provide a

slightly conservative estimate for collector-storage wall hybrid systems.

Figures 2.5.3 and 2.5.4 show plots of the f-Chart time distribution correction factor (ΔF_a) derived from TRNSYS simulations as a function of annual active solar fraction (F_a) and annual passive solar fraction (F_p) for active storage capacities of 314 and 157 KJ/C-m^2, respectively.

The time distribution correction factor is presented on an annual rather than monthly basis because it provides a slightly better estimate of the auxiliary energy requirement if applied on an annual basis. As presented, the correction factor should not be applied on a monthly basis as the monthly passive solar fraction could exceed the limits of the correction factor correlation ($F_p \leq 0.6$). If a monthly auxiliary estimate is necessary, the annual value of ΔF_a can be applied to the monthly active solar fractions to obtain approximate monthly auxiliary values. This does not give a strictly correct monthly distribution of auxiliary energy use, but the error appears to be less than the random error inherent in the f-Chart method.

The error in f-Chart predictions is larger for higher passive fractions and for smaller active storage capacities. This would be expected because both of these conditions would accentuate the problems associated with raising the active storage temperature during the day. The

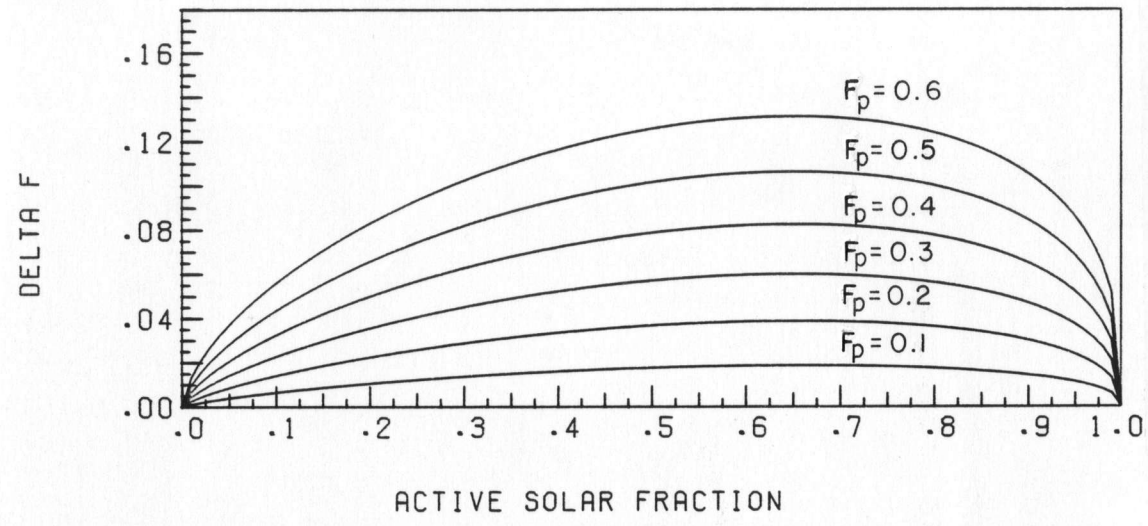

Figure 2.5.4 Active System Load Time Distribution Correction Factor for an Active System Storage Capacity of 157 KJ/C-m^2.

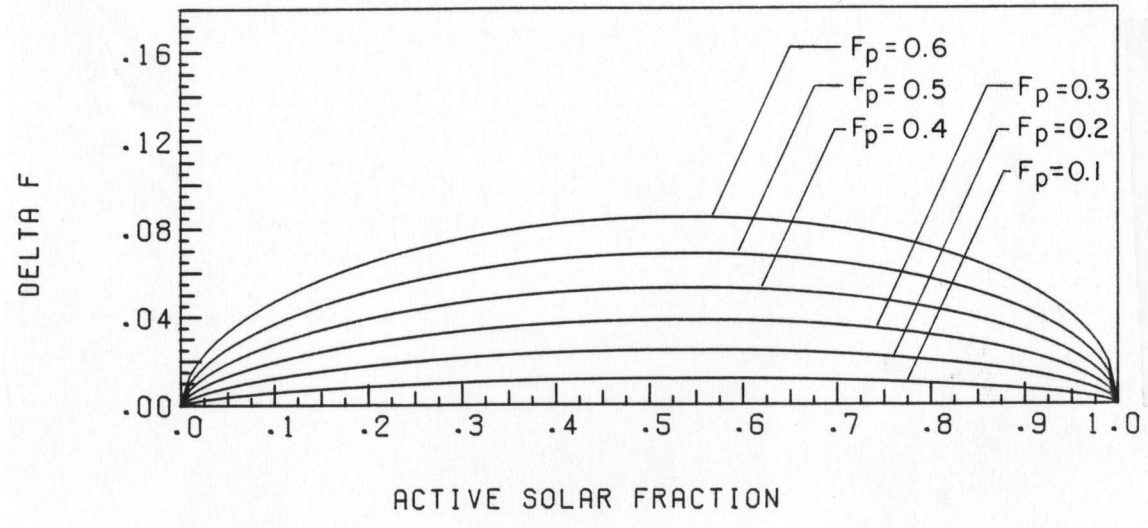

Figure 2.5.3 Active System Load Time Distribution Correction Factor for an Active System Storage Capacity of 314 KJ/C-m^2.

fact that the f-Chart prediction approaches the TRNSYS calculations at active solar fractions of 0% and 100% can also be deduced. At F_a equal to 0%, there is no interaction effect, and the correction factor should be zero. At 100% active solar fraction, the active system is so large relative to the load it must meet, that it supplies all of the necessary energy regardless of the minor interactions with the passive system.

The time distribution correction factor for collector-storage walls always had values less than the corresponding direct-gain values, but they could not be correlated because the effect of location was of the same magnitude as the f-Chart overprediction.

Curve fits for the information in Figures 2.5.3 and 2.5.4 are:

$$F_a = C_1 F_a^{C_2(2.8-F_p)} (1 - F_a)^{C_3(2.8-F_p)} F_p \qquad (2.5.1)$$

	Active Storage Capacity	
	314 KJ/C-m^2	157 KJ/C-m^2
C_1 =	0.287	0.410
C_2 =	0.246	0.285
C_3 =	0.216	0.154

This correction factor should be applied on an annual basis to the active solar fraction predicted by the f-Chart

methods, lowering the uncorrected solar fraction F_a to the value of F'_a as defined in Equation 2.5.2.

$$F_a' = F_a - \Delta F_a \qquad (2.5.2)$$

F_a' can then be used to obtain the auxiliary energy estimate, and does not require iteration. The time distribution correction factor should be used in conjunction with the load magnitude correction factor described previously as they are of similar magnitudes.

2.6 RESULTS

Figures 2.6.1 and 2.6.2 show a comparison of design method and simulation predictions of auxiliary energy use with and without the two hybrid correction factors for 23 examples in Bismark, ND, Caribou, ME, Columbia, MO, and New York, NY. For these plots, the SLR method (3,9) was used for the passive system analysis. The standard deviation of the error for the uncorrected predictions was 3.98 GJ (about 24% of the RMS average auxiliary). When the load magnitude and time distribution correction factors were applied, the standard deviation of the error was reduced to about 1.48 GJ (8.7% of the RMS auxiliary). If the Un-utilizability method is used for the passive calculations, the standard deviation of the error is reduced to 1.33 GJ (7.9%). Further reductions in the average error are

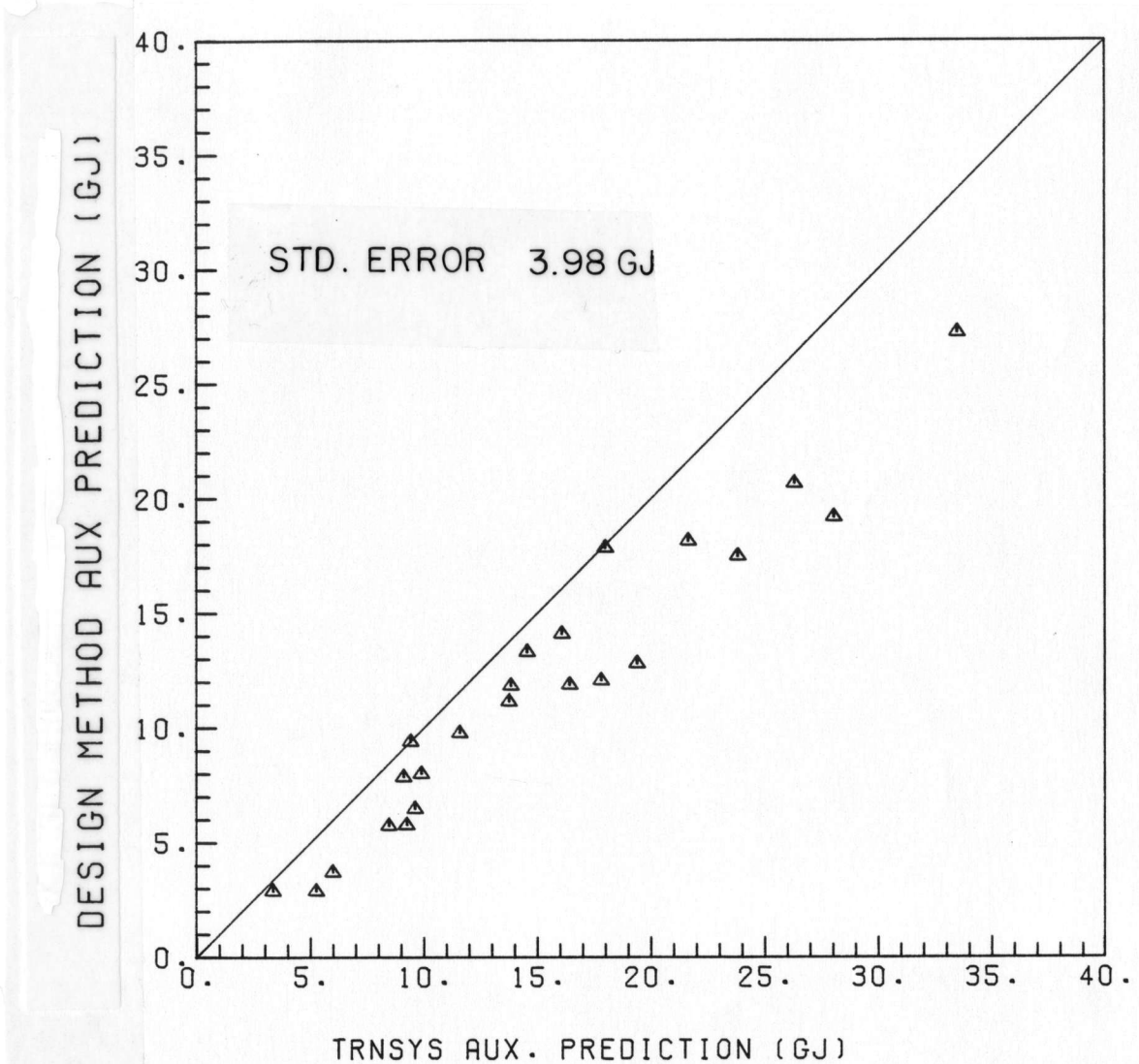

Figure 2.6.1 Uncorrected Design Method Predictions of Auxiliary Energy Use Compared to TRNSYS Simulation Results. The Locations are Caribou, ME, Bismarck, ND, Columbia, MO, and New York, NY.

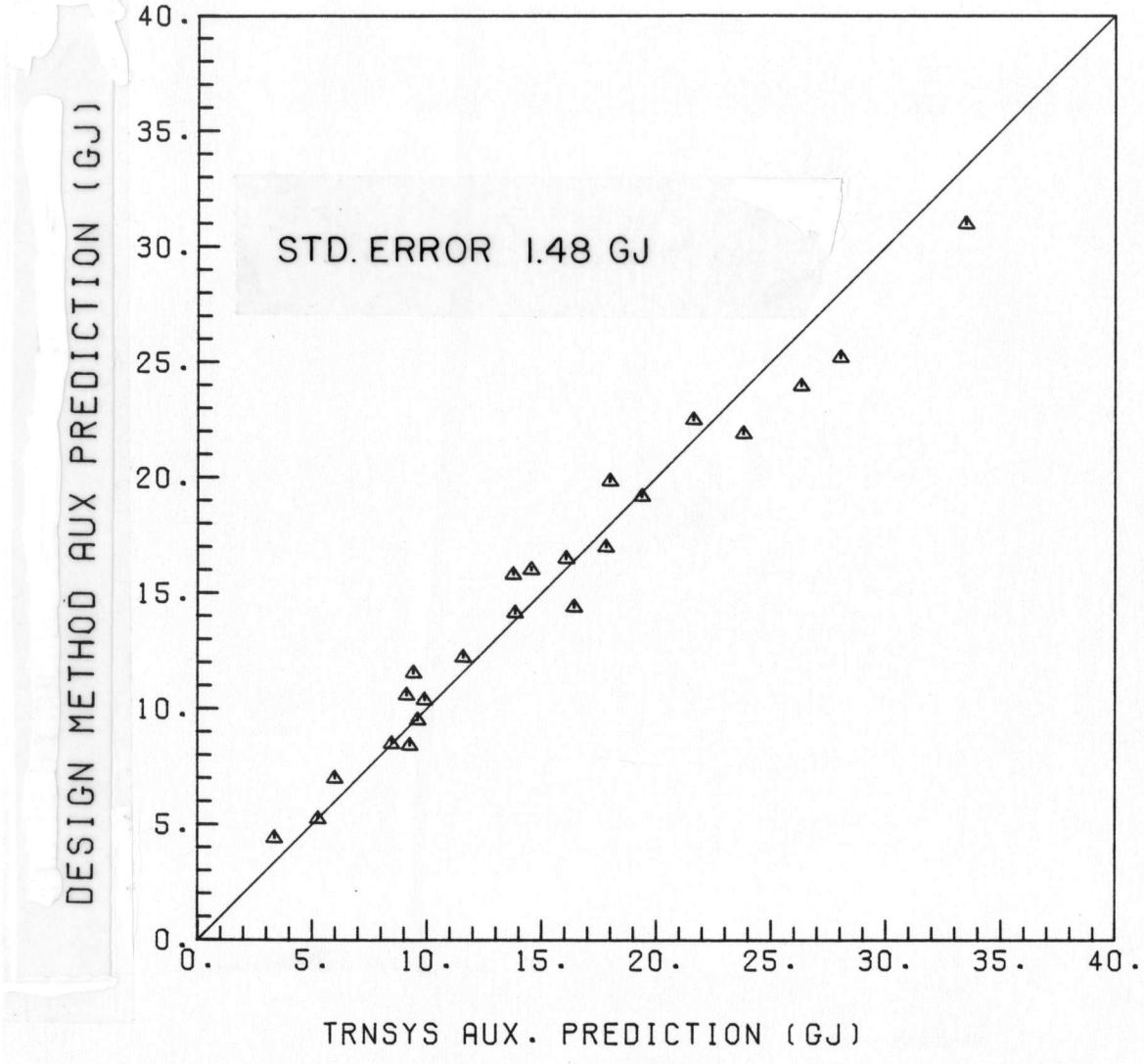

Figure 2.6.2 Design Method Predictions of Auxiliary Energy Use Using the Active System Load Magnitude and Time Distribution Correction Factors Compared to TRNSYS Simulation Results. The Locations are the same as in Figure 2.6.1.

unlikely, since a large portion of this remaining error is inherent in the passive and active design methods.

2.7 EXAMPLE

As an example of the use of the active system load and solar fraction correction factors, a direct-gain hybrid system located in Madison, WI will be analyzed. System parameters and meteorological data for January are given in Table 2.7.1.

Tilted surface radiation for both the active and passive systems was calculated using the method of Klein and Theilacker (13), with the monthly diffuse fraction estimated using the correlation developed by Erbs, et al. (14). The passive calculations were done using the Un-utilizability method (4) and are summarized in Table 2.7.2. The last column in Table 2.7.2 shows corresponding values from a TRNSYS simulation, giving an idea of the error associated with the passive design method for this system.

From these calculations, the active system load for zero active collector area (L_o) for January is 10.55 GJ. This value is used as a first approximation of the net load on the active system (L). Using the f-Chart method, the active solar fraction for January is found to be:

$$f_a = 0.444$$

The estimated auxiliary for January is

TABLE 2.7.1

EXAMPLE PROBLEM PARAMETERS

LOCATION: MADISON, WI LAT: 43.1°

SYSTEM DATA:

PASSIVE COMPONENTS

Collector area (direct gain)		40 m^2
U_{window}	Day	2.5 $W/m^2°C$
	Night	1.5 $W/m^2°C$
$(\overline{\tau\alpha})$		.7

ACTIVE COMPONENTS

Collector Area ($\beta = 60°$, $\gamma = 0°$)	40 m^2
$F_R(\tau\alpha)$	.7
$F_R(U_L)$	4.72 $W/m^2°C$
Storage Capacity (Water)	75 ℓ/m^2

BUILDING

UA (without passive window)	150 W/°C
Capacitance	17000 KJ/°C
Auxiliary Set Temperature	18°C
Active Set Temperature	19°C
Deadbands	2°C
Allowable Passive Swing Temperature	8°C

JANUARY DATA

$\overline{DD}$ = 819 °C-Days

$\overline{H}_{hor}$ = 5877 KJ/m^2-day

TABLE 2.7.2

PASSIVE SYSTEM ANALYSIS (UN-UTILIZABILITY METHOD)

	Building Losses	Window Losses	L_o	Solar Fraction	TRNSYS L_o
J	10.61 GJ	5.66 GJ	10.60 GJ	.001	9.91 GJ
F	8.70	4.64	7.66	.120	7.19
M	7.98	4.26	5.85	.267	6.03
A	3.73	1.99	1.73	.464	2.10
M	1.94	1.04	0.02	.990	0.76
S	1.13	0.61	0.00	1.00	0.16
O	3.12	1.67	1.19	.619	1.83
N	6.08	3.25	5.22	.142	5.48
D	8.73	4.65	9.13	-.050	9.19
	52.03	27.77	41.41	.204	42.59

$$Q_{aux} = (1 - f_a)(L_o) = 5.87 \text{ GJ}$$

Equation 2.4.8 is now used to correct the estimated load with

DD = 819 C-days; $f_p = 0.001$; $f_a = 0.444$, and the controller settings shown in Table 2.7.1

$$L/L_o = 1.039$$

$$L = 1.039(10.60) = 11.01 \text{ GJ}$$

The new value for L is then used to repeat the f-Chart calculations to obtain a more accurate monthly active system load. Using this load, the f-Chart method gives

$$f_a = 0.405$$

$$Q_{aux} = (1 - 0.405)(11.01) = 6.55 \text{ GJ}$$

A summary of the results for the nine heating-season months is shown in Table 2.7.3. The time distribution correction factor can then be applied to the annual active solar fraction. Using the annual passive solar fraction, F_p = 0.204, and the annual active solar fraction, F_a = 0.582, Equation 2.5.1 gives a ΔF_a value of 0.025. The actual active solar fraction F_a' can then be found

$$F_a' = 0.582 - 0.025 = 0.557$$

This gives an annual auxiliary energy use of

$$Q_{aux} = (1 - 0.557)(46.62) = 20.65 \text{ GJ}$$

TABLE 2.7.3

ACTIVE SYSTEM ANALYSIS (f-Chart METHOD)

	First Approximation			Second Approximation	
	f_a	DD	L/L_o	L	f_a
J	.444	819	1.039	11.01	.405
F	.676	672	1.074	8.22	.634
M	.878	616	1.139	6.66	.923
A	1.0	288	1.447	2.50	1.0
M	1.0	150	48.55	0.97	1.0
S	1.0	87	——	0.0	——
O	1.0	241	1.776	2.11	1.0
N	.581	469	1.100	5.74	.588
D	.304	673	1.031	9.41	.253
	.583			46.62	.582

TABLE 2.7.4

COMPARISON OF DESIGN METHOD AND SIMULATION RESULTS

	DESIGN METHOD		TRNSYS SIMULATION	
	L	Q_{AUX}	L	Q_{AUX}
J	11.01 Gj	6.55	10.18	6.59
F	8.22	3.01	7.68	3.46
M	6.66	.51	6.98	1.05
A	2.50	0.00	2.85	0.04
M	0.97	0.00	1.15	0.06
S	0.0	0.00	0.33	0.0
O	2.11	0.00	2.59	0.0
N	5.74	2.36	6.01	2.79
D	9.41	7.03	9.39	6.73
	46.52	19.46*	47.15	20.71

* Including the time distribution correction factor, the annual Design Method auxiliary prediction is 20.65 GJ.

Table 2.7.4 shows the design method results for active system loads and auxiliary energy, compared to detailed TRNSYS simulation results. On an annual basis, the design method active system load for this example is within 1.2% of the simulation results. The predicted annual auxiliary is within 1% of the simulation results.

2.8 CONCLUSIONS

A study of hybrid space heating systems has found that there are two major sources of systematic error associated with using existing design methods successively on the passive and active subsystems. The first is associated with the effect of the active system controller which increases the load on the active system as a function of controller parameters, active solar fraction and passive solar fraction. An analytical equation has been developed to correct the active system load predicted by a passive design method for the controller error.

The second systematic error is caused by the effect of the passive system on the time distribution of the active system load. An empirical correction factor for the f-Chart method has been developed to account for the effect of load distribution in a combined direct-gain,active hybrid system. In all cases, the direct-gain passive system will be the worst in terms of interfering with the active system in a way in which the f-Chart method cannot

predict. This interaction occcurs because the direct-gain competes directly with the active system during the day, resulting in higher collector inlet temperatures, and therefore lower collector efficiency. Collector-storage walls, on the other hand, offset the passive gains somewhat. The thicker the wall, the more the gains will be distributed and will more closely resemble a distributed load, thereby having less effect upon the active system. The time distribution correction factor will therefore give a conservative estimate of the active system performance in collector-storage wall hybrid systems.

In all cases, the error in f-Chart is relatively small and may be overshadowed by other uncertainties. Errors in such factors as passive system design calculations, load calculations, building capacitance, and meteorological data can give errors of a similar or larger magnitude.

CHAPTER 3 ACTIVE COLLECTION-PASSIVE STORAGE HYBRID SYSTEMS

3.1 INTRODUCTION

In this chapter, a design method is presented for the analysis of active collection-passive storage space heating systems. These systems use conventional active collectors with forced circulation of either air or liquid, but use only the capacitance of the building as the energy storage medium.

The design method for these systems is based on the concept of solar radiation utilizability (7) which has been used previously in estimating the thermal performance of active solar collectors by Klein and Beckman (7), and direct-gain passive systems by Monsen,et al. (4). These two methods are combined and modified to allow monthly performance calculations for active collection-passive storage systems. The modifications which are necessary to the methods in references (7) and (4) are of several types. The Utilizability method for active systems is modified to account for the variation in collector inlet temperature which results from allowing the building temperature to rise for energy storage purposes. The Un-utilizability method for direct-gain systems is modified to account for collector losses and the effect of collector efficiency on

the energy dumping critical radiation level. Modifications to the collector parameters to account for fluid flowrate, duct heat losses, and heat exchanger efficiencies are also needed. The combined method is compared to detailed simulations with the TRNSYS (1) transient simulation program for a variety of locations to verify that the design method predictions closely match the simulation results.

3.2 SYSTEM DESCRIPTION

Active solar space heating systems are ordinarily designed with an active storage component such as a water storage tank or a pebble bed. Storage is necessary for systems designed to meet a significant fraction of the load so that energy collected during a sunny day can be used at night or during a subsequent cloudy day. For certain applications however, such as retrofitting a solar system to an existing structure, it can be difficult to find an accessible location for a storage component. In addition, the storage component, along with the pipes (or ducts) and controls, can represent a substantial portion of the initial investment, providing an economic advantage for an active system which does not use active storage. An alternative to active storage is to use the mass of the building structure and furnishings to store energy (i.e., passive storage). In the systems considered here, a fluid,

generally air but possibly a liquid, is circulated through the collector bank when the incident radiation is sufficient to provide a useful energy gain. The energy collected is transferred to the building interior (using a heat exchanger if necessary) which offsets building energy losses. If the energy collected is greater than the instantaneous building energy losses, the excess energy is stored within the building by increasing the indoor temperature. The active collection-passive storage system is similar to a direct-gain passive solar system in this respect. Depending upon the effective building energy storage capacitance and the allowable indoor temperature swing, the use of passive storage may eliminate the need for an active storage component. Methods have been developed (6) to predict the performance of two specific configurations of active collection-passive storage systems. This chapter presents a more generalized design method for these types of systems.

3.3 SIMULATION MODEL FOR ACTIVE COLLECTION-PASSIVE STORAGE SYSTEMS

The TRNSYS 11.1 transient simulation program was used to model a building with capacitance, coupled to a collector bank. A special TRNSYS component, developed by Braun (15), was used. This component internally solves the combined collector-building energy balance, resulting in

much greater computational efficiency than could have been obtained by linking together standard TRNSYS components. The special component was compared to simulation results from an equivilent system composed of standard components and gave identical performance at approximately one-fourth of the computational cost.

The building-collector bank model assumes that the building has a one node (lumped) capacitance, specified by the user. The losses from the building are calculated using the product of the overall bulding energy loss coefficient, UA_b , and the inside to ambient temperature difference.

The collector model can represent either a liquid or air system, including a heat exchanger if necessary. The system is controlled such that any collectable solar energy is used in the building if it is needed. If the building temperature is greater than the maximum allowable temperature, the collectors are not turned on and cooling is added to maintain the indoor temperature at the upper set point.

The collector efficiency is modeled as being a linear function of the difference between the inlet and ambient temperatures divided by the total incident radiation. ASHRAE 93-77 collector test results can then be used for the intercept efficiency, $F_R(\tau\alpha)_n$, and the negative of the slope of efficiency versus $\Delta T/I_T$, $F_R U_L$. Incidence angle

modification can also be included.

3.4 THEORETICAL LIMITS OF PERFORMANCE

The upper and lower bounds of performance for active collection-passive storage systems can be defined by making assumptions about the effectiveness of the passive energy storage. If the energy storage capacity is assumed to be infinite, such as in a very massive building, all of the energy collected by the system will be usable and the auxiliary energy will be at a minimum compared to the same system with less effective storage. If the building has no energy storage capacity, (i.e., if the building temperature is not allowed to vary) only that amount of collected energy which can be used immediately to offset building energy losses is useful. Any collected energy which is in excess of the instantaneous heating load must be "dumped" from the building and will not offset auxiliary energy. Energy dumping can occur by forced ventilation or by turning the collector fluid circulator off during periods in which useful energy collection is possible. Zero energy storage capacity will therefore cause the auxiliary energy to be at a maximum. A real system will give performance somewhere between these two extremes, storing some fraction of the collected energy that is in excess of the instantaneous load.

The monthly average energy collected by the collectors will be the same for both zero and infinite storage capacity, but some of the energy will be dumped for the zero storage case. On a monthly basis, an energy balance on the collector array will give $Q_{c,a}$, the amount of useful energy that is collected.

$$Q_{c,a} = A_{c,a}\bar{H}_T N(F_R(\tau\alpha)_n)(F_R'/F_R)(\overline{\tau\alpha})/(\tau\alpha)_n \bar{\phi}_c \qquad (3.4.1)$$

$A_{c,a}$ is the active collector area; $\bar{H}_T$ is the monthly average daily radiation incident on the collector; N is the number of days per month; $F_R(\tau\alpha)_n$ is the intercept value from the ASHRAE 93-77 collector test; and $(\overline{\tau\alpha})/(\tau\alpha)_n$ is the ratio of monthly average to normal incidence transmittance-absorptance products (7). F_R'/F_R is the collector-heat exchanger penalty factor (deWinter) which is one for systems with air heaters which do not require a heat exchanger (7). An algorithm for calculating the collector-heat exchanger penalty factor, as well as pipe or duct loss and flow rate modifications to the collector parameters are given in Appendix A.

$\bar{\phi}_c$ is the monthly collector utilizability factor which is the fraction of the energy incident on the collector that is not lost to the environment as collector losses. $\bar{\phi}_c$ is a nonlinear function of the collector critical radiation

level, $I_{c,c}$, and can be calculated by methods given in Appendix B. The critical radiation level is the radiation level below which there is no useful energy. It is given by

$$I_{c,c} = F_R'U_L(\bar{T}_i - \bar{T}_a)/F_R'(\overline{\tau\alpha}) \qquad (3.4.2)$$

where F_RU_L is the negative of the slope of the ASHRAE 93-77 collector test, $\bar{T}_i$ is the monthly average collector fluid inlet temperature, and $\bar{T}_a$ is the monthly average ambient temperature. $I_{c,c}$ is shown in Figure 3.4.1. If the radiation level is below $I_{c,c}$, then the collectors (if operated) will lose more energy than they absorb. If the radiation level is greater than $I_{c,c}$, a net energy gain is possible. In an active collection-passive storage system, air from the building interior is circulated through the collectors (or collector heat exchanger). Thus, the monthly-average collector fluid inlet temperature, $\bar{T}_i$ is the average building indoor air temperature and assumed to be constant over the month. This assumption is exact for the zero and infinite storage capacity limits since in either case, the building air temperature is constant. For a finite capacity building, this assumption is not strictly true, because as the building stores energy the indoor temperature and therefore the collector inlet temperature will increase. This increase in temperature does

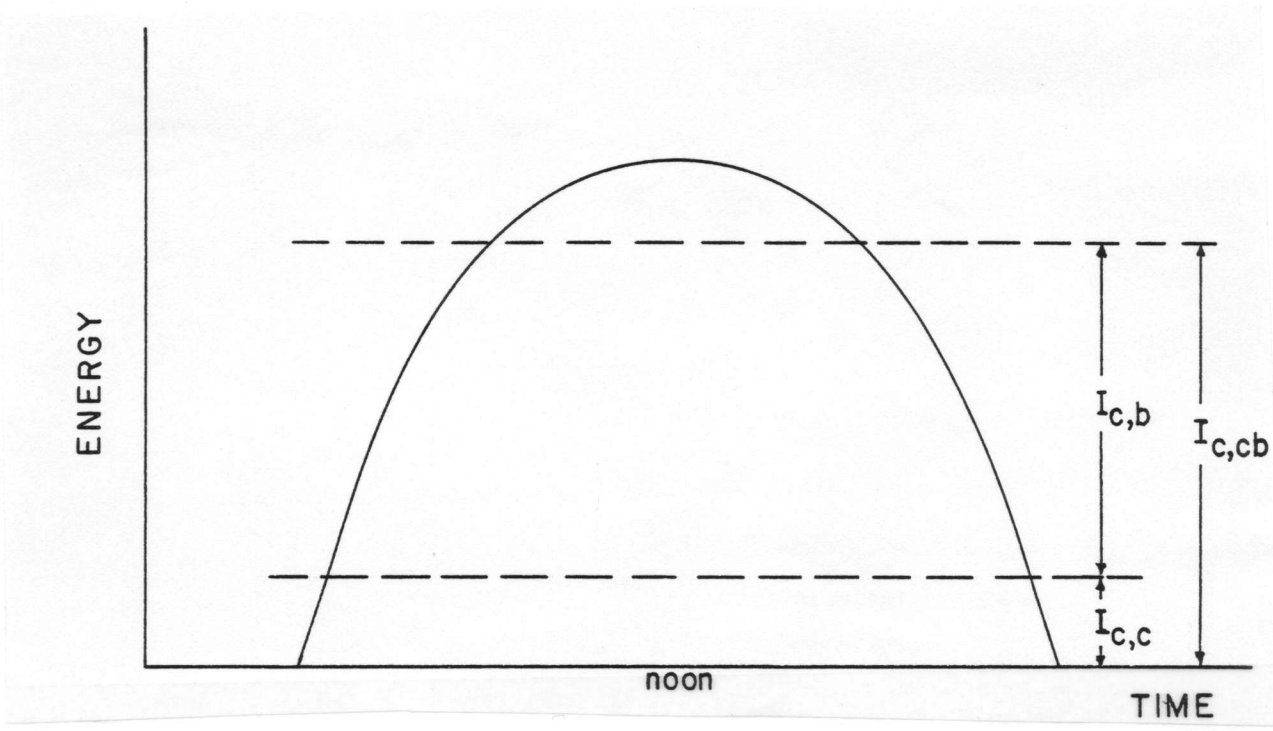

Figure 3.4.1 Collector and Building Critical Radiation Levels Compared to a Plot of Solar Radiation For a Typical Day.

significantly affect system performance as shown in section 3.5.

The auxiliary energy required by the infinite storage limit can be calculated using the total heating load for the month, L, and the collected solar energy.

$$Q_{aux,i} = (L - Q_c)^+ \qquad (3.4.3)$$

where the + superscript indicates that only positive values of auxiliary energy are considered (monthly carryover is not allowed). The monthly solar fraction can be calculated from the auxiliary energy and the load:

$$f_{a,i} = 1 - Q_{aux,i}/L = Q_c/L \qquad (3.4.4)$$

The auxiliary energy required by the zero storage case is somewhat more complicated, as some of the collected energy must be dumped. The amount of radiation which is just necessary to meet the building heating load, called the building critical radiation level, $I_{c,b}$, is a function of the building total energy loss coefficient, UA_b; the average ambient and indoor temperatures; and the product of the collector area and $F_R'(\overline{\tau\alpha})$.

$$I_{c,b} = UA_b(T_b - \overline{T}_a)/A_{c,a}F_R'(\overline{\tau\alpha}) \qquad (3.4.5)$$

$I_{c,b}$ is the monthly average radiation level that would be necessary to meet the heating load if there were no losses from the collectors. Collector losses are characterized by the collector critical level $I_{c,c}$. As a result, the total amount of radiation incident on the collectors that is necessary to meet the heating load is $I_{c,cb}$ where

$$I_{c,cb} = I_{c,c} + I_{c,b} \tag{3.4.6}$$

Figure 3.4.1 also shows $I_{c,b}$ and $I_{c,cb}$ in relation to $I_{c,c}$. For buildings with zero energy storage capacity, any radiation above $I_{c,cb}$ must be dumped, and this unutilizable fraction of the incident radiation can be calculated using utilizability factors.

$$Q_{dump} = A_{c,a}\bar{H}_T F_R'(\overline{\tau\alpha})N\bar{\phi}_{cb} \tag{3.4.7}$$

The auxiliary energy and solar fraction for the zero storage case can then be written:

$$Q_{aux,z} = (L - (Q_c - Q_{dump}))^+ \tag{3.4.8}$$

$$f_{a,z} = 1 - Q_{aux,z}/L = (Q_c - Q_{dump})/L \tag{3.4.9}$$

This has been shown by Erbs (16) to be in close agreement for the zero storage case.

3.5 PERFORMANCE OF SYSTEMS WITH FINITE STORAGE CAPACITY

The analysis presented above is very similar to the analysis of direct-gain passive space heating systems done by Monsen, et al. (4,5). For direct-gain systems with finite energy storage capacity, Monsen correlated f, the fraction of the load supplied by solar energy, to the solar to load ratio (X), the storage to dump ratio (Y), and the utilizability factor based on the building critical level. Monsen's correlation can be used for active collection-passive storage systems provided that a number of changes are made to correctly model the physics of the active-passive system.

First, the solar to load ratio must be modified to account for collector performance. From Monsen, the solar-load ratio (X) is defined:

$$X = A_{c,a}\bar{H}_T N(\overline{\tau\alpha})/L \qquad (3.5.1)$$

The modification necessary to X to make it suitable for active-passive systems is to replace the transmittance-absorptance product with the collector parameter $F_R'(\overline{\tau\alpha})$. The solar to load ratio can then be written

$$X = A_{c,a}\bar{H}_T N F_R'(\overline{\tau\alpha})/L \qquad (3.5.2)$$

The storage to dump ratio, Y, must also be redefined. The passive energy storage capacity, $Q_{s,p}$, remains the same, being defined as the product of effective building capacitance (C) and the allowable indoor temperature swing (ΔT_s)

$$Q_{s,p} = C\Delta T_s \tag{3.5.3}$$

The denominator of the storage-dump ratio is the amount of energy which would be dumped from a building with zero energy storage capacity, defined in Equation 3.4.7.

The storage to dump ratio can therefore be written:

$$Y = (C\Delta T_s N)/A_{c,a}\bar{H}_T F_R'(\overline{\tau\alpha})\, N\bar{\phi}_{cb} \tag{3.5.4}$$

Monsen correlated the solar to load ratio and the storage to dump ratio along with the un-utilizabiltiy factor for the zero energy storage case to obtain the following equation to predict solar fractions for direct-gain passive systems with finite energy storage capacity.

$$f = PX + (1 - P)(3.082 - 3.142\bar{\phi}_b)\,(1 - \exp(-0.329X)) \tag{3.5.5}$$

where

$$P = (1 - \exp(-0.294Y))^{0.652} \qquad (3.5.6)$$

Monsen's correlation can be generalized to include active collection-passive storage systems by including the collector utilizability factor, $\overline{\phi}_c$, in the first term of Equation 3.5.5, and by replacing the building un-utilizability factor with a system un-utilizability factor, $\overline{\phi}_u$, defined below. $\overline{\phi}_u$ is composed of the energy lost from the collectors, $(1-\overline{\phi}_c)$, and the amount dumped from the building, $\overline{\phi}_{cb}$. The equation for P remains the same.

$$\overline{\phi}_u = 1 - \overline{\phi}_c + \overline{\phi}_{cb} \qquad (3.5.7)$$

$$f_a = PX\overline{\phi}_c + (1 - P)(3.082 - 3.142\overline{\phi}_u)$$
$$(1 - \exp(-0.329X)) \qquad (3.5.8)$$

These modifications are necessary for Equation 3.5.8 to reduce down to the limits of infinite and zero energy storage. For infinite energy storage, P equals unity, causing the second term of Equation 3.5.8 to drop out and the solar fraction becomes $X\overline{\phi}_c$. This can be rewritten as Q_c/L which is equivalent to Equation 3.4.4. Equation 3.5.8 approximately reduces to the zero energy storage case for small values of X. In this case, P equals zero and the first term of Equation 3.5.8 drops out. The exponent in the second term can be expanded in a power series, and for

small values of X, the higher terms can be ignored. For this case, the solar fraction can be written (8):

$$f_a = (1.032 - 1.034\overline{\phi}_u)X$$
$$\simeq (\overline{\phi}_c - \overline{\phi}_{cb})X = (Q_c - Q_{dump})/L \qquad (3.5.9)$$

This is the zero capacitance limit derived in Equation 3.4.9. This more generalized version of Monsen's correlation can be reduced to the original equation for a direct-gain passive system. In a direct-gain system, the collector critical level is zero (i.e., all energy entering the window is collected), giving a collector utilizability of unity. The system un-utilizability factor therefore equals $\overline{\phi}_{cb}$ which is equal to the building un-utilizability factor for a collector critical level of zero. Similarly, the storage to dump and solar to load ratios defined for the active-passive system will reduce to the direct-gain case as F_R' will be unity and $\overline{\phi}_{cb}$ will equal $\overline{\phi}_b$.

The previous analysis is based on a constant collector inlet temperature equal to the auxiliary set temperature. For a building with finite capacity , the actual building temperature will be greater than the set temperature whenever solar energy is stored in the building mass. The increase in building temperature can be approximated by assuming that the average building temperature when the solar system is operating is higher than the auxiliary set

temperature by one half of the allowable temperature swing. The fraction of the time that the solar system is operating is assumed to be linearly proportional to the solar fraction, leading to a linear relationship between monthly average building temperature and solar fraction:

$$\overline{T}_b = T_{set,aux} + 0.5(\Delta T_s)f_a \qquad (3.5.10)$$

This relationship is analogous to the relationship derived in Chapter 2 for active-passive combined systems. In this case however, the average building temperature is much more approximate as active collection-passive storage systems have less precise controls. On some days, the building may never reach the maximum allowable temperature, causing the average temperature to be lower than $\overline{T}_b$. In other cases, the building temperature may stay at the maximum for an extended period, increasing the average temperature.

Figure 3.5.1 shows a plot of predicted monthly average building temperatures versus the values for the corresponding TRNSYS simulations. The standard deviation for this method of approximating the average building temperatures was 1.1 C. A large portion of the error was due to months in which conduction gains increased the average building temperature. These can be seen in Figure 3.5.1 as the horizontal line across the center of the graph, and are not accounted for in this simplified

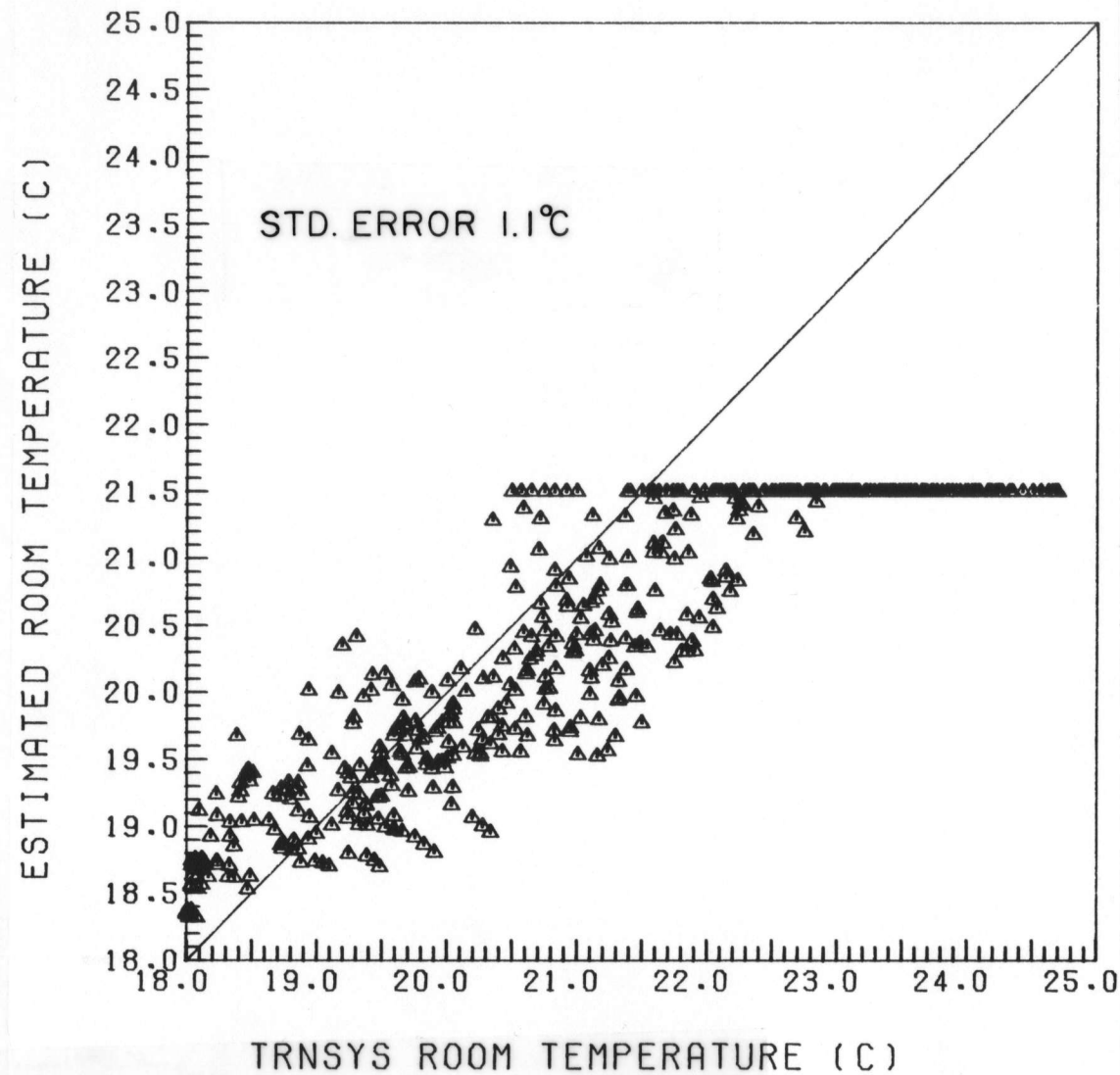

Figure 3.5.1 Comparison of Estimated Monthly Average Building Temperatures with TRNSYS Simulation Results. The Points are for Madison, WI, Albequerque, NM, and Boston, MA.

TABLE 3.5.1

RANGE OF PARAMETERS INVESTIGATED FOR

ACTIVE COLLECTION-PASSIVE STORAGE SYSTEMS

LOCATIONS	Madison, WI Albuquerque, NM Boston, MA Bismarck, ND
SYSTEM PARAMETERS	
Collector Area	0-150 m^2
$F_R'(\overline{\tau\alpha})$	0.5-0.8
$F_R'U_L$	2.5-4.5 W/C-m^2
Collector Slope	30-90
Collector Azimuth	$\pm$30
BUILDING PARAMETERS	
Effective Capacitance	0.4-200 MJ/C
Allowable Temperature Swing	0-11 C
UA_b	80-420 W/C

approach. Use of the collector inlet temperature modification requires an iterative procedure similar to that outlined in Section 2.4.

The generalized correlation was compared with detailed simulation results using the TRNSYS 11.1 (1) simulation program, both with and without the inlet temperature modification. Four locations and a wide range of system parameters were tested to ensure that the correlation was valid for active collection-passive storage systems. Table 3.5.1. gives the range of parameters for which the simulation and correlation results were compared. Figure 3.5.2 shows a plot of the simulation results and correlation predictions of annual auxiliary energy use for 228 years of simulations in Madison, Albuquerque, Boston, and Bismarck, for the design method without inlet temperature modification. The correlation had a standard deviation of 1.48 GJ for these examples. If the collector inlet temperature is modified to account for the increase in building temperature, the standard deviation is reduced only to 1.46 GJ, indicating that the effect of assuming constant building temperature equal to the auxiliary set temperature is minimal.

3.6 DISCUSSION

There are a number of differences which can be observed between space heating systems with active storage

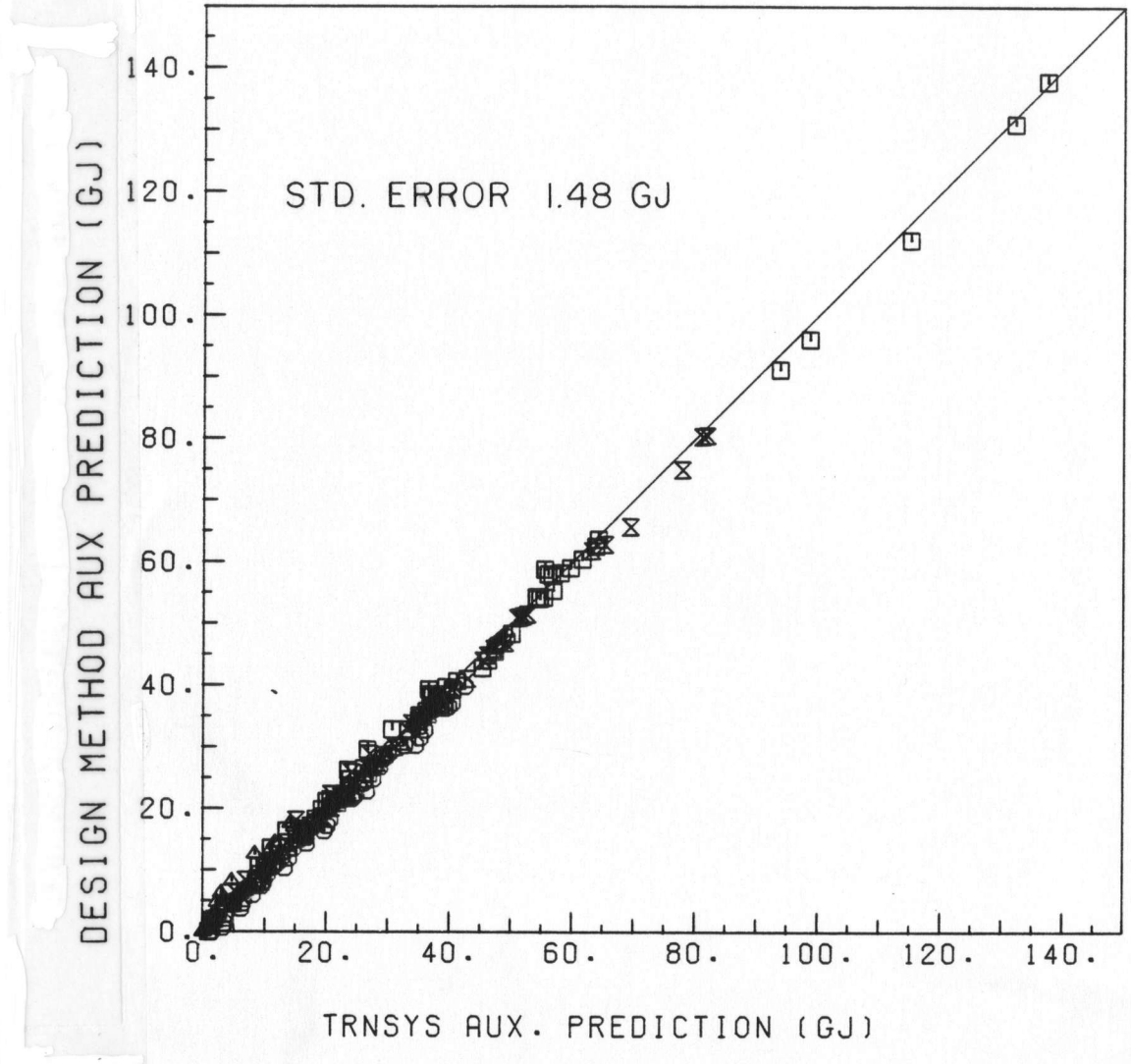

Figure 3.5.2 Comparison of Simulation and Design Method Predictions of Auxiliary Energy Use in Active Collection-Passive Storage Buildings.

and passive storage. These differences can be easily and quickly explored using the design method previously described for active systems with passive storage, and using the f-Chart method (2) for conventional active systems. The following comparisons were all done using these two design methods.

The first comparison concerns the point at which active storage will provide significantly better performance than passive storage for otherwise identical systems. The storage capacity of an active system is usually chosen in proportion to the collector area. A typical capacity is 350 KJ/C per square meter of collector area (7). In this case, as the collector area is increased, the storage capacity also increases and the system can meet a higher fraction of the load. Active collection-passive storage systems, however, have a fixed amount of storage capacity for a given building. As the collector area is increased for these systems, storage capacity becomes the limiting factor and the solar fraction becomes nearly constant at large collector areas. Figure 3.6.1 shows this effect in a plot of solar fraction versus collector area for a system with active storage and a system with passive storage in Madison, WI. For the systems shown in Figure 3.6.1 there is no difference in performance until the collector area becomes greater than about $25m^2$. The collector area at which the difference

becomes significant can best be characterized by the ratio of the active storage capacity to passive storage capacity. The amount of active storage capacity, $Q_{s,a}$, for this ratio can be approximated by assuming that there is a 75 degree Celsius allowable temperature swing in the active storage device:

$$Q_{s,a} = A_{c,a}(mC_p)_s 75 \qquad (3.6.1)$$

$A_{c,a}$ is the collector area and $(mC_p)_s$ is the amount of energy storage capacity per unit of collector area per degree Celsius of temperature difference. The passive storage capacity has been previously expressed in Equation 3.5.3. If Figure 3.6.1 is replotted as the difference between the active and passive solar fractions, $F_{a,p}$, versus the ratio of active to passive storage, $Q_{s,p}/Q_{s,a}$, general guidelines can be found for determining when active storage is not necessary. Figure 3.6.2 shows a plot of $F_{a,p}$ versus $Q_{s,p}/Q_{s,a}$ for a wide range of systems in Albuquerque, NM, Madison, WI and Boston, MA. A difference in solar fraction of 5% was chosen as a criterion for the purpose of determining when the active storage began to significantly outperform the passive storage. The standard active systems used in the comparison of Figure 3.6.2 were all based on the f-Chart standard storage capacity of 350 KJ/Cm^2 for $(mC_p)_s$, and some variation from this data will

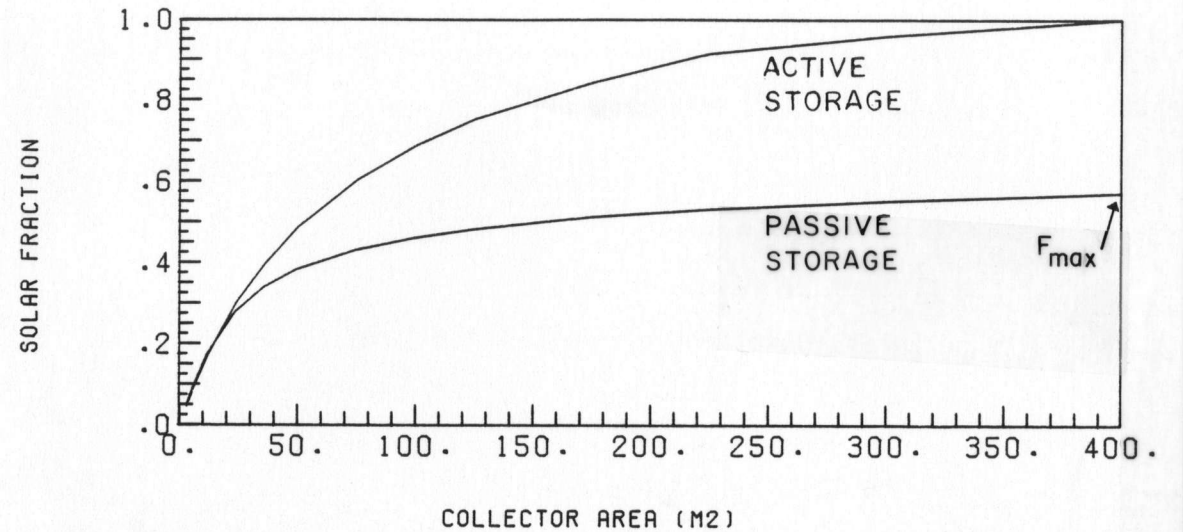

Figure 3.6.1 Solar Fraction Plotted as a Function of Collector Area for Two Similar Systems Located in Madison, WI.

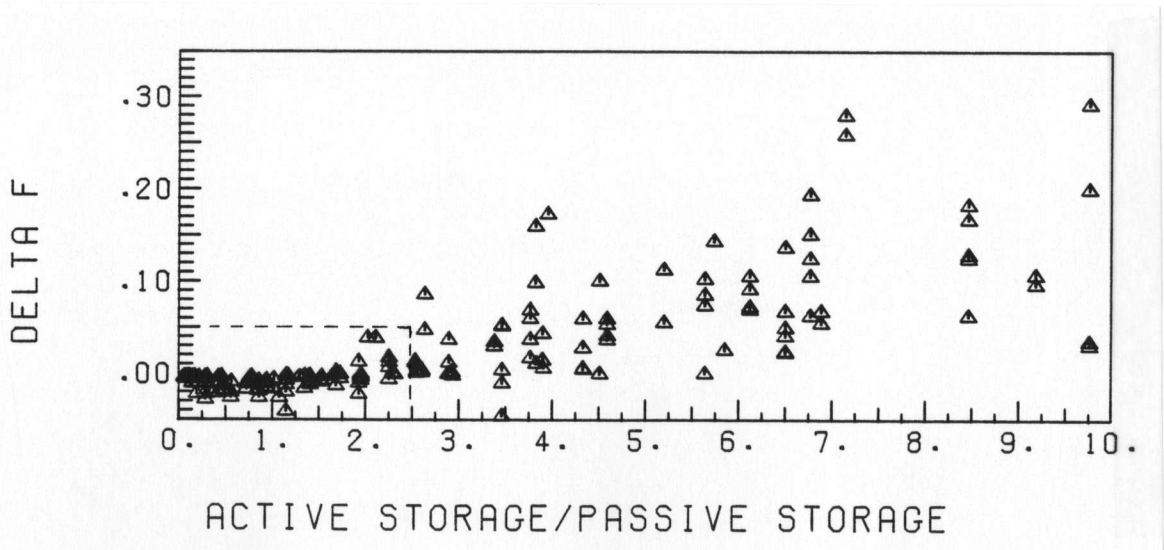

Figure 3.6.2 Difference in Performance Between Systems with Active Storage and Passive Storage. The Dotted Lines Indicate the $Q_{s,a}/Q_{s,p}$ Ratio at Which Some Active Storage Systems Begin to Outperform Passive Storage Systems by More Than 5%.

occur for other active storage sizes. Figure 3.6.2 indicates that active storage will not give any improvement in performance over passive storage if the active storage capacity is less than 2.5 times the potential passive storage capacity. For values of $Q_{s,p}/Q_{s,a}$ greater than 2.5, a passive storage system may or may not perform to within 5% of a similar system with active storage. Systems which fall into this category should be analyzed using the design method described in this chapter and the f-Chart method to determine if there is any advantage of active storage over passive storage. An economic analysis can then be used to determine if the active storage component is cost effective.

The second important difference between systems with active and passive storage is that for passive storage systems, the solar fraction is limited by the fixed amount of storage offered by the building mass. The maximum solar fraction for the system with passive storage shown in Figure 3.6.1 is indicated by F_{max}. The maximum attainable solar fraction for active collection-passive storage systems can be generally correlated on an annual basis as a function of the passive storage capacity per m^2 of floor area, $Q'_{s,p}$, and the yearly heating load per m^2 of floor area, L':

$$F_{max} = 0.655(Q'_{s,p}/L')^{0.36} \qquad (3.6.2)$$

This correlation was developed from data for nine locations and will give F_{max} to within $\pm 6\%$ for a 90% confidence interval compared to the design method. F_{max} is of interest because it can very quickly give an indication of the limit of solar contribution. Figures 3.6.3-3.6.6 are plots of F_{max} versus L' for light, medium, and heavy construction. The National Research Council of Canada (17) has defined a quick (and rough) link between values of $Q_{s,p}'$ and building construction, shown in Table 3.6.1. The L' values used to generate Figures 3.6.3-3.6.6 were designed to bracket the possible ranges of building insulation levels, from uninsulated (R-10 ceiling; R-5 walls; R-0 slab perimeter) to very well insulated (R-60 ceiling; R-30 walls; R-10 slab perimeter).

The value of F_{max} given by Figures 3.6.3-3.6.6 or Equation 3.6.2 is the limit of active-passive performance and cannot be obtained except at very large collector areas. It does however, give an indication of how building construction (both interior mass and exterior insulation) as well as the allowable indoor temperature swing can affect the performance of active-passive systems.

3.7 EXAMPLE

Consider a solar space heating system with active collectors and passive energy storage with the system

TABLE 3.6.1

EFFECTIVE BUILDING STORAGE CAPACITY FOR TYPICAL CONSTRUCTION (FROM REF. 17)

	Thermal Capacity MJ/ Km^2 Floor Area	Description
Light	0.060	Standard frame construction, 12.7 mm gyproc walls and ceilings, carpet over wooden floor.
Medium	0.153	As above, but 50.8 mm gyproc walls and 25.4 mm gyproc ceiling.
Heavy	0.415	Interior wall finish of 101.6 mm brick, 12.7 mm, gyproc ceiling, carpet over wooden floor.
Very heavy	0.810	Very heavy commercial office building 304.8 mm concrete floor.

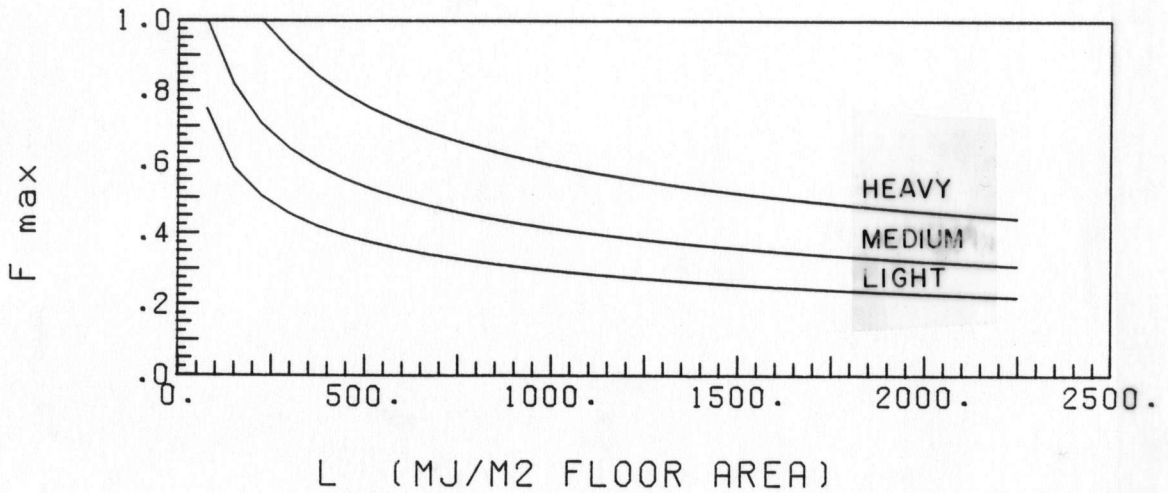

Figure 3.6.3 Maximum Attainable Solar Fraction For Active Collection-Passive Storage Systems Plotted as a Function of Annual Heat Loss Per Square Meter of Floor Area and Building Construction Weight for an Allowable Indoor Temperature Swing of 5 C.

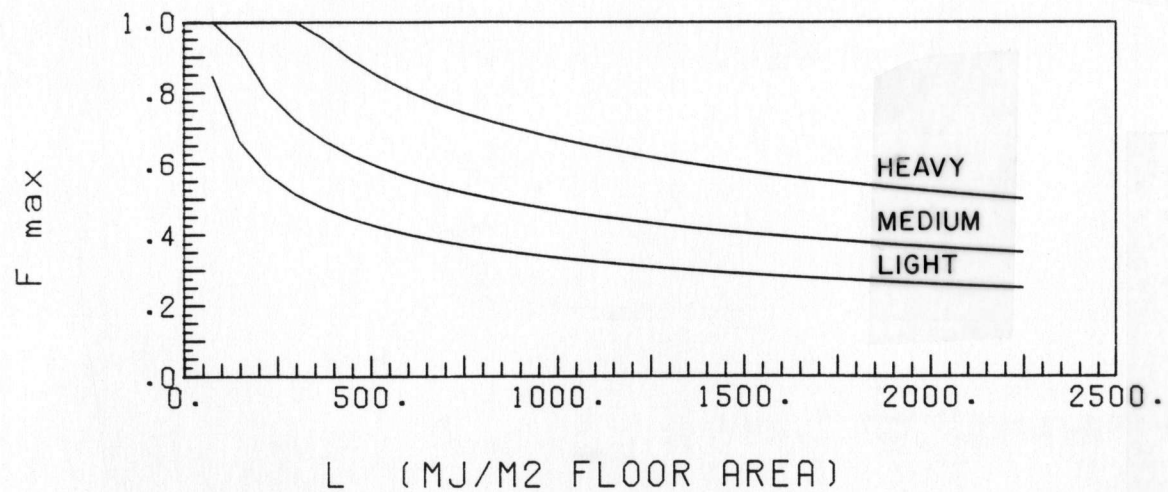

Figure 3.6.4 Maximum Attainable Solar Fraction For Active Collection-Passive Storage Systems Plotted as a Function of Annual Heat Loss Per Square Meter of Floor Area and Building Construction Weight for an Allowable Indoor Temperature Swing of 7 C.

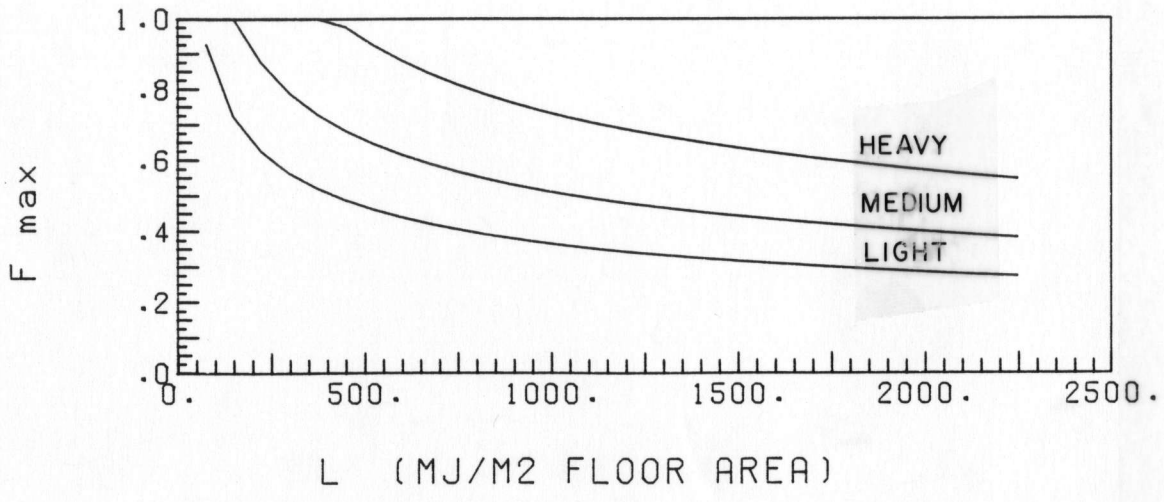

Figure 3.6.5 Maximum Attainable Solar Fraction For Active Collection-Passive Storage Systems Plotted as a Function of Annual Heat Loss Per Square Meter of Floor Area and Building Construction Weight for an Allowable Indoor Temperature Swing of 9 C.

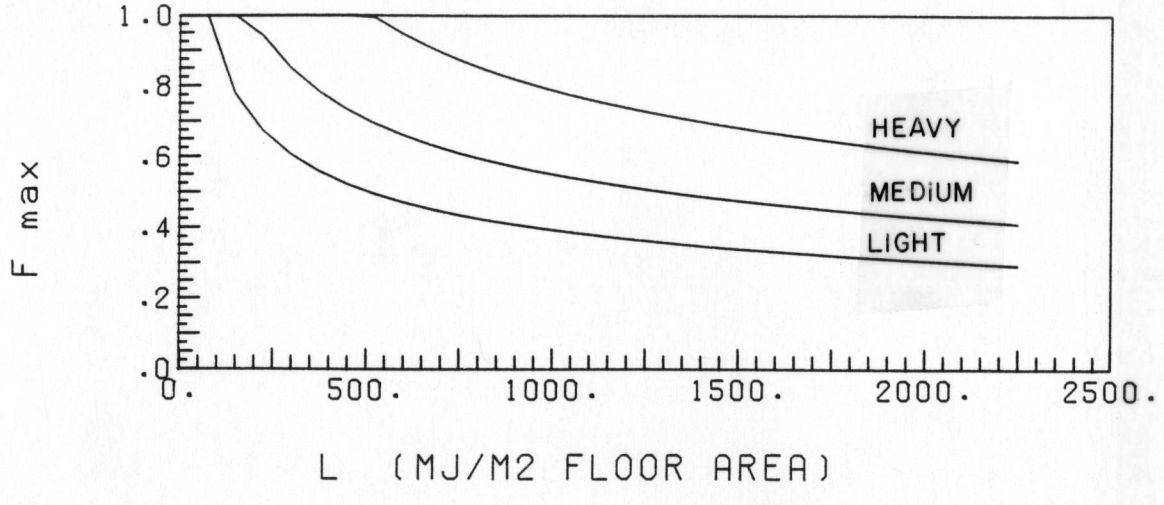

Figure 3.6.6 Maximum Attainable Solar Fraction For Active Collection-Passive Storage Systems Plotted as a Function of Annual Heat Loss Per Square Meter of Floor Area and Building Construction Weight for an Allowable Indoor Temperature Swing of 11 C.

parameters shown in Table 3.7.1, located in Madison, WI. Tilted surface radiation was calculated using the method of Klein (13), with the monthly diffuse fraction estimated using the correlation developed by Erbs, et al. (14). Weather data used in this example are the monthly average values for the typical meteorological year data (18) used in the TRNSYS simulations, and therefore will differ slightly from published monthly average weather data (7,19).

The monthly heating load for the building can be calculated using the monthly degree-days and the building energy loss coefficient. For January, the heating load is

$$L = 210\ W/C(86400\ S/DAY)(818.5\ C\text{-}DAYS) = 14.85\ GJ$$

The remaining monthly heating loads are summarized in Table 3.7.2 for the nine heating months. The solar to load ratio for January is found by using Equation 3.5.2:

$$X = 25(1.06 \times 10^{7})(31)(.51)/14.85 \times 10^{9} = .282$$

The storage to dump ratio requires the passive energy storage capacity of the building and the un-utilizability factor for the energy dumped from the house. The energy storage capacity is constant for all months:

$$Q_{s,p} = 27.54x10^{6} \text{ J/C(7 C)} = 0.193 \text{ GJ/DAY}$$

The house dumping un-utilizability factor is a function of $I_{c,cb}$ (Equation 3.4.6) and is found using the method of Klein (20). For January:

$$I_{c,c} = 3.1(18-(-8.4))/0.51 = 160.5 \text{ W/m}^2$$

$$I_{c,b} = 210(18-(-8.4))/25(0.51) = 434.8 \text{ W/m}^2$$

$$I_{c,cb} = 160.5 + 434.8 = 593.3 \text{ W/m}^2$$

$$\overline{\phi}_{cb} = 0.134$$

The storage to dump ratio for January is (using Equation 3.5.4):

$$1.928x10^{8}(31)/\{25(1.06x10^{7})(0.51)(31)(0.134)\} = 10.73$$

The solar fraction can then be estimated using Equations 3.5.6, 3.5.7 and 3.5.8, where $\overline{\phi}_c$ is found from $I_{c,c}$.

$$\overline{\phi}_c = 0.633$$

$$\overline{\phi}_u = 1-0.633 + 0.134 = 0.501$$

$$P = (1-\exp(-0.294(10.73)))^{0.652} = 0.972$$

$$F = 0.972(0.282)(0.633) + (1-0.972)(3.082-3.142(0.501)) (1-\exp(-0.329(.292))) = 0.18$$

The auxiliary energy required for January is:

$$Q_{aux} = (1-0.18)14.85 = 12.23 \text{ GJ}$$

The solar fractions and auxiliary energy estimates are summarized in Table 3.7.2. Simulation results for the same system are shown in the last two columns of Table 3.7.2 for comparison. For this example, the design method under predicted by 1.26 GJ, which is within 2.5% of the simulation results.

The general rules presented in the discussion section can determine the performance of an active-passive system relative to a typical active system with 350 KJ/C-m^2 of active storage.

The total amount of active storage for an equivalent system is found using Equation 3.6.1:

$$Q_{s,a} = 25m^2(350 \text{ J/C-m}^2\text{x}10^3)75 \text{ C} = 6.56\text{x}10^8 \text{ J/DAY}$$

The ratio of active to passive storage is:

TABLE 3.7.1

PARAMETERS FOR EXAMPLE PROBLEM

Collector Area	$25m^2$
$F_R'U_L$	$3.1\ W/m^2°C$
$F_R'(\tau\alpha)$	.51
Collector Slope	60°
Collector Azimuth	0°
Floor Area	$180m^2$
Building UA	210 W/°C
Effective Capacitance (Med. Const.)	27,540 KJ/°C
Auxiliary Set Temperature	18°C
Allowable Temperature Swing	7°C

TABLE 3.7.2

SUMMARY OF EXAMPLE PROBLEM

Month	Heating Load	Design Method SF	Design Method Q_{aux}	TRNSYS SF	TRNSYS Q_{aux}
Jan	14.85 GJ	0.18	12.23 GJ	0.17	12.39 GJ
Feb	12.18	0.26	9.02	0.24	9.22
Mar	11.17	0.37	7.04	0.41	6.62
Apr	5.22	0.64	1.87	0.62	1.97
May	2.72	1.00	0.00	0.71	.80
Sep	1.59	1.00	0.00	0.97	.05
Oct	4.37	0.71	1.28	0.65	1.52
Nov	8.51	0.28	6.12	0.28	6.16
Dec	12.21	0.15	10.37	0.14	10.49
	72.84 GJ	0.34	47.94 GJ	0.33	49.20 GJ

$$Q_{s,a}/Q_{s,p} = 6.56x10^{8}/1.928x10^{8} = 3.4$$

This value is in the range (greater than 2.5) where it is necessary to use a design method for the active system to determine the relative performance. This was done using the computer program F-CHART 3.0 (10), and gave the results shown below (monthly solar fractions):

	Active-Passive	Typical Active
Jan	0.18	0.19
Feb	0.26	0.29
Mar	0.37	0.42
Apr	0.64	0.69
May	1.00	1.00
Sep	1.00	1.00
Oct	0.71	0.74
Nov	0.28	0.26
Dec	0.15	0.14
Yr	0.34	0.38

Active storage in this case gives an increase in performance of about four percentage points on an annual basis.

Another question of interest is to find the maximum attainable solar fraction for this active collection-passive storage system. The yearly load per square meter of floor area is 404.7 MJ/m^2 , and the building is of medium weight construction. Figure 3.6.4 can then be used to find the maximum solar fraction for an allowable

temperature swing of 7 C :

$$F_{max} = 0.63$$

If the allowable temperature swing had been something other than 5, 7, 9, or 11 C, Equation 3.6.2 could have been used to find the maximum solar fraction.

The example system performs well below the maximum solar fraction, therefore improved performance could be expected with increased collector area. If the collector area is increased to $35m^2$ the annual solar fraction will increase to 0.40. Whether this increase in performance is worth the extra $10m^2$ of collector must be determined through an economic analysis. Generally, if the solar fraction for a system is two-thirds to three-quarters of the maximum solar fraction, performance will increase very slowly with increasing collector area.

3.8 CONCLUSIONS

Space heating systems with active collectors which use the building mass as the energy storage medium can be analyzed using the concept of monthly average utilizability. The upper and lower bounds of performance for these active-passive systems can be found by assuming that the passive energy storage capacity is infinite and zero respectively. Modifications to Monsen's un-

utilizability design method for direct-gain passive systems allow it to be used for analyzing active-passive systems with finite energy storage capacity on a monthly basis.

The use of active storage in space heating systems may not be necessary in some cases. A solar system with passive energy storage may be able to meet the same fraction of the heating requirements as a system with active storage, depending upon the building construction, building heating load, and allowable temperature swing. Even in situations for which active storage provides better performance than passive storage, the increase may not be worth the added expense of the active storage component.

CHAPTER 4 COMBINED ACTIVE COLLECTION-PASSIVE STORAGE AND DIRECT-GAIN HYBRID SYSTEMS

4.1 INTRODUCTION

In this chapter, a modification to the design method descibed in Chapter 3 is presented which allows for combination of active collection-passive storage and direct-gain solar systems. Nearly all active collection-passive storage systems fall into this category to some extent, as most buildings have windows which could give a net solar gain.

A possible method to account for the combination of direct-gain and active collection-passive storage systems would be to calculate the solar gains from one system, and reduce the heating load on the other system correspondingly. This method assumes that the gains are evenly distributed over the entire twenty-four hour day. Active collection-passive storage and direct-gain systems, however, both have the same time distribution of energy input, and will therefore directly compete with each other during the daytime period. Simply analyzing the systems separately and adding the solar gains will cause an overprediction of the solar contribution. The degradation of performance associated with the competition of the two systems is potentially much greater than the degradation of

active system performance for the hybrid systems described in Chapter 2. The systems described in this chapter use only the building mass as the energy storage medium. Depending upon the effective building capacitance and the collector areas, it is easily possible for the storage to become fully charged (i.e., the room temperature reaches the upper set point). In this case, both active and passive systems will dump energy, either by venting, shutting off the fluid circulator (for the active system), or blocking off the collector aperture (for the passive system). The active subsystem of the hybrid systems analyzed in Chapter 2 has a thermally separate storage tank (or pebble bed), thereby isolating it to some extent from the passive subsystem, which uses the building mass as storage. In these systems the active and passive subsystems can dump separately , reducing the effects of one upon the other.

A better solution to this problem is to assume that the passive and active collectors in active plus passive collection-passive storage systems deliver energy in essentially the same fashion and time distribution, and therefore can be represented as a single system. The Un-utilizability method can then be modified to analyze the combined system.

The modifications necessary to the Un-utilizability method for this system are primarily related to calculating

the critical radiation level for energy dumping from the building. Sections 4.2 and 4.3 describe the modifications necessary for systems in which the passive and active collectors are at the same slope and azimuth. This is not an unlikely situation, since most direct-gain passive collectors are south facing and vertical, and the collectors in active collection-passive storage systems are often installed directly onto a south facing wall. Section 4.4 outlines a procedure to account for circumstances in which the active and passive collectors are not at the same slope and/or azimuth.

4.2 THEORETICAL LIMITS OF PERFORMANCE

The upper and lower bounds of performance for combined active plus passive collection-passive storage systems can be determined in a parallel analysis to that given in Section 3.4.

The upper bound assumes that the building has infinite energy storage capacity. The auxiliary energy and solar fraction for this case can be found by calculating the losses from the building and subtracting the energy collected from the active and passive collectors. The collected energy for the active subsystem is exactly the same as in Section 3.4. On a monthly basis:

$$Q_{c,a}=A_{c,a}\bar{H}_{T,a}F_R'(\overline{\tau\alpha})N\bar{\phi}_c \qquad (4.2.1)$$

where $\overline{\phi}_c$ is the monthly average collector utilizability factor, based on $I_{c,c}$ which is the monthly average collector critical radiation level (Equation 3.4.2).

The energy collected by the passive collector takes a similar form, with the exception that the collector utilizability factor is always unity. Collector losses do not need to be accounted for in the calculation of the energy collected by the passive collectors because the energy directly enters the building. The losses are however, included as part of the building energy losses.

$$Q_{c,p} = A_{c,p}\overline{H}_{T,p}(\overline{\tau\alpha})N \qquad (4.2.2)$$

The building energy losses can be calculated using the building shell energy loss coefficient, UA_b, the passive collector energy loss coefficient, UA_c, and the monthly heating degree-days at the building base temperature. Night insulation on the passive collectors can be accounted for by averaging the nighttime and daytime values of UA_c. The overall energy loss coefficient is the degree-day weighted average of the two values, assuming that the night insulation is put in place at sunset and removed at sunrise (8).

$$\overline{UA}_c = \frac{UA_{c,d}DD_d + UA_{c,n}DD_n}{(DD_d + DD_n)} \qquad (4.2.3)$$

Where $UA_{c,d}$ is the daytime value of the passive collector energy loss coefficient and $UA_{c,n}$ is the nighttime value of the passive collector energy loss coefficient. DD_d and DD_n are the daytime and nighttime degree-days for the month, which can be found by the method of Erbs (28). The total building energy losses can then be found:

$$L = (UA_b + \overline{UA}_c)DD \qquad (4.2.4)$$

The auxiliary energy required by the combined system with infinite energy storage capacity is the load minus the energy collected by both collectors (or zero if more energy is collected than is needed during any given month).

$$Q_{aux,i} = (L - (Q_{c,a} + Q_{c,p}))^+ \qquad (4.2.5)$$

The solar fraction can then be found from Q_{aux} and L :

$$f_{a+p,i} = 1 - Q_{aux,i}/L = (Q_{c,a} + Q_{c,p})/L \qquad (4.2.6)$$

The calculation of the auxiliary energy required by the zero energy storage limit involves determining the amount of energy dumped by the building. In the case of the combined active plus passive system, the dumping critical radiation level must be found as a function of

both collectors. An energy balance on the combined system for a radiation level at which the building heating requirements are just met by solar gives:

$$(I_{c,a} - I_{c,c})A_{c,a}F_R'(\overline{\tau\alpha}) + I_{c,p}A_{c,p}(\overline{\tau\alpha})$$

$$= (UA_b + \overline{UA}_c)(T_b - \overline{T}_a) \qquad (4.2.7)$$

$I_{c,c}$ is known (Equation 3.4.2) and for the case where the active and passive collectors have the same slope and azimuth, $I_{c,a}$ is equal to $I_{c,p}$. The dumping critical level can then be written:

$$I_{c,a+p} = \frac{(UA_b + UA_c)(T_b - \overline{T}_a) + (F_R'U_L(\overline{T}_R - \overline{T}_a)A_{c,a}}{F_R'(\overline{\tau\alpha})A_{c,a} + (\overline{\tau\alpha})A_{c,p}} \qquad (4.2.8)$$

The amount of energy dumped by the combined system can them be found as a function of the dumping utilizabiltiy factor $\overline{\phi}_{c,b}$, which is found using $I_{c,a+p}$.

$$Q_{dump} = (A_{c,a}\overline{H}_{T,a}F_R'(\overline{\tau\alpha})N + A_{c,p}\overline{H}_{T,p}N)\overline{\phi}_{cb} \qquad (4.2.9)$$

This gives the following equations for solar fraction and auxiliary energy use in the zero energy storage limit :

$$Q_{aux,z} = (L - ((Q_{c,a} + Q_{c,p}) - Q_{dump}))^+ \qquad (4.2.10)$$

$$f_{a+p,z} = (Q_{c,a} + Q_{c,p} - Q_{dump})/L \qquad (4.2.11)$$

4.3 MODIFICATIONS TO THE UN-UTILIZABILTIY METHOD FOR COMBINED ACTIVE COLLECTION-PASSIVE STORAGE PLUS DIRECT-GAIN SYSTEMS

The generalized version of Monsen's Un-utilizability correlation, described in Chapter 3, requires several slight additional modifications for combined active plus passive collection-passive storage systems. The solar to load ratio, X, can be broken down into a passive solar to load ratio, X_p, and an active solar to load ratio, X_a.

$$X_p = (A_{c,p}\bar{H}_{T,p}(\overline{\tau\alpha})N)/L \qquad (4.3.1)$$

$$X_a = (A_{c,a}\bar{H}_{T,a}F_R'(\overline{\tau\alpha})N/L \qquad (4.3.2)$$

$$X = X_p + X_a \qquad (4.3.3)$$

The passive energy storage capacity remains the same as Equation 3.5.3. The storage to dump ratio, Y, retains a form similar to Equation 3.5.4, with Equation 4.2.9 replacing Equation 3.4.7 as the denominator.

$$Y = \frac{C\Delta T_s N}{(A_{c,a}\bar{H}_{T,a}F_R'(\overline{\tau\alpha}) + A_{c,p}\bar{H}_{T,p}(\overline{\tau\alpha}))N\bar{\phi}_{cb}} \qquad (4.3.4)$$

Both X and Y will reduce to the Equations given in Chapter 3 for the special case where there is no passive collector. The correlation for solar fraction must also be modified somewhat to allow it to reduce to the zero and infinite storage cases.

$$f_{a+p} = P(X_p+X_a\bar{\phi}_c) + (1-P)\left[(3.082-3.142\bar{\phi}_{cb})\right.$$
$$(1- \exp(-0.329X)) - (3.142-3.142\bar{\phi}_c)$$
$$\left.(1- \exp(-0.329X_a))\right] \qquad (4.3.5)$$

$$P = (1 - \exp(-0.294Y))^{0.652} \qquad (4.3.6)$$

For the infinite storage case, P equals unity, and Equation 4.3.5 is equal to Equation 4.2.6. The zero storage case, assuming small values of X, and using a power series expansion of the exponential terms Equation 4.3.5 reduces to:

$$f_{a+p} = (1.014-1.034\bar{\phi}_{cb})X - (1.034-1.034\bar{\phi}_c)X_a \qquad (4.3.7)$$

$$\simeq (Q_{c,p} - Q_{dump} + Q_{c,a})/L \qquad (4.3.8)$$

Equation 4.3.8 is equal to Equation 4.2.11, the solar

fraction for the zero storage limit. Equation 4.3.5 is an even more generalized version of Monsen's correlation than Equation 3.5.8 as it can be used for systems with direct-gain, active collection-passive storage, or combinations of both.

The correlation was compared to detailed TRNSYS simulations for a variety of systems in Madison, WI, Boston, MA, and Albuquerque, NM. The system parameters included in this comparison are listed in Table 4.3.1. Figure 4.3.1 shows a plot of design method predictions of auxiliary energy use compared to the values from corresponding TRNSYS simulations. The correlation had a standard deviation of 2.8 GJ for these examples, which is within the 3.3 GJ standard error originally cited for Monsen's correlation (4).

4.4 NON-EQUAL PASSIVE AND ACTIVE COLLECTOR ORIENTATIONS

The previous analysis is strictly valid only for systems which have the passive and active collectors at the same orientation. If the active and passive collectors have different orientations, it is not possible to solve Equation 4.2.7 for an explicit critical radiation level. Erbs (21) has suggested the use of an "effective" critical radiation level, $I_{c,a+p}$, which is the weighted average of the critical radiation levels incident on the two collectors.

TABLE 4.3.1

PARAMETERS INVESTIGATED FOR DESIGN METHOD AND SIMULATION COMPARISONS

LOCATIONS	Madison,WI Albuquerque, NM Boston, MA
ACTIVE SYSTEM PARAMETERS	
Collector Area	0-80 m^2
$F_R(\overline{\tau\alpha})$	0.51
$F_R U_L$	3.1 W/C-m^2
Collector Slope	90
Collector Azimuth	0
PASSIVE SYSTEM PARAMETERS	
Collector Area	0-80 m^2
U	2.1 W/C-m^2
$\overline{\tau\alpha}$	0.85
Collector Slope	90
Collector Azimuth	0
BUILDING PARAMETERS	
Effective Capacitance	10-50000 KJ/C
Auxiliary Set Temperature	18 C
Allowable Temperature Swing	7 C
UA_b	180 W/C

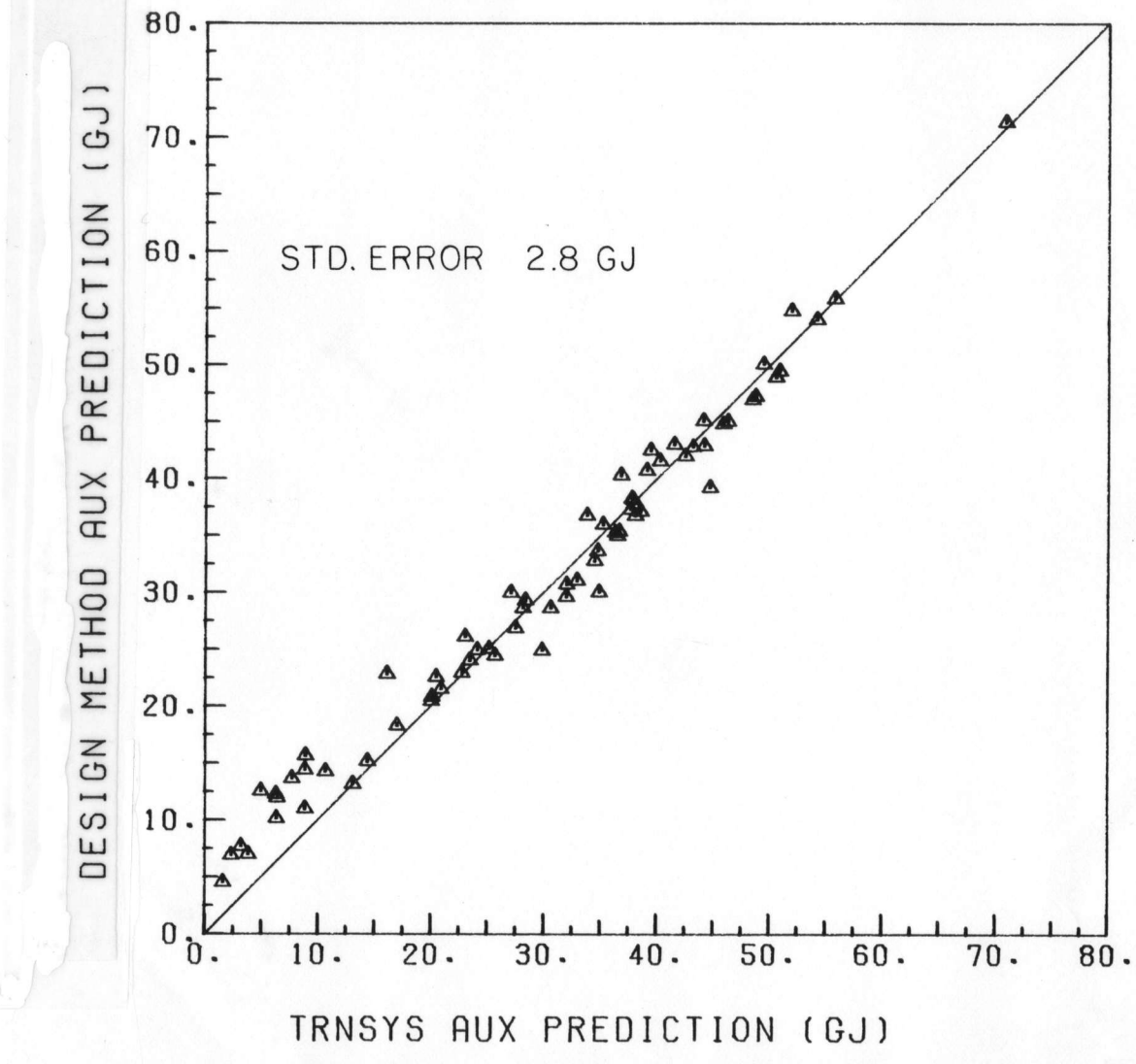

Figure 4.3.1 Comparison of Design Method and Simulation Predictions of Auxiliary Energy Use for Active Plus Passive Collection-Passive Storage Systems with Equal Active and Passive Collector Orientations. Locations Investigated were Madison, WI, Boston, MA, and Albequerque, NM.

$$\bar{I}_{c,a+p} = \frac{I_{c,a}F_R'(\overline{\tau\alpha})A_{c,a} + I_{c,p}(\overline{\tau\alpha})A_{c,p}}{A_{c,a}F_R'(\overline{\tau\alpha}) + A_{c,p}(\overline{\tau\alpha})} \qquad (4.4.1)$$

Equation 4.2.7 can then be solved for $\bar{I}_{c,a+p}$:

$$\bar{I}_{c,a+p} = \frac{(UA_b + \overline{UA}_c)(T_b - \bar{T}_a) + (F_R'U_L(\bar{T}_R - \bar{T}_a)A_{c,a}}{F_R'(\overline{\tau\alpha})A_{c,a} + (\overline{\tau\alpha})A_{c,p}} \qquad (4.5.2)$$

This is exactly the same as Equation 4.2.8, but the associated energy dumping utilizability factor, $\bar{\phi}_{cb}$ must be found using an energy weighted average collector slope and azimuth.

$$\bar{\beta} = \frac{\beta_a(\bar{H}_{T,a}F_R'(\overline{\tau\alpha})A_{c,a}) + \beta_p(\bar{H}_{T,p}(\overline{\tau\alpha})A_{c,p})}{\bar{H}_{T,a}F_R'(\overline{\tau\alpha})A_{c,a} + \bar{H}_{T,p}(\overline{\tau\alpha})A_{c,p}} \qquad (4.4.4)$$

$$\bar{\gamma} = \frac{\gamma_a(\bar{H}_{T,a}F_R'(\overline{\tau\alpha})A_{c,a}) + \gamma_p(\bar{H}_{T,p}(\overline{\tau\alpha})A_{c,p})}{\bar{H}_{T,a}F_R'(\overline{\tau\alpha})A_{c,a} + \bar{H}_{T,p}(\overline{\tau\alpha})A_{c,p}} \qquad (4.4.5)$$

β_a and γ_a are the slope and azimuth of the active collector and β_p and γ_p are the slope and azimuth of the passive collector. The modified $\bar{\phi}_{cb}$ can then be used to calculate the storage to dump ratio (using Equation 4.3.4), and hence the solar fraction. (The solar to load ratios remain the same as defined in Equations 4.3.1-4.3.3).

Figure 4.4.1 provides a comparison of TRNSYS simulation results and design method predictions of auxiliary energy use for 24 examples in Madison, WI. The range of parameters covered by these examples is given in Table 4.4.1. The standard deviation of the error for these examples was 3.23 GJ. This is somewhat of an increase in error over the systems which had equal passive and active collector orientation, presumably due to problems in evaluating $\overline{\phi}_{cb}$ for the average collector properties.

4.5 EXAMPLE

Consider the example from Chapter 3, with the addition of 20 square meters of south facing direct-gain windows, and with the active collectors mounted vertically. The system parameters are listed in Table 4.5.1. Tilted surface radiation was calculated using the method of Klein (13), with the diffuse fraction estimated using the correlation developed by Erbs et al. (14).

The monthly heating load can be calculated using the monthly degree-days and the combined building plus passive collector energy loss coefficients. For this example no night insulation is used, therefore the average collector energy loss coefficient is equal to the daytime value. For January:

$$L=(210+2.1(20))(86400)(818.5) = 17.82 \text{ GJ}$$

TABLE 4.4.1

PARAMETERS INVESTIGATED FOR DESIGN METHOD AND SIMULATION COMPARISONS

LOCATIONS	Madison,WI
ACTIVE SYSTEM PARAMETERS	
Collector Area	0-80 m^2
$F_R(\overline{\tau\alpha})$	0.51
$F_R U_L$	3.1 W/C-m^2
Collector Slope	45-90
Collector Azimuth	$\pm$30
PASSIVE SYSTEM PARAMETERS	
Collector Area	0-80 m^2
$\frac{U}{\tau\alpha}$	2.1 W/C-m^2
	0.85
Collector Slope	90
Collector Azimuth	$\pm$30
BUILDING PARAMETERS	
Effective Capacitance	30000 KJ/C
Auxiliary Set Temperature	18 C
Allowable Temperature Swing	7 C
UA_b	180 W/C

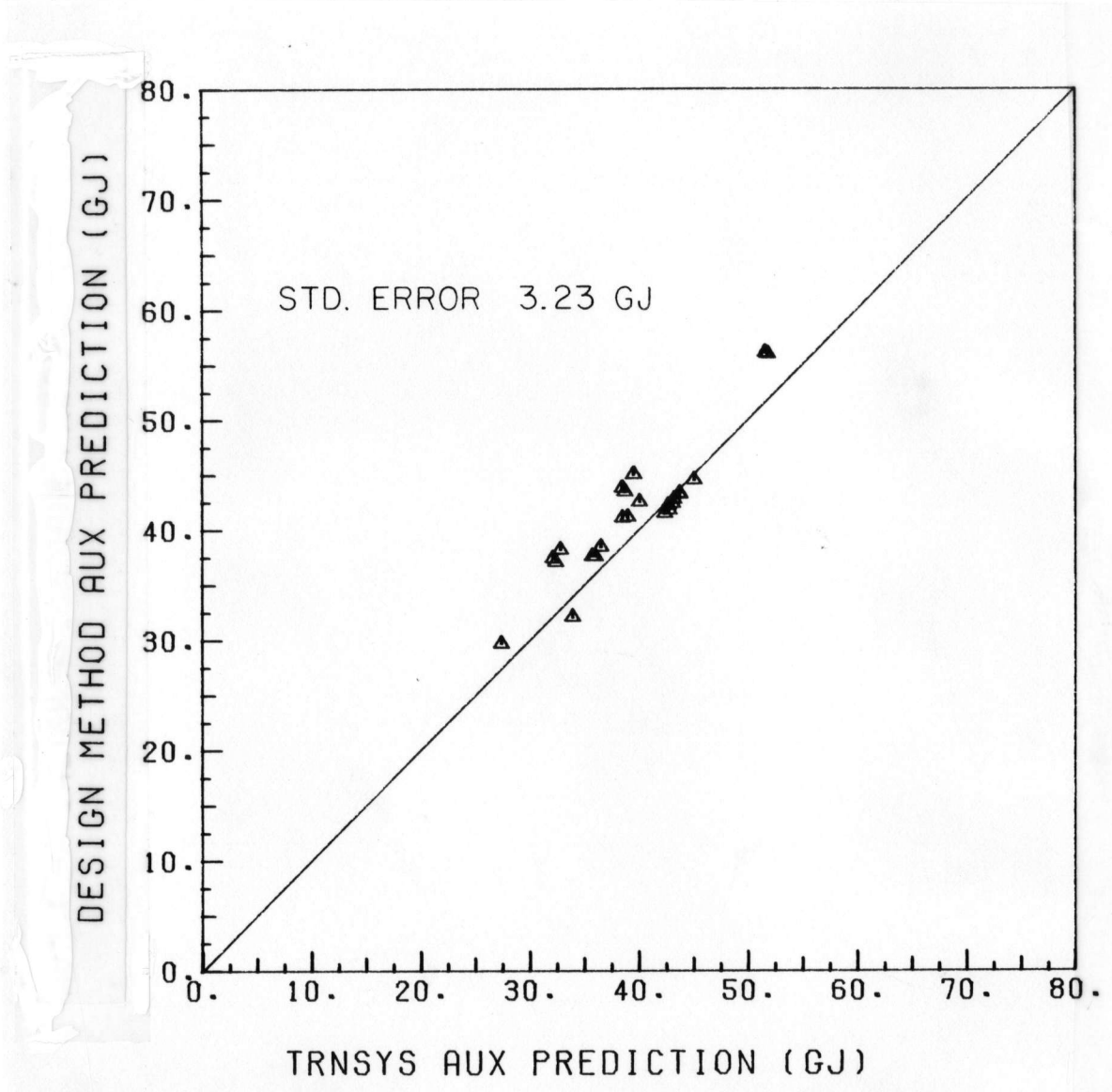

Figure 4.4.1 Comparison of Design Method and Simulation Predictions of Auxiliary Energy Use for Active Plus Passive Collection-Passive Storage Systems with Unequal Active and Passive Collector Orientations in Madison, WI.

The remaining monthly heating loads are summarized in Table 4.5.2. The passive and active solar to load ratios, X_p and X_a, can be found using Equations 4.3.1 and 4.3.2.

$$X_p = 20(1.06\text{x}10^7)(31)(.85)/17.82\text{x}10^9 = 0.286$$

$$X_a = 25(1.06\text{x}10^7)(31)(.51)/17\text{x}10^9 = 0.214$$

$$X = 0.286 + 0.214 = 0.500$$

The storage to dump ratio, Y, can be found using Equation 4.3.4, with the dumping un-utilizability factor found using $I_{c,a+p}$.

$$I_{c,a+p} = 251.7(18-(-8.4))+3.1(18-(-8.4))25/$$
$$((.51)25+(.85)20) = 292.13 \text{ W/m}^2$$

$$\overline{\phi}_{cb} = 0.392$$

$$Y = 1.928\text{x}10^8/((25)1.07\text{x}10^7(.51)+$$
$$20(1.07\text{x}10^7)(.85))0.392 = 1.712$$

The solar fraction for January can then be estimated from Equations 4.3.5 and 4.3.6:

$$P = (1-\exp(-0.294(1.712)))^{0.652} = 0.546$$

$$f_{a+p} = 0.546(0.286+0.214(0.607)) + (1-0.546)$$
$$[(3.082-3.142(.392))(1-\exp(-0.329(0.5))) -$$
$$(3.142-3.142(0.607))(1-\exp(-0.329(0.214)))]$$
$$= 0.317$$

The auxiliary energy use for January is:

$$Q_{aux} = (1-0.317)(17.82) = 12.17 \text{ GJ}$$

The solar fractions and monthly auxiliary energy estimates are summarized in Table 4.4.2. For this example, the design method predicted the auxiliary energy to within 1.09 GJ (2.4%) of the simulation results on an annual basis.

TABLE 4.5.1

PARAMETERS FOR EXAMPLE PROBLEM

LOCATION	Madison,WI
ACTIVE SYSTEM PARAMETERS	
Collector Area	25 m^2
$F_R(\overline{\tau\alpha})$	0.51
$F_R U_L$	3.1 W/C-m^2
Collector Slope	90
Collector Azimuth	0
PASSIVE SYSTEM PARAMETERS	
Collector Area	20 m^2
$\overline{U}$	2.1 W/C-m^2
$\overline{\tau\alpha}$	0.85
Collector Slope	90
Collector Azimuth	0
BUILDING PARAMETERS	
Effective Capacitance (Med. Wt. Constr.)	27540 KJ/C
Auxiliary Set Temperature	18 C
Allowable Temperature Swing	7 C
UA_b	210 W/C

TABLE 4.5.2

EXAMPLE PROBLEM SUMMARY

Month	Heating Load	Design Method SF	Design Method Q_{aux}	TRNSYS SF	TRNSYS Q_{aux}
Jan	17.80 GJ	0.32	12.16 GJ	0.35	11.55 GJ
Feb	14.60	0.40	8.83	0.44	8.24
Mar	13.39	0.49	6.85	0.55	6.03
Apr	6.26	0.70	1.87	0.73	1.69
May	3.26	1.00	0.00	0.78	0.70
Sep	1.90	1.00	0.00	0.95	0.09
Oct	5.24	0.79	1.09	0.72	1.47
Nov	10.20	0.42	5.92	0.42	5.90
Dec	14.64	0.29	10.45	0.29	10.40
	87.30 GJ	0.46	47.16 GJ	0.47	46.07 GJ

CHAPTER 5 EFFECTIVE CAPACITANCE

5.1 INTRODUCTION

Both the active collection-passive storage, and combined active collection-passive storage plus direct-gain space heating systems rely on the bulding mass as the energy storage medium. Some means must be employed to determine the energy storage capacity of the building mass in order for the design methods presented in Chapter 3 and 4 to be used. The method usually recommended for determining building energy storage capacity is to use the product of an "effective capacitance" and an allowable indoor temperature swing.

The use of an effective capacitance assumes that the different components of the building can be lumped, i.e., the indoor air, furnishings, and some portion of the building mass are all at the same temperature. In reality, the air, walls and furnishings are distributed capacitances and could all be at different temperatures, with temperature gradients within each object, leading to a very complicated, time dependent function for energy storage capacity.

For either a real or lumped representation of building capacitance the energy flows are cyclic in nature. When

excess energy is available (such as during a sunny day for an active collection-passive storage system that is large relative to the heating load) the building heats up and energy is stored in the mass ("charging"). Alternately, when the losses from the building are greater than the gains, the additional energy needed can be obtained by allowing the building temperature to decay ("discharging").

The effective capacitance which is used to represent the distributed capacitances of a real building is a function of a number of parameters. As a limit, the effective capacitance must be less than or equal to the total capacitance of the building*, where the total capacitance is the sum over all of the building components of the product of the mass of each component and its specific heat.

The pecentage of the total capacitance which is effective for energy storage purposes is dependent upon the conductance of the building materials, the convection heat transfer coefficient between the air and the building components, and the time scale over which the charge-discharge cycle takes place. Additional conditions such as whether solar radiation is incident upon some of the internal mass, and the allowable temperature swing, may

* Horn (24) has found instances when the effective capacitance is greater than the total capacitance. This only occured for a cooling load, however, and therefore does not concern this analysis.

also influence the effective capacitance.

The conductance of the building material and the convection heat transfer coefficient characterize the resistance to energy transfer into or out of the building mass. If the conductance or convection coefficient (or both) are small, either a very long time or a large temperature difference would be required between the room air and the building mass to allow much energy to penetrate into the mass. This would cause the effective capacitance to be much smaller than the total capacitance for the time scales and temperature swings typical in buildings using passive storage (i.e., time scales of 12-48 hours, and temperature swings of less than 10 C). If, on the other hand, the resistance to energy transfer from the room air to the building mass were very small, the entire building mass would be essentially isothermal, and the effective capacitance would approach the total capacitance.

There are several ways of determining the effective capacitance of a building. All of these are very approximate, and generally are not well defined in relationship to specific building constructions. The ASHRAE Handbook of Fundamentals (22) recommends the use of three categories of construction weight; light, medium, and heavy. These correspond to numerical capacitance values of 112, 261, and 485 KJ/C per square meter of floor area. How to determine the category of a particular construction type

and whether the values of capacitance are the effective or total capacitance is not clear.

Mitchell (23) has tabulated a number of experimental values for the effective capacitance of residential structures. The values approximately correspond to the ASHRAE light weight construction values.

The National Research Council of Canada (17) has also established values for effective capacitance. Table 3.6.1 is a summary of their results. The values in Table 3.6.1 were determined by using the ASHRAE transfer function method in an hourly simulation model. The ASHRAE standard response factors are given primarily for commercial buildings, so the researchers at the National Council of Canada calculated non-standard transfer functions for the constructions given in Table 3.6.1.(17). Exactly how the values of capacitance were determined is not stated, but similar results can be obtained by using the TRNSYS transfer fucntion building model and using a procedure similar to the one outlined in Section 5.3.

Horn (24) devoted an entire Masters thesis to developing an analytical or empirical relationship for effective capacitance. His overall recommendation is to use one half of the total capacitance of the structure plus the capacitance of the air and furnishings as the effective capacitance. Included with this recommendation is the admonition that relatively large errors could result, and

that the effective capacitance seems to be a function of interior and exterior conditions, wall construction, and type of load.

5.2 BUILDING TEMPERATURE DECAY METHOD OF DETERMINING EFFECTIVE CAPACITANCE

5.2.1 BACKGROUND

An experimental method which has been used to determine the effective capacitance of buildings is to measure the temperature decay of the building over a period of a few days during a time of relatively constant ambient temperatures. An energy balance on the building can then be used to derive an equation to calculate the effective capacitance that would have had the same temperature decay rate.

$$C\frac{dT}{dt} = -UA_b(T(t)-T_a) \qquad (5.2.1)$$

C is the effective capacitance of the building, UA_b is the overall building energy loss coefficient, and T_a is the ambient temperature during the test. This can be solved as a function of the initial and final temperatures of the building, the length of the test, UA_b, and T_a, assuming that the capacitance is not a function of the other variables.

$$C = \frac{-UA_b(t-t_o)}{\ln((T(t)-T_a)/(T(t_o)-T_a))} \qquad (5.2.2)$$

There are several problems with this type of test on actual buildings. First, the building must be built before the capacitance can be determined. Then, the overall energy loss coefficient must be determined, and the ambient temperature must remain at an appropriate constant temperature for several days.

5.2.2 SIMULATED TEMPERATURE DECAY TESTING

This section presents a means of using a detailed, distributed capacitance building model to perform simulated temperature decay test to evaluate effective capacitance.

The building model used in these simulations is the TRNSYS 12.1 Type 19 transfer function model (25). The Type 19 model simulates single zone buildings with capacitance in the individual walls, a flat roof and floor. Multiple zone buildings can be modeled by combining several Type 19 components. The heat transfer through the structure is modeled using the ASHRAE transfer function method (26). Standard ASHRAE walls (listed in references 22 and 27) can be specified, or specially constructed walls may be used by supplying the transfer function coefficients for the sol-air temperature, equivalent zone temperature and heat flux.

Radiative gains and radiative exchange between interior surfaces is accounted for in the calculation of the equivalent zone temperature. Infiltration rate can be specified as proportional to the difference between the indoor and ambient air temperatures, proportional to the wind speed, or on a constant air change per hour basis. A complete mathematical description can be found in reference (25).

The Type 19 building model is used in simulated decay tests by fixing the ambient temperature input at some arbitrary value. The indoor building temperature is held at the upper set point temperature until the building reaches a steady-state condition. (At the initiation of the simulation, the walls, roof and floor are assumed to be isothermal at the initial room temperature). The building temperature is then allowed to float until it reaches the lower set point. The length of time from the beginning of the floating room temperature, the initial set temperature, and the building energy loss coefficient can then be used in Equation 5.2.1 to calculate an effective capacitance.

Three different building constructions were simulated as examples to test this method of determining effective capacitance. The first example building is of frame construction with a one-inch wood floor. Example building construction two is similar to the first, except that the wood floor is replaced with four inches of heavy weight

concrete. The third example utilizes masonry external walls with a two-inch concrete floor. The complete descriptions of the three construction types are listed in Table 5.2.1. For these simulations, the infiltration rate was fixed at one-half air change per hour, and there were no windows to allow solar gains.

5.2.3 RESULTS

The example buildings were simulated using a variety of ambient temperatures. For each test, the effective capacitance was calculated on a continuous basis, using the elapsed time since the room temperature was allowed to float, t, the initial room set temperature, $T(t_0)$, and the room temperature at time t in Equation 5.2.2. Figure 5.2.1 shows the estimated room capacitance as a function of time for example building constructions 1 and 2. The effective capacitance starts out at a very small value, equal to the capacitance of the indoor air (which has a capacitance of only about 500 KJ/C for these examples). The effective capacitance is equal to the indoor air capacitance initially, because there is no temperature differance between the wall surfaces and the indoor air. Heat cannot therefore be convected from the walls to the air, and the capacitance of the walls does not affect the temperature decay rate. Thus, the indoor air temperature drops rapidly during the first few hours of the simulated decay test. As

TABLE 5.2.1

DESCIPTION OF EXAMPLE BUILDING CONSTRUCTIONS

EXAMPLE CONSTRUCTION 1

Walls	ASHRAE Type 97: Frame Construction With 3/4" Plaster Interior Finish
Roof	ASHRAE Type 39: Flat Roof with 6" Insulation and 1" Wood Interior Finish
Floor	ASHRAE Type 28: Frame Construction With 1" Wood Floor
UA_b	190.1 W/C

EXAMPLE CONSTRUCTION 2

Walls	ASHRAE Type 97: Frame Construction With 3/4" Plaster Interior Finish
Roof	ASHRAE Type 39: Flat Roof with 6" Insulation and 1" Wood Interior Finish
Floor	ASHRAE Type 34: 4" Heavy Weight Concrete
UA_b	190.1 W/C

EXAMPLE CONSTRUCTION 3

Walls	ASHRAE Type 102: 12" Light-Weight Concrete Block Wall with 4" Face Brick
Roof	ASHRAE Type 40: Flat Roof with 6" Insulation and 2" Wood Interior Finish
Floor	ASHRAE Type 32: 2" Heavy Weight Concrete
UA_b	188.0 W/C

GENERAL INFORMATION

Infiltration Rate	0.5 Air Ch./Hr
Auxiliary Set Temperature	18 C
Allowable Temperature Swing	7 C

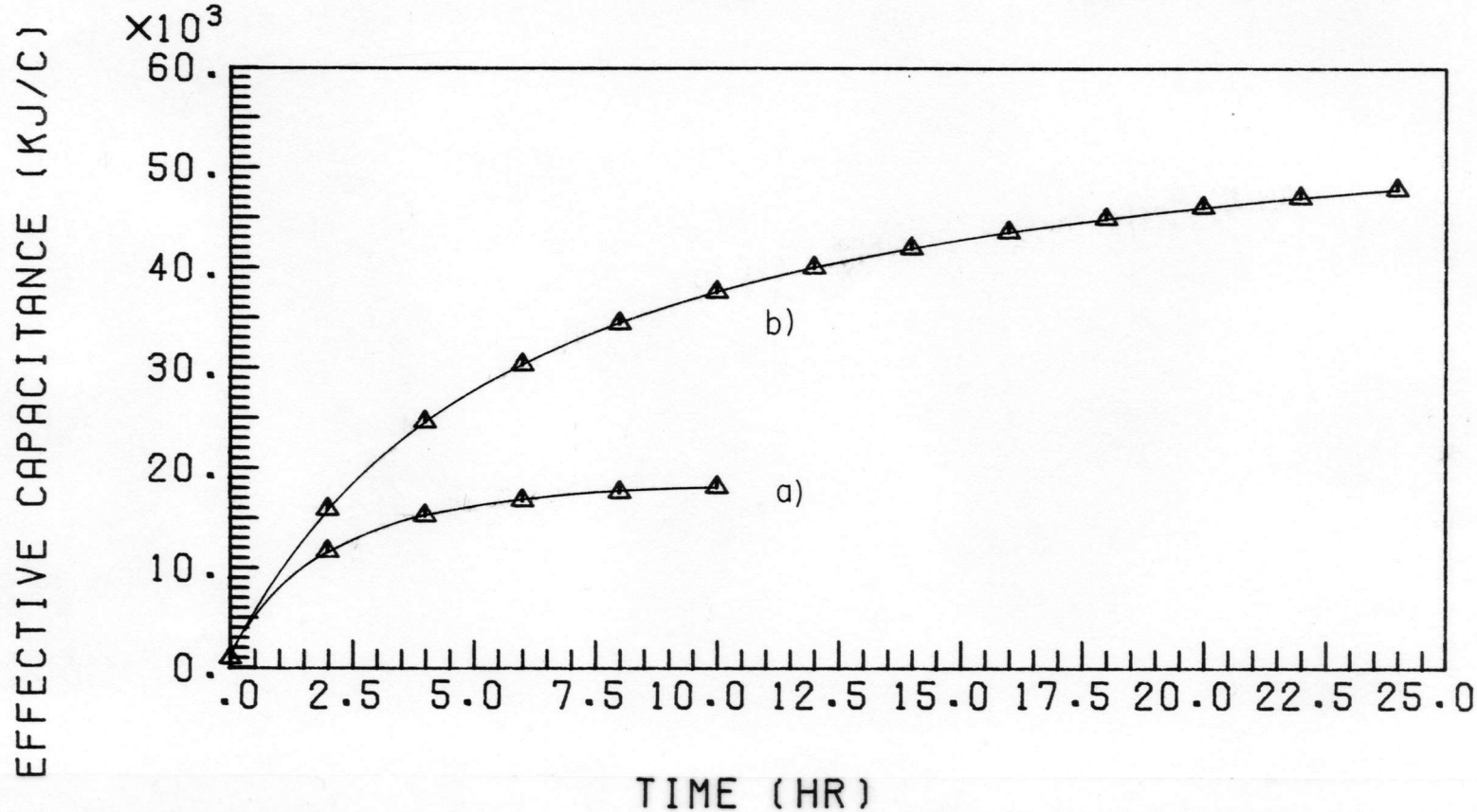

Figure 5.2.1 Effective Capacitance as a Function of Time Elapsed Since the Start of the Simulated Decay Test. The Upper Setpoint was 25 C and the Lower Setpoint was 18 C. a)Example Building Construction 1. b) Example Building Construction 2.

the interior air temperature drops, the temperature difference between the air and wall surfaces becomes great enough to allow heat to convect from the walls to the room air. The convection from the walls will then tend to balance the infiltration losses and the effective building capacitance becomes nearly constant. Figures 5.2.2-5.2.4 also show this effect by plotting the temperature decay from the simulation results as a function of time compared to the temperature decay of a lumped capacitance. The lumped capacitance used for these plots is the effective capacitance calculated at the end of the simulation, when the room air temperature is at the minimum set point.

If the ambient temperature used in the decay simulation is varied, the building temperature decay rate, and hence the calculated effective capacitance also varies. Figure 5.2.5 shows a plot of the effective capacitance at the end of the decay test as a function of the ambient temperature used in the test. There is about a 10 percent variation over the range of ambient temperatures used, although there seems to be an increasing rate of change at the lower ambient test temperatures for the more massive building construction.

The type of construction affects not only the absolute magnitude of the effective capacitance, but also the ratio of the effective capacitance to the total capacitance of the building. The less conductive materials, such as wood,

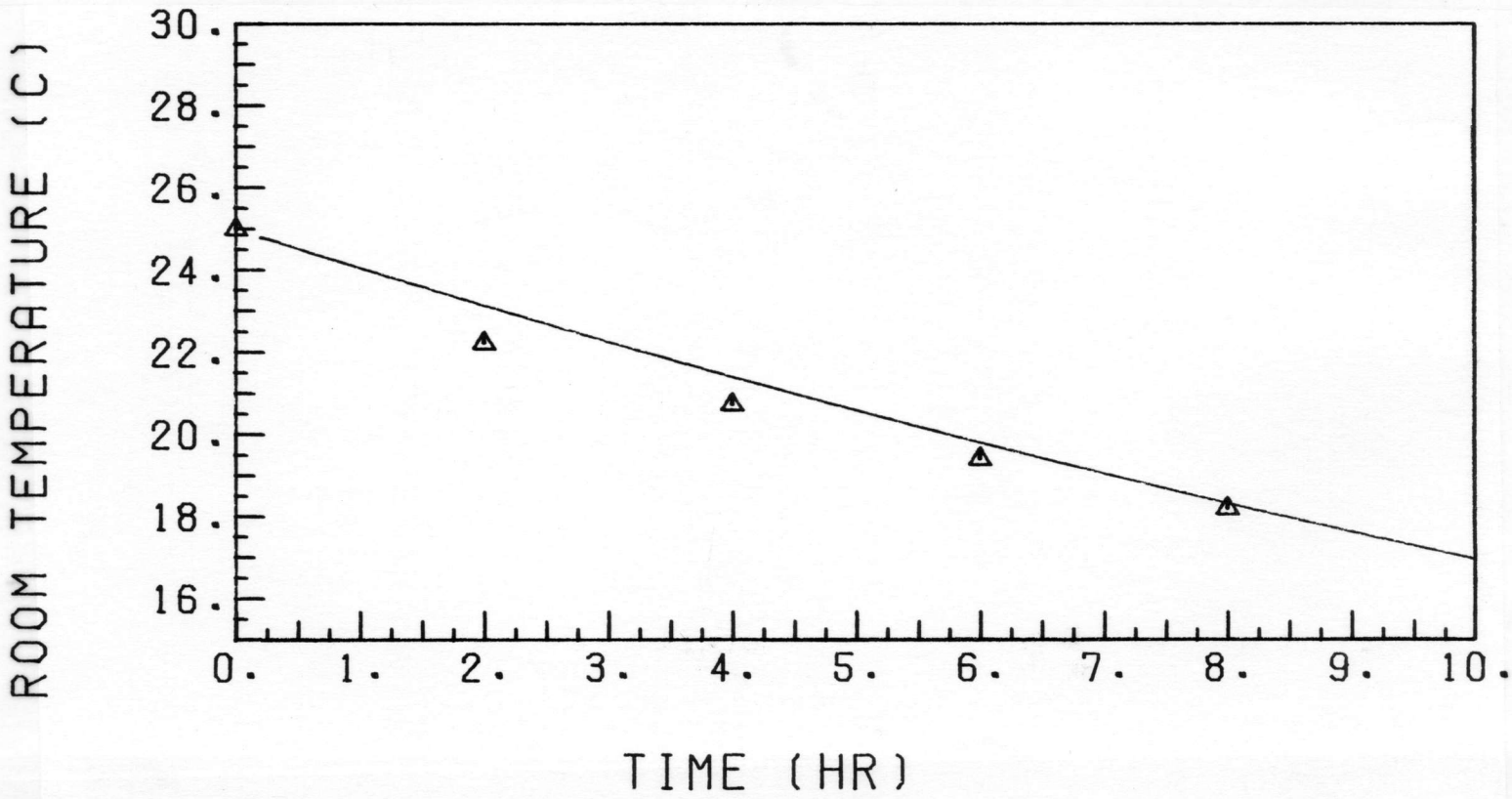

Figure 5.2.2 Data Points of Simulated Temperature Decay Test of the Transfer Function Building Model (⚠) Compared to the Temperature Decay of a Lumped Capacitance for Example Building Construction 1.

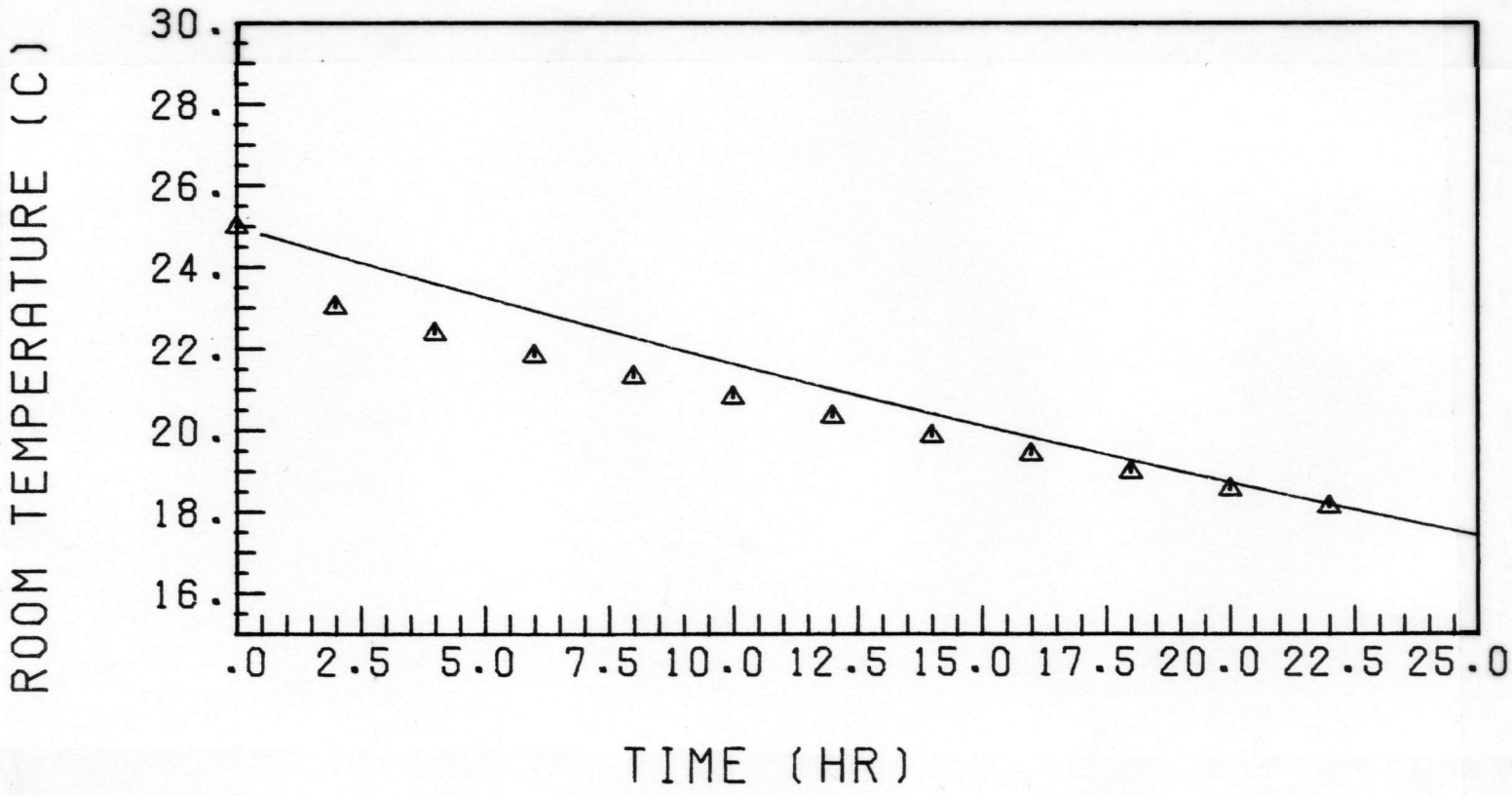

Figure 5.2.3 Data Points of Simulated Temperature Decay Test of the Transfer Function Building Model (⚠) Compared to the Temperature Decay of a Lumped Capacitance for Example Building Construction 2.

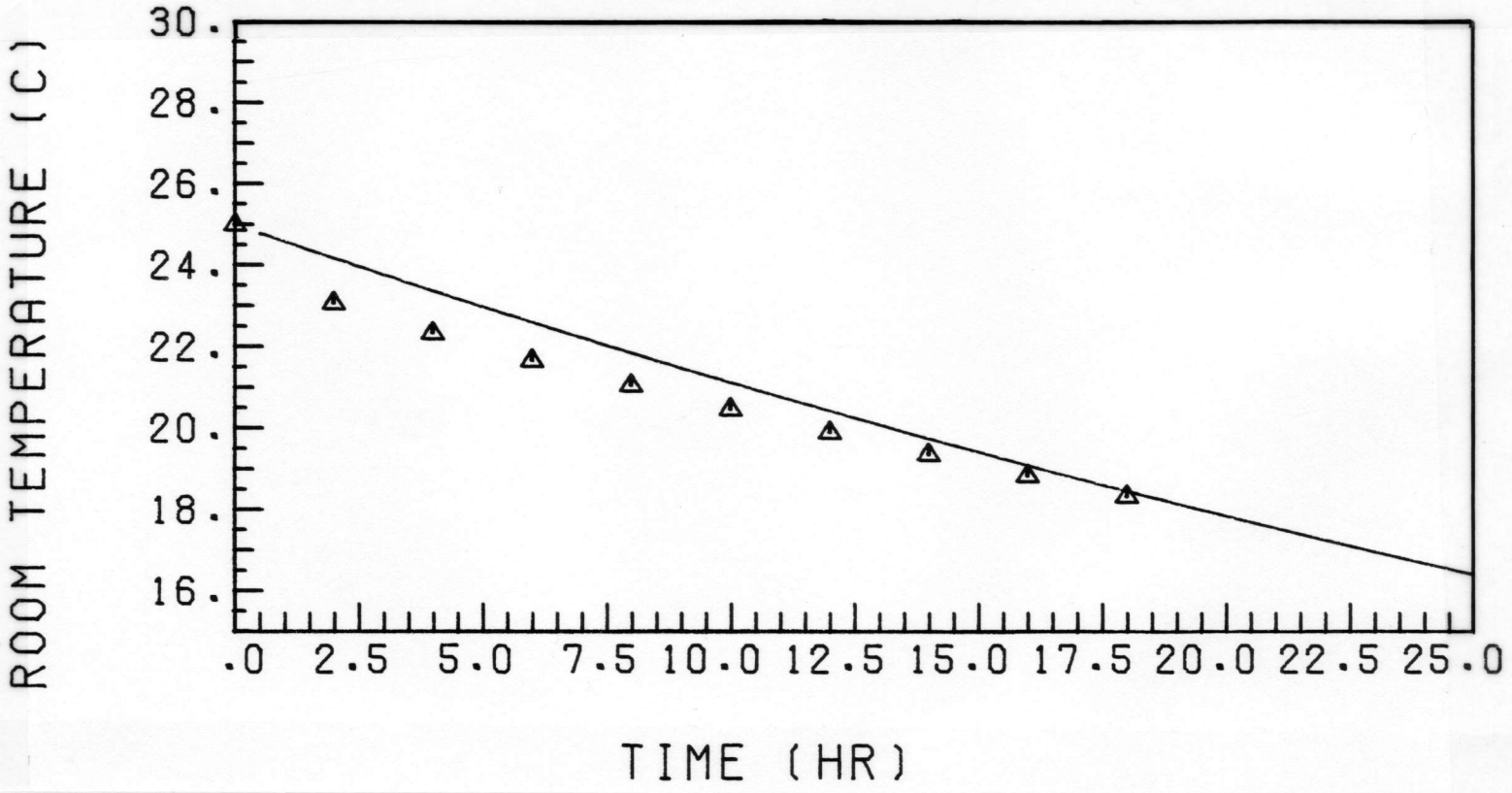

Figure 5.2.4 Data Points of Simulated Temperature Decay Test of the Transfer Function Building Model (△) Compared to the Temperature Decay of a Lumped Capacitance for Example Building Construction 3.

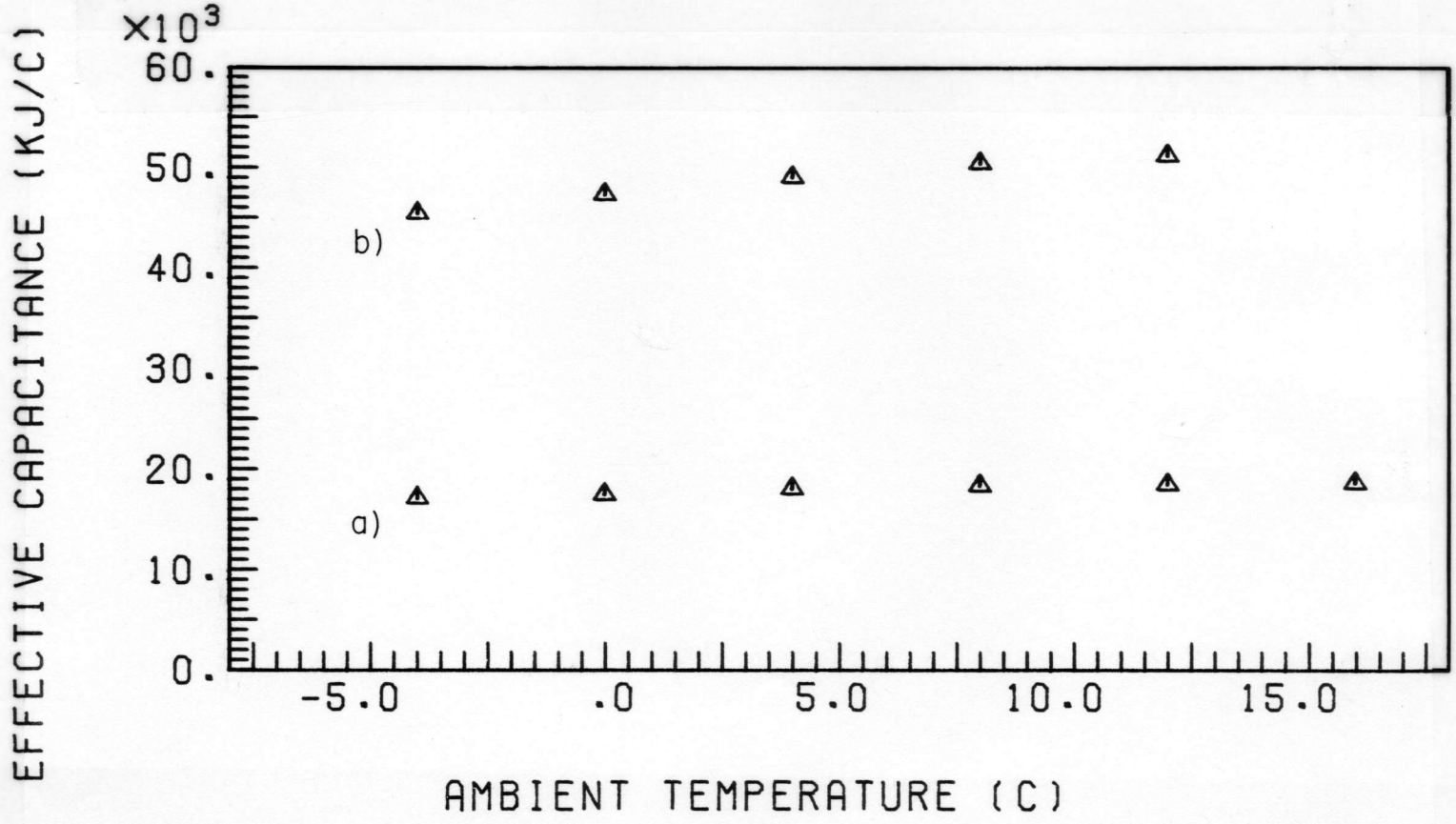

Figure 5.2.5 Effective Capacitance as a Function of the Ambient Temperature Used in the Decay Test. a) Example Building Construction 1. b) Example Building Construction 2.

should have a lower ratio of effective capacitance to total capacitance, because the energy cannot discharge from the material as quickly. Table 5.2.2 shows that this is true for the three example building constructions. Example construction number 3, although of heavier wall construction than example construction number 2, has a lower effective to total capacitance ratio because the lightweight concrete blocks used on the interior of the walls have a lower conductivity than the plaster used in the second example.

5.3 COMPARISON OF EFFECTIVE CAPACITANCE AND SIMULATION RESULTS ON AN ANNUAL BASIS

In order to determine if the effective capacitance from the short term simulations gives an appropriate representation of energy storage capacity for longer periods of time, annual TRNSYS simulations using the Type 19 building model were compared to design method calculations using effective capacitance.

The three example building constructions were simulated with various size active collection-passive storage solar systems in Madison, WI. The results from these simulations were compared to predictions from the design method presented in Chapter 3. The effective capacitance used in the design method was the cumulative value from the simulated decay test at an ambient

TABLE 5.2.2

COMPARISON OF EFFECTIVE AND ACTUAL

BUILDING CAPACITANCE

	EXAMPLE CONSTR. 1	EXAMPLE CONSTR. 2	EXAMPLE CONSTR. 3
TOTAL CAPACITANCE	28200 KJ/C	58400 KJ/C	51500 KJ/C
EFFECTIVE CAPACITANCE	17600 KJ/C	47300 KJ/C	40500 KJ/C
EFFECTIVE TO TOTAL RATIO	0.62	0.81	0.78

temperature equal to the heating season average temperature. The cumulative value was the value after the room temperature had decayed from the upper to the lower set points. The allowable temperature swing used in the design method was the difference between the two set points.

Table 5.3.1 gives the range of solar system parameters covered by the comparisons. The building heating load calculated by the simulations is found using transfer function relationships, taking into account the effects of solar radiation on the exterior wall surfaces, and the effects of capacitance in the walls. The building load cannot, therefore, be exactly found in a design method calculation *.Therefore, the loads for the design method were calculated by a TRNSYS simulation with no active collection-passive storage system to eliminate any error associated with calculating the building load on a monthly basis.

Figure 5.3.1 shows a plot of the TRNSYS simulation results compared to the design method predictions on an annual basis. The standard deviation of the error for these twenty-one examples was 0.97 GJ. Table 5.3.2. shows a comparison of TRNSYS and design method monthly auxiliary

* The sol-air degree-day method of Erbs (21) can be used to account for solar radiation on exterior walls, but does not account for the capacitance of the walls.

predictions for the three example building constructions for an active collection-passive storage system with 120 m^2 of collector. On a monthly basis, there is somewhat more variability in the predictions, but well within the error limits originally cited for Monsen's correlation (4). This seems to indicate that the effective capacitance given by the tests is a reasonable value to use on an annual basis.

5.4 LIMITATIONS

The simulated decay test method of determining effective capacitance assumes that the allowable temperature swing for the entire building is limited by the upper and lower thermostat set temperatures, which measure only the indoor air temperature. This is a reasonable assumption for active collection-passive storage systems, because the energy is transferred from the collectors to the room air, and then to the internal masses. Therefore, if the room air temperature is confined to upper and lower bounds, the internal mass will also be confined to the same bounds.

Direct-gain systems, on the other hand, have solar radiation incident upon some portion of the inside surfaces. This can give surface temperatures higher than the maximum allowable room temperature without necessarily overheating the room. This increases the temperature swing

TABLE 5.3.1

RANGE OF PARAMETERS INVESTIGATED FOR

DESIGN METHOD AND SIMULATION COMPARISONS OF

ACTIVE COLLECTION-PASSIVE STORAGE SYSTEMS

LOCATIONS	Madison, WI
SYSTEM PARAMETERS	
Collector Area	0-120 m^2
$F_R'(\tau\alpha)$	0.51
$F_R U_L$	3.1 W/C-m^2
Collector Slope	60
Collector Azimuth	0
BUILDING PARAMETERS	
Effective Capacitance	17.6-47.3 MJ/C
Allowable Temperature Swing	7 C
UA_b	190 W/C

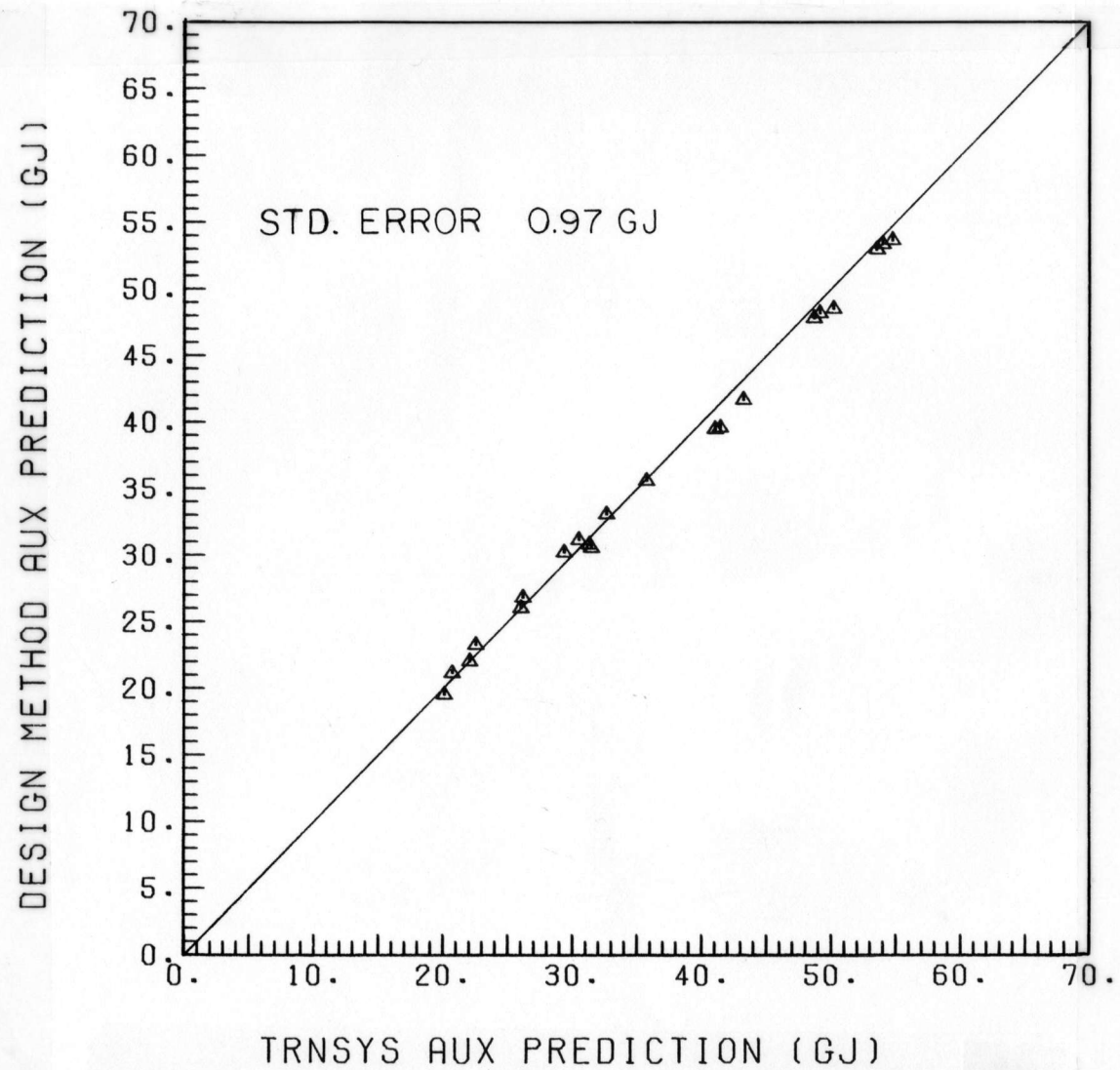

Figure 5.3.1 Comparison of TRNSYS Transfer Function Model Simulation Results for Active Collection-Passive Storage Systems and Design Method Calculations Using the Simulated Decay Test Effective Capacitance. Parameters for These Comparisons are Listed in Table 5.3.1.

TABLE 5.3.2

COMPARISON OF MONTHLY AUXILIARY PREDICTIONS FROM TRNSYS SIMULATIONS AND THE GENERALIZED UN-UTILIZABILITY METHOD

Auxiliary Energy Use
(Collector Area of 120 m^2)

	EXAMPLE CONSTR. 1		EXAMPLE CONSTR. 2		EXAMPLE CONSTR. 3	
	TRN	UN-UT	TRN	UN-UT	TRN	UN-UT
J	7.73 GJ	8.61 GJ	5.97 GJ	6.61 GJ	6.07 GJ	6.85 GJ
F	5.04	6.04	3.26	3.91	3.41	4.28
M	3.67	4.29	1.64	1.60	1.75	2.12
A	0.77	0.19	0.18	0.00	0.24	0.00
M	0.24	0.00	0.09	0.00	0.10	0.00
S	0.03	0.00	0.02	0.00	0.01	0.00
O	0.67	0.00	0.15	0.00	0.18	0.00
N	3.89	3.76	2.64	1.75	2.76	2.01
D	7.32	7.29	6.16	5.65	6.19	5.86
	29.36 GJ	30.18 GJ	20.12 GJ	19.52 GJ	20.73 GJ	21.13 GJ

for those surfaces exposed to the sun, and thus will increase their energy storage capacity. Direct-gain systems will therefore have a somewhat higher passive energy storage capacity than would be predicted by the simulated temperature decay test.

The work presented here indicates that there is potential for this method to give accurate estimates of effective capacitance for a variety of building constructions. Until further research is conducted however, this method should be used with caution for solar systems which have a large portion of the solar gains from direct radiation onto the interior surfaces. The use of the simulated decay test effective capacitance will give a conservative estimate of the energy storage capacity for these systems because of the increased temperature swing of the masses exposed to the direct radiation.

CHAPTER 6 SUMMARY AND RECOMMENDATIONS

6.1 SUMMARY

The objective of this research was to develop simplified design methods for active-passive hybrid solar space heating systems. Three types of hybrid systems have been analyzed; active system-passive system, active collection-passive storage, and active plus passive collection-passive storage hybrids.

Active system-passive system heating systems, which are comprised of either a direct-gain or collector-storage wall passive solar system combined with an active solar space heating system are analyzed in Chapter 2. The design method for these systems uses any of the existing passive solar design methods (i.e., the SLR method (3), or the Un-utilizability method (4,5)) to determine the passive subsystem energy contribution. The passive gains are then used to reduce the heating load the active solar subsystem must meet. A correction factor is presented to further modify the load on the active subsystem to account for effects caused by the active and auxiliary system controllers. The controllers affect the active system load by causing an increase in the average building temperature whenever the active subsystem is operating due to the

difference in active and auxiliary system set temperatures. This causes a higher active system load than would be calculated assuming perfect controllers. The active system load is then used in the active system design method (i.e., the f-Chart method (2)) to predict the active subsystem solar contribution. A second correction factor is presented to modify the f-Chart method for interaction effects caused by direct-gain passive, active hybrid systems. The passive system meets much of the load during the day, causing the active system to store more energy than it would if there were no passive system, thereby reducing the efficiency of the active collectors. The correction factor can also be used for collector-storage wall, active system hybrids, but will tend to give conservative estimates of the active subsystem performance. The standard deviation of the error for the combined hybrid analysis was 1.5 GJ on an annual basis.

Chapter 3 presents a design method for active collection-passive storage systems. These systems use active collectors, but use only the building mass as the energy storage medium. The design method for these systems is a modification of Monsen's Un-utilizability method for direct-gain systems (4,5). The modifications to Monsen's method generalize it to include collector efficiency and losses, and allow it to be used for either direct-gain or active collection-passive storage systems. The standard

alternative forms may provide better estimates of the solar fraction. The current correlation seems to give better predictions for active collection-passive storage systems than for direct-gain systems. The causes of this should be investigated.

2) The combined active plus passive collection-passive storage systems with non-equal active and passive collector orientations require the calculation of an average utilizability factor. The accuracy of the method presented in Chapter 4 is unknown, and better means of determining the utilizability factors for average surfaces might be found.

3) The short term simulated decay test method of determining effective capacitance should be further investigated. It seems possible that this method can be used to develop a relatively simple correlation for effective capacitance in terms of the building materials, building energy loss coefficient, allowable temperature swing, and other variables.

4) The design method for active system-passive system hybrids presented in Chapter 2 should be tested with active design methods other than the f-Chart method. The correction factors were developed in such a manner as to be independent of the active system design method, but this has not yet been tested.

5) Additional hybrid system designs still require

deviation of the error for the design method was 1.48 GJ for 228 examples in Madison, WI, Albuquerque, NM, Boston, MA, and Caribou, ME.

The design method for active collection-passive storage hybrid systems is expanded in Chapter 4 to include combinations of active and passive collectors with passive storage. These systems are broken down into two categories. The first is systems in which the active and passive collectors are at the same orientation. In this case, the utilizability factor for energy dumping can be found using conventional methods. Systems which have the active and passive collectors at different slopes and/or azimuths require a slightly more complicated and approximate means of evaluating a weighted average utilizability factor.

Chapter 5 briefly reviews the concept of effective capacitance, and presents a method of using short term simulations to evaluate the effective capacitance of different building constructions.

6.2 RECOMMENDATIONS

A number of recommendations can be made for future study of hybrid space heating systems.

1) With the increased utility of Monsen's un-utilizability concept, it is worthwhile to reexamine the form of his solar fraction correlation, as

analysis. Combinations of collector-storage wall passive systems and active collection-passive storage systems have not been dealt with here.

APPENDIX A

COLLECTOR PERFORMANCE PARAMETER MODIFICATIONS

Collector performance is usually characterized by two parameters, $F_R(\tau\alpha)_n$, and F_RU_L. F_R is the collector heat removal factor, which is analogous to a heat exchanger effectiveness. $(\tau\alpha)_n$ is the transmittance-absorbtance product of the collector cover-absorber combination for radiation perpendicular to the collector surface. U_L is the total heat loss coefficient of the collector. These parameters are determined through performance tests (such as the ASHRAE 93-77 test). The instantaneous efficency, η_i (defined as the ratio of delivered energy to the incident radiation) is plotted as a function of $(T_i - T_a)/G_T$*.

$$\eta_i = Q_u/A_cG_T = F_R(\tau\alpha)_n - F_RU_L(T_i - T_a)/G_T \qquad (A1)$$

Where T_i is the collector inlet temperature, T_a is the ambient temperature, G_T is the incident radiation per square meter, Q_u is the delivered energy, and A_c is the collector area.

* Efficency can also be presented as a function of the collector outlet or the average of the collector inlet and outlet temperature, ambient temperature difference. Duffie and Beckman (7) give conversion equations to obtain $F_R(\tau\alpha)$ and F_RU_L from these types of test data.

Presented in this form, the efficency is a linear function of $(T_i - T_a)/G_T$, with $F_R(\tau\alpha)_n$ being the intercept efficency and F_RU_L being the negative of the slope.

A number of factors can cause the performance of collectors in actual applications to differ from the test performance. The tests are performed at a specific fluid flowrate, and with the radiation nearly normal to the collector surface. The fluid flowrate may, however, differ considerably from the test value, and the radiation incidence angle will vary considerably. Additionally, pipe or duct losses, several collectors in series, and the inclusion of a heat exchanger between the collector and the storage device will detract from collector performance.

Modifications to $F_R(\tau\alpha)_n$ and F_RU_L can account for these effects by defining an equivolent collector with a different intercept efficency and efficency slope. The following correction factors (summarized from Duffie and Beckman (7)) can be applied individually, or sequentially in the order given.

A.1 FLUID FLOWRATE MODIFICATION

$$F_R(\tau\alpha)_n|_{use} = rF_R(\tau\alpha)_n|_{test} \qquad (A.1.1)$$

$$F_R(U)_L|_{use} = rF_R(U)_L|_{test} \qquad (A.1.2)$$

where

$$r = \frac{(mC_{pc}/A_cF_R'U_L)\ (1-e^{-A_cF'U_L/mC_{pc}})|_{use}}{(mC_{pc}/A_cF_R'U_L)\ (1-e^{-A_cF'U_L/mC_{pc}})|_{test}} \quad (A.1.3)$$

$$F'U_L = \frac{-mC_{pc}}{A_c} \ln\left[1-\frac{F_RU_LA_c}{mC_{pc}}\right] \quad (A.1.4)$$

mC_{pc} = Collector fluid capacitance flow rate

The $|_{use}$ and $|_{test}$ indicate that the values should be evaluated at the use and test flowrates respectively.

A.2 COLLECTORS IN SERIES

Additional modifications can be applied for the effects of having several collectors in series. For identical collectors:

$$F_R(\tau\alpha)_n = F_R(\tau\alpha)_n\{(1 - (1 - K)^N)/NK\} \quad (A.2.1)$$

$$F_R(U)_L = F_R(U)_L\{(1 - (1 - K)^N)/NK\} \quad (A.2.2)$$

where N is the number of collectors in series

$$K = A_cF_RU_L/mC_{pc} \quad (A8)$$

A.3 PIPE OR DUCT LOSSES

Correction factors can be applied to $(\tau\alpha)$ and U_L to account for pipes or ducts that are exposed to the ambient, leading to and from the collectors.

$$(\tau\alpha)' = (\tau\alpha)\{1/(1 + U_d A_o/(mC_{pc}))\} \qquad (A.3.1)$$

$$U_L' = \frac{U_L\{1-U_d a_i/(mC_{pc}) + U_d(A_i+A_o)/A_c F_R U_L\}}{1 + U_d A_o/(mC_{pc})} \qquad (A.3.2)$$

where A_i = Surface area of inlet pipe(duct)
A_o = Surface area of outlet pipe(duct)
U_d = loss coefficent of the pipe(duct)
mC_{pc} = collector fluid capacitance flowrate

A.4 COLLECTOR LOOP HEAT EXCHANGER

F_R can be modified to account for a collector loop heat exchanger. The modified collector heat removal factor, F_R', depends upon the capacitance flowrate of the collector loop, mC_{pc}, the heat exchanger efficency, ε, and the minimum of the collector and storage loop capacitance flowrates, $mC_{p,min}$.

$$F_R' = F_R\left[1+\left(\frac{A_c F_R U_L}{mC_{pc}}\right)\left(\frac{mC_{pc}}{\varepsilon mC_{p,min}} - 1\right)\right]^{-1} \qquad (A.4.1)$$

A.5 AVERAGE TRANSMITTANCE-ABSORBTANCE PRUDUCT

The last collector parameter modification presented here accounts for the dependence of $(\tau\alpha)$ on the angle of incidence of the solar radiation. On a monthly average basis, the overall average transmittance-absorbtance product, $(\overline{\tau\alpha})$, is the energy weighted average of the monthly average value beam, diffuse, and reflected radiation. The average transmittance-absorbtance product for beam radiation, $(\overline{\tau\alpha})_b$, can be approximated by evaluating $(\tau\alpha)$ at the incidence angle that occurs on the average day of the month, 2.5 hours from noon (7).

$$(\overline{\tau\alpha})_b = (\tau\alpha)_n\{1 + b_o(1/\cos\ - 1)\} \qquad \text{(A.5.1)}$$

where $b_o = -0.10$ for a 1 glass cover collector

$b_o = -0.17$ for a 2 glass cover collector

$b_o = -0.45$ for a mylar honeycomb plus 1 glass cover collector

This is limited to incidence angles of less than 60^o. The average $(\overline{\tau\alpha})$ for diffuse sky and ground radiation, $(\overline{\tau\alpha})_d$ and $(\overline{\tau\alpha})_g$, can be found using Equation A.5.1 and an effective beam radiation angle (7).

APPENDIX B

CALCULATION OF MONTHLY AVERAGE UTILIZABILITY FACTORS

Two algorithms for evaluating montly average utilizability factors ($\bar{\phi}$) are presented here. The first, developed by Klein (20) is applicable only to south facing collectors. The second , by Clark, et al., (29) can be used for collectors of any orientation.

KLEIN ALGORITHM (Adapted from Reference 20)

Monthly average utilizability factors for south facing surfaces are dependent upon the critical radiation level, location, time of year, collector orientation , and the incident solar radiation. Location, time of year, and collector orientation can be accounted for in two parameters, $\bar{K}_T$ (the monthly average clearness index) and $\bar{R}/R_N$. $\bar{K}_T$ is given for many locations in references (7,19). $\bar{R}$ is the ratio of montly radiation incident on a tilted surface to the radiation incident on a horizontal surface.

$$\bar{R} = (1-\bar{H}_d/\bar{H})\bar{R}_b+(\bar{H}_d/\bar{H})(1+\cos\ )/2+\ (1-\cos\ )/2 \quad (B.1.1)$$

where β = collector slope

ρ = ground reflectance

$\bar{R}_b$ = ratio of monthly average beam radiation on a tilted surface to that on a horizontal surface

$\bar{H}_d/\bar{H}$ = monthly diffuse faction

$\bar{H}_d/\bar{H}$ can be found using a number of correlations (7). The diffuse fraction correlation of Erbs (14) is given below.

$$\bar{H}_d/\bar{H} = 1.317 - 3.023\bar{K}_T + 3.372\bar{K}_T^2 - 1.76\bar{K}_T^3 \quad \text{(B.1.2)}$$

$\bar{R}_b$ can be approximated for south facing surfaces by calculating the ratio of extraterrestrial radiation on a tilted surface to that on a horizontal surface.

$$\bar{R}_b = \frac{\cos(\ell-\beta)\cos\delta\sin(\omega_s')+(\pi/180)\omega_s'\sin(\ell-\beta)\sin\delta}{\cos\ell\cos\delta\sin\omega_s+(\pi/180)\omega_s\sin\ell\sin\delta} \quad \text{(B.1.3)}$$

where $\omega_s' = \text{MIN}\begin{cases}\omega_s=\cos^{-1}(-\tan\ell\tan\delta)\\ \cos^{-1}(-\tan(\ell+\beta)\tan\delta\end{cases}$

ℓ = latitude

δ = solar declination

ω_s = sunset hour angle on a horizontal surface

ω_s' = sunset hour angle on a tilted surface

R_N, the ratio of radiation on a tilted surface to that on a horizontal surface at noon, can be found using equations B.1.5-B.1.9.

$$R_N=(1-(r_{d,n}/r_{T,n})H_d/H)R_{b,N}+(r_{d,N}/r_{T,N})H_d/H(1+\cos\beta)/2 +(1-\cos\beta)/2 \quad \text{(B.1.5)}$$

$$r_{d,N}=(\pi/24)(1-\cos\omega_s)/(\sin\omega_s-(\pi/180)\omega_s\cos\omega_s) \quad \text{(B.1.6)}$$

$$r_{T,N}=r_{d,N}(1.07+0.025\sin(\omega_s-60)) \quad \text{(B.1.7)}$$

where $r_{T,N}$ is the ratio of radiation at noon to the daily total radiation, from Rabl (20), and $r_{d,N}$ is the ratio of diffuse radiation at noon to the daily diffuse radiation. $R_{b,N}$ is the ratio of beam radiation on a tilted surface to that on a horizontal surface. For a south facing surface:

$$R_{b,N} = \frac{\cos(\ell-\beta)\cos\delta+\sin(\ell-\beta)\sin\delta}{\cos\ell\cos\delta+\sin\ell\sin\delta} \quad \text{(B.1.8)}$$

H_d/H, the daily diffuse fraction can be estimated using the correlation developed by Erbs (14).

The critical radiation level, I_c, is incorperated into a dimensionless critical radiation level, X_c. X_c is the ratio of I_c to the radiation level at noon for the average day of the month.

$$X_c = I_c/(r_{T,N}R_N\bar{K}_T\bar{H}_o) \quad \text{(B.1.9)}$$

From the three dimensionless parameters X_c, $\bar{R}/R_N$, and $\bar{K}_T$, $\bar{\phi}$

can be found using equations B.1.10-B.1.13:

$$\bar{\phi} = \exp((A+B(R_N/\bar{R}))(X_c+CX_c^2\}))) \quad \text{(B.1.10)}$$

where $A = 2.943-9.271\bar{K}_T+4.031\bar{K}_T^2$ (B.1.11)

$B = -4.345+8.853\bar{K}_T- 3.062\bar{K}_T^2$ (B.1.12)

$C = -0.170-0.306\bar{K}_T+ 2.936\bar{K}_T^2$ (B.1.14)

CLARK ALGORITHM (Adapted from Reference 29)

The method for calculating $\bar{\phi}$ developed by Clark et al. (29) encompasses a somewhat different approach than Klein's algorithm. The monthly average daily utilizability, $\bar{\phi}$, can be broken down into monthly average hourly utilizability factors, ϕ, for each hour of the day. ϕ can then be found for surfaces with any orientation, including non-south facing surfaces. The energy weighted average of the hourly ϕ values on the average day of the month is the monthly average daily utilizability, $\bar{\phi}$.

$$\bar{\phi} = (\Sigma \bar{I}_T \phi) / \Sigma \bar{I}_T \quad \text{(B.2.1)}$$

Monthly average hourly ϕ's can be determined in a similar manor to the $\bar{\phi}$ algorithm of Klein. Emperical correlations of two dimensionless parameters, X_c, and X_m, account for the collector orientation , location, and

critical radiation level.

$$X_c = I_c/\bar{I}_T \qquad (B.2.2)$$

where $\bar{I}_T$ is the monthly average radiation incident on the collector for a given hour interval.

$$X_m = 1.85+0.169\bar{R}/\bar{k}^2-0.0696(\cos\beta)/\bar{k}^2-0.981k/(\cos\delta)^2 \qquad (B.2.3)$$

where $\bar{R}$ = the ratio of total radiation on a tilted surface to that on a horizontal surface
β = collector slope
δ = solar declination
$\bar{k}$ = the monthly average hourly clearness index

$\bar{k}$ can be estimated from the monthly average daily clearness index, $\bar{K}_T$ using a correlation developed by Collares-Periera and Rabl (30).

$$\bar{k} = \bar{K}_T(a+b\cos\omega) \qquad (B.2.4)$$

$$a=0.409+0.5016\sin(\omega_s-60) \qquad (B.2.5)$$

$$b=0.6609-0.4767\sin(\omega_s-60) \qquad (B.2.6)$$

where ω is the hour angle for the hour of interest.

$\bar{I}$, the monthly average total radiation on a horizontal surface can be found using $\bar{k}$ and the extraterrestrial radiation, $\bar{I}_o$.

$$\bar{I} = \bar{I}_o \bar{k} \qquad (B.2.7)$$

The diffuse fraction of radiation can be found using the relationship of Liu and Jordan (31), combined with Equation B.2.4.

$$\bar{I}_d/\bar{I} = (\bar{H}_d/\bar{H})(a+b\cos\omega)^{-1} \qquad (B.2.8)$$

where $\bar{H}_d/\bar{H}$ is defined in Appendix A. $\bar{R}$ can be found for hourly values in an analogous manor to Equation B.1.1.

$$\bar{R} = (1-\bar{I}_d/\bar{I})R_b+(\bar{I}_d/\bar{I})(1+\cos\beta)/2+ (1-\cos\beta)/2 \qquad (B.2.9)$$

R_b, the ratio of beam radiation on a tilted surface to that on a horizontal surface is:

$$R_b = \cos\theta/\cos\theta_z \qquad (B.2.10)$$

where θ is the incidence angle of the radiation on the tilted surface and θ_z is the incidence angle on a horizontal surface. The total radiation on the tilted surface, $\bar{I}_T$, can then be found using $\bar{R}$ and $\bar{I}$.

$$\bar{I}_T = \bar{R}\ \bar{I} \qquad (B.2.11)$$

BIBLIOGRAPHY

1) TRNSYS 11.1, EES Report 38, University of Wisconsin-Madison, WI (1981).

2) Klein, S.A., et al., "A Design Procedure for Solar Heating Systems," SOLAR ENERGY, 18, 113 (1976).

3) Jones, R.W., editor; Balcomb, J.D. et al., Passive Solar Design Handbook, 3, U.S. Dept. of Energy, DOE/CS-0127/3, (1982).

4) Monsen, W.A., et al., "Prediction of Direct Gain Solar Heating System Performance," SOLAR ENERGY, 27, 143 (1981).

5) Monsen, W.A., et al., "The Un-utilizability Method for Collector Storage Walls," SOLAR ENERGY, 29, 421 (1982).

6) Swisher, J., "Active Charge/Passive Discharge Solar Heating System: Thermal Analysis," AS/ISES Philadelphia, PA, 587 (1981).

7) Duffie, J.A. and Beckman, W.A., Solar Engineering of Thermal Processes, Wiley-Interscience, New York, (1980).

8) Monsen, W.A., "Design Methods for Building-Integrated Solar Heating Components," M.S. Thesis, University of Wisconsin-Madison (1980).

9) Balcomb, J.D., et al., "Expanding the SLR Method," PASSIVE SOLAR JOURNAL, 1, 67 (1982).

10) F-CHART 3.0, EES Report 49, University of Wisconsin-Madison, (1978).

11) Klein, S.A. and Beckman, W.A., "A Generalized Design Method for Closed-Loop Solar Energy Systems," SOLAR ENERGY, 22, 269 (1979).

12) F-CHART 4.1, EES Report 50, University of Wisconsin-Madison, (1980).

13) Klein, S.A. and Theilacker, J.C., "An Algorithm for Calculating Monthly-Average Radiation on Inclined Surfaces," ASME JOURNAL OF SOLAR ENERGY ENGR., 103, 29 (1981).

14) Erbs, D.G., et al., "Estimation of the Diffuse Radiation Fraction for Hourly, Daily, and Monthly-Average Global Radiation," SOLAR ENERGY, 28(4), 293, (1982).

15) Braun, J.E., "Seasonal Storage of Energy in Solar Heating," M.S. Thesis, University of Wisconsin-Madison (1980).

16) Erbs, D.G., "Models and Applications for Weather Statistics Related to Building Heating and Cooling Loads," to be completed Dec. (1983).

17) Barakat, S.A. and Sander, D.M., Building Research Note No. 184, Division of Building Research, National Research Council of Canada (1982).

18) SOLMET Typical Meterological Year, NOAA, Environmental Data Service, National Climatic Center, Asheville,

North Carolina.

19) Cinanemani, V., et al., "Input Data for Solar Systems," U.S. Dept. of Energy (1978).

20) Klein, S.A., "Calculation of Flat Plate Collector Utilizability," SOLAR ENERGY, 21, 393 (1978).

21) Erbs, D.G., et al., "Sol-air Heating and Cooling Degree-Days," to be published in SOLAR ENERGY.

22) ASHRAE Handbook of Fundamentals, New York: American Society of Heating, Refrigeration, and Air Conditioning Engineers Incorporated, (1982).

23) Mitchell, J.W., Personal Communication (1983).

24) Horn, J.C., "Investigation of Various Thermal Capacitance Models," M.S. Thesis, University of Wisconsin-Madison (1982).

25) TRNSYS 12.1, EES Report to be Published by January 1 (1984).

26) Mitalas, G.P., "Calculation of Transient Heat Flow Through Walls and Roofs, "ASHRAE Transactions, 74, 182-188 (1968).

27) ASHRAE Handbook of Fundamentals, New York: American Society of Heating, Refrigeration, and Air Conditioning Engineers Incorporated, (1977).

28) Erbs, D.G., "Estimation of Degree-Days and Ambient Temperature Bin Data From Monthly Average Temperatures," ASHRAE Journel, June (1983).

29) Clark, D.R., Klein, S.A., and Beckman, W.A., "Algorithm for Evaluating the Hourly Radiation Utilizability Function," JOURNAL OF SOLAR ENERGY ENGINEERING, Vol 105,(August) 281 (1983).

30) Collares-Pereia, M. and Rabl, A., "The Average Distribution of Solar Radiation-Correlations Between Daily and Hourly Insolation Values," SOLAR ENERGY 22, 155 (1979).

31) Liu, B.Y.H. and Jordan, R.C., "The Interrelationship and Characteristic Distribution of Direct,Diffuse, and Total Radiation," SOLAR ENERGY 4, 1 (1960).